

FATIGUE LIFE CALCULATION
BY
RAINFLOW CYCLE COUNTING METHOD

A THESIS SUBMITTED TO
THE GRADUATE SCHOOL OF NATURAL AND APPLIED SCIENCES
OF
MIDDLE EAST TECHNICAL UNIVERSITY

BY

SEÇİL ARIDURU

IN PARTIAL FULFILLMENT OF THE REQUIREMENTS
FOR
THE DEGREE OF MASTER OF SCIENCE
IN
MECHANICAL ENGINEERING

DECEMBER 2004

Approval of the Graduate School of Natural and Applied Sciences

Prof. Dr. Canan ÖZGEN
Director

I certify that this thesis satisfies all the requirements as a thesis for the degree of Master of Science.

Prof. Dr. S.Kemal İDER
Head of Department

This is to certify that we have read this thesis and that in our opinion it is fully adequate, in scope and quality, as a thesis for the degree of Master of Science.

Prof. Dr. Mehmet ÇALIŞKAN
Supervisor

Examining Committee Members

Prof. Dr. Levent PARNAS (METU,ME) _____

Prof. Dr. Mehmet ÇALIŞKAN (METU,ME) _____

Assoc.Prof. Dr. Suat KADIOĞLU (METU,ME) _____

Assis.Prof. Dr. Serkan DAĞ (METU,ME) _____

M.S. Gürol İPEK (BİAS) _____

I hereby declare that all information in this document has been obtained and presented in accordance with academic rules and ethical conduct. I also declare that, as required by these rules and conduct, I have fully cited and referenced all material and results that are not original to this work.

SEÇİL ARIDURU

ABSTRACT

FATIGUE LIFE CALCULATION BY RAINFLOW CYCLE COUNTING METHOD

ARIDURU, Seçil

M.S., Department of Mechanical Engineering

Supervisor: Prof. Dr. Mehmet ÇALIŞKAN

December 2004, 119 pages

In this thesis, fatigue life of a cantilever aluminum plate with a side notch under certain loading conditions is analyzed. Results of experimental stress analysis of the cantilever aluminum plate by using a uniaxial strain gage are presented. The strain gage is glued on a critical point at the specimen where stress concentration exists. Strain measurement is performed on the base-excited cantilever beam under random vibration test in order to examine the life profile simulation.

The fatigue analysis of the test specimen is carried out in both time and frequency domains. Rainflow cycle counting in time domain is examined by taking the time history of load as an input. Number of cycles is determined from the time history. In frequency domain analysis, power spectral density function estimates of normal stress are obtained from the acquired strain data sampled at 1000 Hz. The moments of the power spectral density estimates are used to find the probability density function estimate from Dirlik's empirical expression. After the total

number of cycles in both time and frequency domain approaches are found, Palmgren-Miner rule, cumulative damage theory, is used to estimate the fatigue life. Results of fatigue life estimation study in both domains are comparatively evaluated. Frequency domain approach is found to provide a marginally safer prediction tool in this study.

Keywords: fatigue, dynamic strain measurement, rainflow cycle counting, Palmgren-Miner rule

ÖZ

YAĞMURAKIŞI DÖNGÜ SAYMA YÖNTEMİ İLE YORULMA ÖMRÜNÜN HESAPLANMASI

ARIDURU, Seçil

Y. Lisans, Makina Mühendisliği Bölümü

Tez Yöneticisi : Prof. Dr. Mehmet ÇALIŞKAN

Aralık 2004, 119 sayfa

Bu çalışmada, bir kenarından sabitlenmiş, belirli bir yük altında, yan çentiği bulunan alüminyum profilin yorulma ömrü incelenmiştir. Serbest giriş alüminyum profilin deneysel gerilme analizi sonuçları, tek eksen uzama teli kullanılarak sunulmuştur. Gerilme yoğunluğunun olduğu test biriminin kritik noktasına uzama teli yapıştırılmıştır. Rassal titreşim testi altında olan serbest giriş alüminyum profilinin, ömür profil benzeşimini incelemek için gerilme ölçümü yapılmıştır.

Test edilen birimin yorulma analizi, zaman ve frekans alanlarında incelenmiştir. Zaman alanında yağmurakışı döngü sayımı, girdi olarak zaman aralığı alınarak yapılmıştır. Zaman aralığından döngü sayısı bulunmuştur. Frekans alanında, gerilme verisinden güç spektrum yoğunluğu fonksiyon kestirimleri, 1000 Hz'de örneklenen kazanılmış gerilme verisinden elde edilmiştir. Dirlik'in deneysel anlatımından olasılık yoğunluk fonksiyon kestirimini bulmak için, güç spektrum yoğunluğu hesaplarından elde edilen alanlar kullanılmıştır. Zaman ve frekans alanlarından toplam döngü sayıları bulunduktan sonra, birikimsel hasar

kuramlardan biri olan Palmgren-Miner kuralı, yorulma ömrünü tahmin etmek için kullanılmıştır. Yorulma ömrü tahmini üzerine yapılan çalışmaların sonuçları, her iki alanda karşılaştırmalı olarak değerlendirilmiştir. Bu çalışmada, frekans alanı yaklaşımı, biraz daha güvenli bulunmuştur.

Anahtar kelimeler: yorulma, dinamik birim uzama ölçümü, yağmurakışı döngü sayımı, Palmgren-Miner kuralı

ACKNOWLEDGMENTS

I would like to express my deepest gratitude and appreciation to Prof. Dr. Mehmet Çalışkan for his guidance, advices, encouragements and insight throughout the research.

I would like to express my deepest gratitude to my parents for their encouragements and understanding throughout this study.

I would like to thank to M.S. Gürol İpek for his support.

TABLE OF CONTENTS

	PAGE
PLAGIARISM.....	iii
ABSTRACT.....	iv
ÖZ.....	vi
ACKNOWLEDGMENTS.....	viii
TABLE OF CONTENTS.....	ix
LIST OF FIGURES.....	xii
LIST OF TABLES.....	xv
NOMENCLATURE.....	xvi
 CHAPTER	
1. INTRODUCTION.....	1
1.1. General.....	1
1.2. Applications of Fatigue Life Calculations.....	3
1.3. Scope and Objective of the Thesis.....	4
2. FATIGUE FAILURE.....	6
2.1. Fatigue.....	6
2.2. Stress-Life Based Approach.....	9
3. RAINFLOW CYCLE COUNTING	13
3.1. Original Definition.....	13
3.2. Practical Definition.....	19
4. RAINFLOW CYCLE COUNTING IN TIME DOMAIN AND FREQUENCY DOMAINS.....	23
4.1. Introduction.....	23
4.2. Rainflow Cycle Counting in Time Domain.....	24

4.3. Rainflow Cycle Counting in Frequency Domain.....	25
4.3.1. Probability Density Function.....	26
4.3.2. Expected Zeros, Peaks and Irregularity Factor.....	27
4.3.3. Moments from the Power Spectral Density.....	29
4.3.4. Expected Zeros, Peaks and Irregularity Factor from a Power Spectral Density.....	30
4.3.5. Estimation of Probability Density Function from Power Spectral Density Moments.....	31
5. PALMGREN-MINER RULE.....	33
6. DESIGN OF THE EXPERIMENTS.....	37
6.1. Vibration Test System.....	37
6.2. Test Material.....	39
6.3. Strain Gages.....	41
6.3.1. Strain Gage Characteristics.....	44
6.3.2. The Measuring Circuit.....	47
6.3.2.1. Quarter Bridge Circuit.....	48
6.3.3. Shunt Calibration of Strain Gage.....	50
6.4. Test Procedure.....	51
7. RESULTS OF MODAL ANALYSIS AND EXPERIMENTAL STUDIES	60
7.1. Modal Analysis.....	60
7.2. Experimental Results.....	63
7.2.1. Experimental Results in Time Domain.....	63
7.2.2. Experimental Results in Frequency Domain.....	68
7.3. Palmgren-Miner Rule Application.....	73
7.3.1. Total Damage Calculation in Time Domain by Palmgren-Miner Rule.....	74
7.3.2. Total Damage Calculation in Frequency Domain by	

Palmgren-Miner Rule.....	75
7.4. Statistical Errors Associated with the Spectral Measurements...	75
7.4.1. Random Error.....	77
7.4.2. Bias Error.....	78
8. SUMMARY AND CONCLUSION.....	81
8.1. Summary.....	81
8.2. Conclusion.....	85
REFERENCES.....	90
APPENDICES	
A. EXPERIMENTAL WORK FOR THE TEST SPECIMEN DETERMINATION.....	94
B. TABLES.....	101
C. FIRST NATURAL FREQUENCY CALCULATION OF THE CANTILEVER ALUMINUM PLATE.....	105
D. COMMUNICATION.....	107
E. SUBROUTINE FOR RAINFLOW COUNTING.....	108
F. SOLUTION METHODS.....	112
G. COUNTING METHODS FOR THE ANALYSIS OF THE RANDOM TIME HISTORY.....	114

LIST OF FIGURES

FIGURE	PAGE
1.1. Description of fatigue process.....	2
2.1. The basic elements of the fatigue design process.....	7
2.2. The cumulative damage analysis process.....	9
2.3. Functional diagram of engineering design and analysis.....	10
2.4. A typical S-N material data.....	11
3.1. Stress-strain cycles.....	14
3.2. Random stress fluctuation.....	14
3.3. The drop released from the largest peak.....	15
3.4. Flow rule of the drop from a peak.....	16
3.5. Drop departure from a valley.....	17
3.6. Flow rule of the drop from a valley.....	17
3.7. Rainflow cycle counting.....	18
3.8. Practical definition of the rainflow cycle counting.....	21
4.1. Time history.....	23
4.2. Random processes.....	24
4.3. General procedure for time domain fatigue life calculation.....	25
4.4. General procedure for frequency domain fatigue life calculation.....	26
4.5. Probability density function.....	27
4.6. Zero and peak crossing rates.....	28
4.7. Equivalent time histories and power spectral densities.....	29
4.8. One-sided power spectral density function.....	30
5.1. Spectrum of amplitudes of stress cycles.....	34
5.2. Constant amplitude S-N curve.....	35
6.1. Vibration test system.....	37
6.2. Components of the vibration test system.....	38
6.3. Left hand rule.....	38
6.4. Minimum Integrity Test applied to the specimen between 5-500Hz.....	40

6.5. Detail description of the uniaxial strain gage.....	44
6.6. Basic Wheatstone Bridge circuit	48
6.7. The external circuit with active gage illustrated with instrument	49
6.8. Quarter bridge circuit with active gage.....	49
6.9. Shunt calibration of single active gage.....	50
6.10. Aluminum test specimen.....	52
6.11. Side notch in the aluminum test specimen.....	52
6.12. Cantilever aluminum plate.....	53
6.13. Test specimen with fixture.....	54
6.14. Strain gage glued on the aluminum test specimen.....	54
6.15. Side notch placed under the strain gage.....	55
6.16. Uniaxial strain gage.....	55
6.17. Aluminum test specimen, cable and the connector.....	57
6.18. Quarter bridge circuit diagram of the strain gage connector.....	58
6.19. Measuring equipment.....	59
7.1. 1st mode shape of the test specimen obtained by ANSYS.....	62
7.2. 2nd mode shape of the test specimen obtained by ANSYS.....	62
7.3. 3rd mode shape of the test specimen obtained by ANSYS.....	63
7.4. Random data acquired from the test specimen.....	64
7.5. Cycle counting in full range by rainflow method on the test specimen.....	65
7.6. Percentage of cycle counting in full range by rainflow method on the test specimen.....	66
7.7. Cycle counting and mean classes in full range by rainflow method on the test specimen.....	67
7.8. Percentage of cycle counting and mean classes in full range by rainflow method on the test specimen.....	67
7.9. Number of cycles versus stress obtained from the test in time domain.....	68
7.10. Power spectral density function estimates of the test specimen for signal in Figure 7.4.....	69
7.11. Probability density function estimates versus stress amplitude obtained	

from PSD graph of the test specimen in Figure 7.10.....	72
7.12. Number of cycles versus stress obtained from the test in frequency domain.....	73
7.13. Average result of power spectral density estimates versus frequency for 1.024 seconds of each 64 sample time history.....	76
7.14. Average power spectral density estimates versus frequency.....	77
8.1. Number of cycles vs stress diagram (time domain approach).....	87
8.2. Number of cycles vs stress diagram (frequency domain approach).....	87
A.1. Aluminum test specimens.....	94
A.2. Perpendicular S-shaped test specimen under vibration test.....	95
A.3. Crack initiation occurred in the welded points in the vibration test.....	95
A.4. Bending started from the end of the support part in the test specimen.....	96
A.5. Aluminum cantilever plate under a certain loading condition.....	96
A.6. Cantilever aluminum test specimen.....	97
A.7. Crack occurred in the fixed side of the aluminum plate in the vibration test.....	97
A.8. The notch placed on the aluminum plate.....	98
A.9. The notch placed on top surface of the cantilever aluminum plate.....	98
A.10. Polyurethane foam glued on the aluminum plate.....	99
A.11. Notch position on the aluminum plate.....	99
A.12. The notch placed on the bottom surface of the aluminum plate.....	100
A.13. Crack propagation occurred in the vibration test.....	100
G.1. Level crossing counting example.....	115
G.2. Peak counting example.....	117
G.3. Simple range counting example.....	118

LIST OF TABLES

TABLES	PAGE
3.1. Cycle counts.....	22
6.2. Dimensions of the strain gage used in the experiment.....	56
7.1. Material properties of the elements used in the modal analysis.....	60
7.2. Data obtained for the test specimen by MATLAB software.....	71
B.1. Stress versus number of cycles in time domain.....	101
B.2. Stress versus probability density function estimates and number of cycles in frequency domain.....	102
B.3. Standard gage series.....	104

NOMENCLATURE

SYMBOL

A	Area
b	Width
b()	Biased estimate
B	Magnetic flux density (Tesla)
B _e	Effective bandwidth
B _r	Half-power bandwidth
D	Total damage
e	Strain
ε _b	Bias error
ε _r	Random error
E	Modulus of elasticity
E[0]	Number of upward zero crossings per second
E[D]	Expected fatigue damage
E[P]	Number of peaks per second
f	Frequency
f _n	Natural frequency
f _r	Resonance frequency
F	Force (Newton)
F _C	Compression force
F _T	Tension force
g	Acceleration
G(f)	Power spectral density for $0 \leq f \leq \infty$
G _{ave} (f)	Average power spectral density
h	Thickness
H(f)	Frequency response function

I	Current (Amper)
k	Strain sensitivity , stiffness
K	Constant
L	Length (meter), Level
ΔL	Change in length
m	Mass
n	Total number of applied cycles
n_d	Subrecords
N	Number of cycles to failure
R	Resistance
S	Stress
S-T-C	Self-Temperature Compensation
S_t	Total number of cycles
T	Time
Var()	Variance
ζ	Damping ratio
γ	Irregularity factor

CHAPTER 1

INTRODUCTION

1.1. GENERAL

For centuries, man has been aware that by repeatedly bending the wood or metal back and forth with large amplitude, it could be broken. It came as something surprise, however, when he found that repeated stressing would produce fracture even with the stress amplitude held well within the elastic range of the material. Fatigue analysis procedures for the design of modern structures rely on techniques, which have been developed over the last 100 years or so. The first fatigue investigations seem to have been reported by a German mining engineer, W.A.S.Albert who in 1829 performed some repeated loading tests on iron chain. [22] When the railway systems began to develop rapidly about the midst of the nineteenth century, fatigue failures in railway axles became a widespread problem that began to draw the first serious attention to cyclic loading effects. This was the first time that many similar parts of machines had been subjected to millions of cycles at stress levels well below the yield point, with documented service failures appearing with disturbing regularity. This theory was disparaged by W.J.Rankine in 1843. As is often done in the case of unexplained service failures, attempts were made to reproduce the failures in the laboratory. Between 1852 and 1870 the German railway engineer, August Wöhler set up and conducted the first systematic fatigue investigation. [14]

Fatigue is the most important failure mode to be considered in a mechanical design. The physical process of fatigue is described in Figure1.1. Under the action of oscillatory tensile stresses of sufficient magnitude, a small crack will initiate at a point of the stress concentration. Once the crack is initiated, it will tend to grow in a direction orthogonal to the direction of the oscillatory tensile loads.

There are several reasons for the dominance of this failure mode and the problems of designing to avoid it: (1) the fatigue process is inherently unpredictable, as evidenced by the statistical scatter in laboratory data; (2) it is often difficult to translate laboratory data of material behavior into field predictions; (3) it is extremely difficult to accurately model the mechanical environments to which the system is exposed over its entire design lifetime; and (4) environmental effects produce complex stress states at fatigue-sensitive hot spots in the system. It can be thought that fatigue can involve a very complicated interaction of several processes and/or influences.

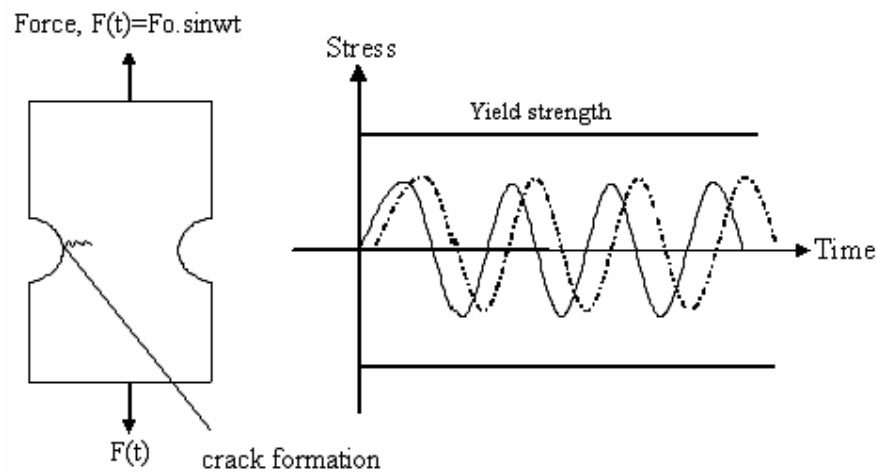


Figure 1.1. Description of fatigue process [13]

Fatigue failures are often catastrophic; they come without warning and may cause significant property damage as well as loss of life. The goal of such new elements in the design process is to perform fatigue and durability calculations much earlier, thereby reducing or removing the need for expensive redesign later on. Actually, fatigue damage is related to cycle amplitudes or ranges and not to peak values. Therefore, in any kind of loading, fatigue damage is caused by statistical properties such as amplitudes and mean values.

Fatigue life is the number of loading cycles of a specified character that a given specimen sustains before failure of a specified nature occurs. When analyzing the fatigue life for the structures, the level crossings have been used for a long time. However, better life predictions are obtained when using a cycle counting method, which is a rule for pairing local minima and maxima to equivalent load cycles. An appropriate cycle identification technique, which is rainflow cycle counting method, is examined in time and frequency domains. Fatigue damage is computed by damage accumulation hypothesis which is illustrated as Palmgren-Miner rule. This rule is used to obtain an estimate of the structural fatigue life.

The fatigue life time depends on several factors, where the most important ones are the manufacturing, the material properties, and the loading conditions, which are all more or less random. Both material properties and dynamical load process are important for fatigue evaluation, and should in more realistic cases be modeled as random phenomena. In order to relate a load sequence to the damage it inflicts to the material, the so called rainflow cycle counting method is often used, together with a damage accumulation model. The damage can then be related to the fatigue life.

The rainflow cycle counting method has been successful, and has now become a standard method for the railway, aircraft and automotive industries in fatigue life estimations.

1.2. APPLICATION OF FATIGUE LIFE CALCULATIONS

In this thesis, the fatigue life of a cantilever aluminum plate with a side notch, under a certain loading condition is investigated. Experiments are performed on cantilever aluminum plate on the vibration test system at room temperature. The results, obtained as time and strain values, are analyzed in time domain and in frequency domain separately. ESAM software is used for the analysis and

MATLAB software is also exploited for the implementation algorithm of the Dirlik's approach. The modal analysis of the specimen is carried to obtain mode shapes and undamped natural frequencies by ANSYS software. Through S-N curve, the fatigue life of the specimen is calculated by Palmgren-Miner rule.

1.3. SCOPE AND OBJECTIVE OF THE THESIS

This thesis contains eight chapters. In Chapter 1, the field of fatigue life and the fatigue process are introduced. The application of the fatigue life calculations is also discussed briefly.

In Chapter 2, the concept of fatigue failure is given in detail. The fundamentals of the fatigue considerations, basic elements of the fatigue design process, stress-life based approach for the fatigue design are presented in this chapter.

In Chapter 3, the original definition of the rainflow cycle counting and the stress-strain behavior of the material which is the basis of the counting are explained. Rainflow cycle counting is illustrated with an example where the cycles are identified in a random variable amplitude loading sequence. The practical definition of the rainflow cycle counting, which is according to the ASTM E-1049 Standard Practices for Cycle Counting in Fatigue Analysis, is also defined and cycles counted are tabulated.

In Chapter 4, the rainflow cycle counting in the time domain and in the frequency domain is studied. The processes that should be followed are given step by step in these domains separately. How to store the stress range histogram in the form of a probability density function of stress ranges, and the calculation of the parameters which are expected zeros, peaks and irregularity factor are given. Spectral moments of the power spectral density function and the parameters in terms of spectral moments are defined. Dirlik's solution is illustrated.

In Chapter 5, most popular cumulative damage theory which is referred as Palmgren-Miner rule is defined for the fatigue life prediction. The assumptions done in the rule are summarized. Constant amplitude S-N curve, total damage and the event of failure are described. Existing limitations in the rule are explained.

In Chapter 6, design of the experiments is described. The theory and the components of the vibration test system and the random vibration profile used in the experiment is explained. The reason for the choice of aluminum as the test material, the strain gages, and its characteristics are described. Also, the measuring circuit and the quarter bridge circuit is used in the experiment and shunt calibration of the strain gage are illustrated. The test procedure followed in the experiment is analyzed.

In Chapter 7, the modal analysis of the test specimen to obtain the vibration characteristics is given. Experimental results in time and in frequency domains for rainflow cycle counting are described. The algorithms written in MATLAB software to obtain the moments of the power spectral density estimates and the probability density function estimates of stress ranges are given. The graphs acquired from the test results are shown and the values found are tabulated. Palmgren-Miner rule application is performed and total damage calculation both in time and frequency domains are calculated. The average power spectral density estimates and the spectral errors, namely, the random and bias errors are determined.

In Chapter 8, summary of the thesis and conclusions are given, the results of the modal analysis, the analysis of the rainflow cycles counting in time and frequency domains, total number of cycles found from the analysis and the graphs obtained, Palmgren-Miner rule solution and the statistical errors in the experimental results are discussed.

CHAPTER 2

FATIGUE FAILURE

2.1. FATIGUE

Fatigue is the process of progressive localized permanent structural change occurring in a material subjected to conditions that produce fluctuating stresses and strains at some point or points and that may culminate in cracks or complete fracture after a sufficient number of fluctuations. If the maximum stress in the specimen does not exceed the elastic limit of the material, the specimen returns to its initial condition when the load is removed. A given loading may be repeated many times, provided that the stresses remain in the elastic range. Such a conclusion is correct for loadings repeated even a few hundred times. However, it is not correct when loadings are repeated thousands or millions of times. In such cases, rupture will occur at a stress much lower than static breaking strength. This phenomenon is known as fatigue.

To be effective in averting failure, the designer should have a good working knowledge of analytical and empirical techniques of predicting failure so that during the predescribed design, failure may be prevented. That is why; the failure analysis, prediction, and prevention are of critical importance to the designer to achieve a success.

Fatigue design is one of the observed modes of mechanical failure in practice. For this reason, fatigue becomes an obvious design consideration for many structures, such as aircraft, bridges, railroad cars, automotive suspensions and vehicle frames. For these structures, cyclic loads are identified that could cause fatigue failure if the design is not adequate. The basic elements of the fatigue design process are illustrated in Figure 2.1.

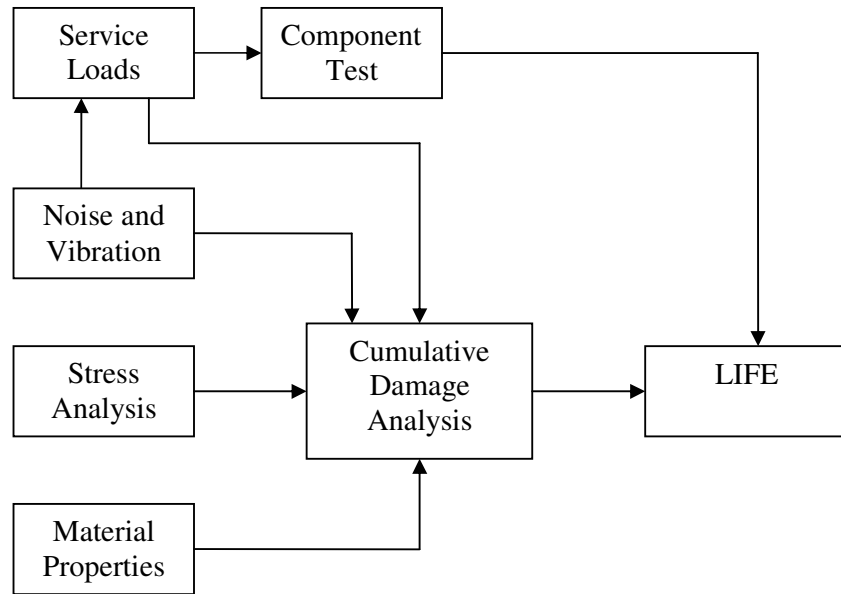


Figure 2.1. The basic elements of the fatigue design process [1]

Service loads, noise and vibration: Firstly, a description of the service environment is obtained. The goal is to develop an accurate representation of the loads, deflections, strains, noise, vibration etc. that would likely be experienced during the total operating life of the component. Loading sequences are developed from load histories measured and recorded during specific operations. The most useful service load data is recording of the outputs of strain gages which are strategically positioned to directly reflect the input loads experienced by the component or structure. Noise and vibration has also effect on insight in the modes and mechanics of component and structural behavior. An objective description of the vibration systems can be done in terms of frequency and amplitude information.

Stress analysis: The shape of a component or structure and boundary conditions dictates how it will respond to service loads in terms of stresses, strains and deflections. Analytical and experimental methods are available to quantify this behavior. Finite element techniques can be employed to identify areas of both

high stress, where there may be potential fatigue problems, and low stress where there may be potential for reducing weight. Experimental methods can be used in situations where components or structures actually exist. Strain gages strategically located can be used to quantify strains at such critical areas.

Material properties: A fundamental requirement for any durability assessment is knowledge of the relationship between stress and strain and fatigue life for a material under consideration. Fatigue is a highly localized phenomenon that depends very heavily on the stresses and strains experienced in critical regions of a component or structure. The relationship between uniaxial stress and strain for a given material is unique, consistent and, in most cases, largely independent of location. Therefore, a small specimen tested under simple axial conditions in the laboratory can often be used to adequately reflect the behavior of an element of the same material at a critical area in a component or a structure. However, the most critical locations are at notches even when loading is uniaxial.

Cumulative damage analysis: The fatigue life prediction process or cumulative damage analysis for a critical region in a component or structure consists of several closely interrelated steps as can be seen in Figure 2.1, separately. A combination of the load history (Service Loads), stress concentration factors (Stress Analysis) and cyclic stress-strain properties of the materials (Material Properties) can be used to simulate the local uniaxial stress-strain response in critical areas. Through this process it is possible to develop good estimates of local stress amplitudes, mean stresses and elastic and plastic strain components for each excursion in the load history. Rainflow counting can be used to identify local cyclic events in a manner consistent with the basic material behavior. The damage contribution of these events is calculated by comparison with material fatigue data generated in laboratory tests on small specimens. The damage fractions are summed linearly to give an estimate of the total damage for a particular load history.

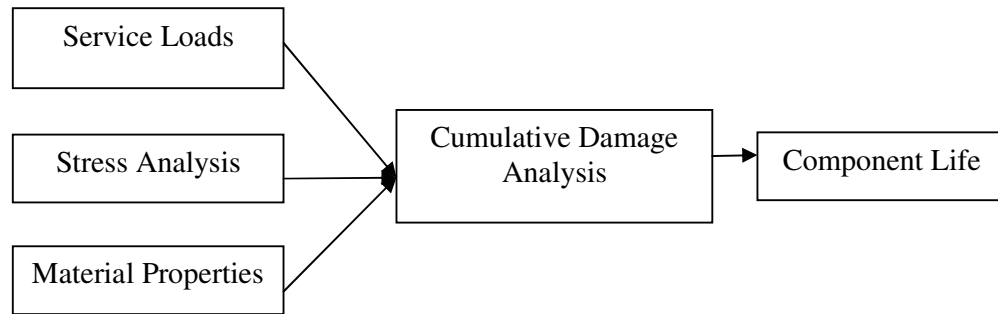


Figure 2.2. The cumulative damage analysis process

Component test: It must be carried out at some stage in a development of a product to gain confidence in its ultimate service performance. Component testing is particularly in today's highly competitive industries where the desire to reduce weight and production costs must be balanced with the necessity to avoid expensive service failures.

Fatigue life estimates are often needed in engineering design, specifically in analyzing trial designs to ensure resistance to cracking. A similar need exists in the troubleshooting of cracking problems that appear in prototypes or service models of machines, vehicles, and structures. That is the reason that the predictive techniques are employed for applications ranging from initial sizing through prototype development and product verification. The functional diagram in Figure 2.3 shows the role of life prediction in both preliminary design and in subsequent evaluation-redesign cycles, then in component laboratory tests, and finally in field proving the tests of assemblies or composite vehicles.

2.2. STRESS-LIFE BASED APPROACH (S-N METHOD)

For the fatigue design and components, several methods are available. All require similar types of information. These are the identification of candidate locations for

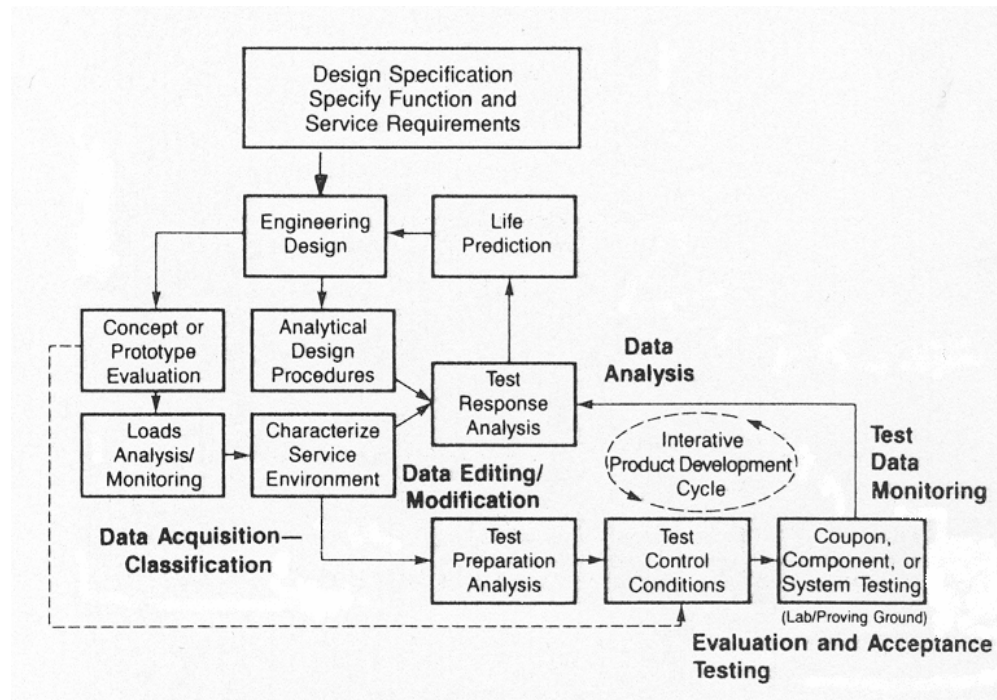


Figure 2.3. Functional diagram of engineering design and analysis [1]

fatigue failure, the load spectrum for the structure or component, the stresses or strains at the candidate locations resulting from the loads, the temperature, the corrosive environment, the material behavior, and a methodology that combines all these effects to give a life prediction. Prediction procedures are provided for estimating life using stress life (Stress vs Number of cycles curves), hot-spot stresses, strain life, and fracture mechanics. With the exception of hot-spot stress method, all these procedures have been used for the design of aluminum structures.

Since the well-known work of Wöhler in Germany starting in the 1850's, engineers have employed curves of stress versus cycles to fatigue failure, which are often called S-N curves (stress-number of cycles) or Wöhler's curve.[14]

The basis of the stress-life method is the Wöhler S-N curve, that is a plot of alternating stress, S, versus cycles to failure, N. The data which results from these tests can be plotted on a curve of stress versus number of cycles to failure. This curve shows the scatter of the data taken for this simplest of fatigue tests. A typical S-N material data can be seen in Figure 2.4. The arrows imply that the specimen had not failed in 10^7 cycles.

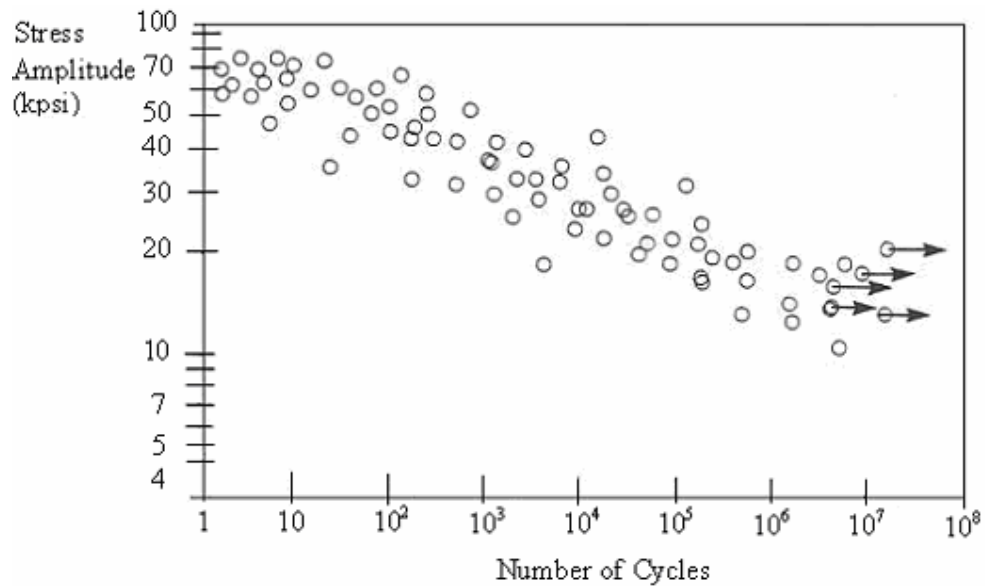


Figure 2.4. A typical S-N material data

The approach known as stress-based approach continues to serve as a widespread-used tool for the design of the aluminum structures. Comparing the stress-time history at the chosen critical point with the S-N curve allows a life estimate for the component to be made.

Stress-life approach assumes that all stresses in the component, even local ones, stay below the elastic limit at all times. It is suitable when the applied stress is nominally within the elastic range of the material and the number of cycles to

failure is large. The nominal stress approach is therefore best suited to problems that fall into the category known as high-cycle fatigue. High cycle fatigue is one of the two regimes of fatigue phenomenon that is generally considered for metals and alloys. It involves nominally linear elastic behavior and causes failure after more than about 10^4 to 10^5 cycles. This regime associated with lower loads and long lives, or high number of cycles to produce fatigue failure. As the loading amplitude is decreased, the cycles-to-failure increase.

CHAPTER 3

RAINFLOW CYCLE COUNTING

3.1. ORIGINAL DEFINITION

Counting methods have initially been developed for the study of fatigue damage generated in aeronautical structures. Since different results have been obtained from different methods, errors could be taken in the calculations for some of them. Level crossing counting, peak counting, simple range counting and rainflow counting are the methods which are using stress or deformation ranges. One of the preferred methods is the rainflow counting method. Other methods are briefly explained in Appendix G.

Rainflow cycle counting method has initially been proposed by M.Matsuiski and T.Endo to count the cycles or the half cycles of strain-time signals. [14] Counting is carried out on the basis of the stress-strain behavior of the material. This is illustrated in Figure 3.1. As the material deforms from point a to b, it follows a path described by the cyclic stress-strain curve. At point b, the load is reversed and the material elastically unloads to point c. When the load is reapplied from c to d, the material elastically deforms to point b, where the material remembers its prior history, i.e. from a to b, and deformation continues along path a to d as if event b-c never occurred.

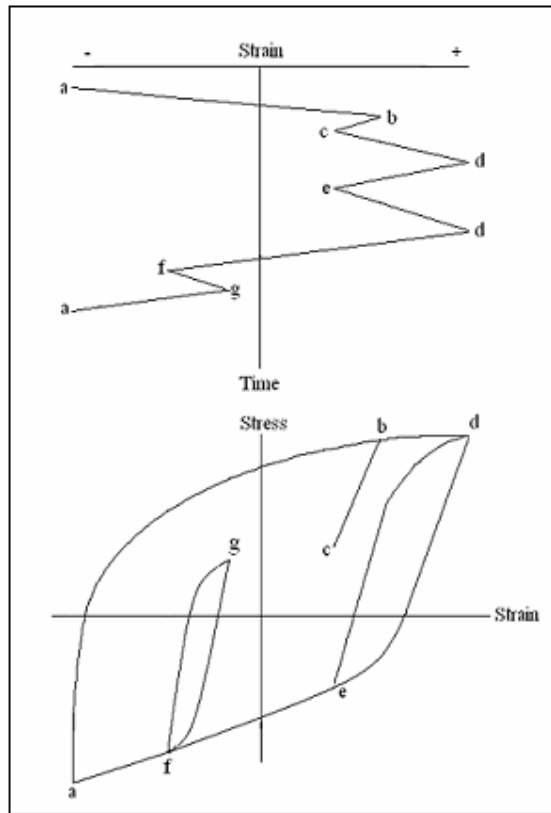


Figure 3.1. Stress-strain cycles

The signal measured, in general, a random stress $S(t)$ is not only made up of a peak alone between two passages by zero, but also several peaks appear, which makes difficult the determination of the number of cycles absorbed by the structure. An example for the random stress data is shown in Figure 3.2.

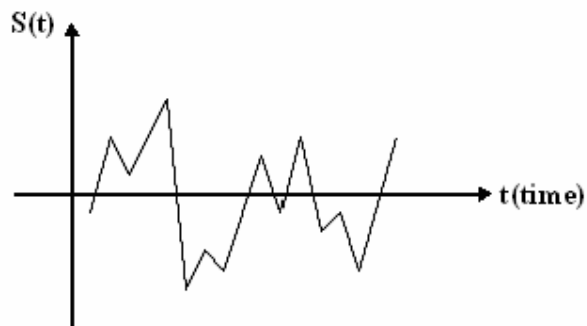


Figure 3.2. Random stress fluctuation

The counting of peaks makes it possible to constitute a histogram of the peaks of the random stress which can then be transformed into a stress spectrum giving the number of events for lower than a given stress value. The stress spectrum is thus a representation of the statistical distribution of the characteristic amplitudes of the random stress as a function of time.

The origin of the name of rainflow counting method which is called 'Pagoda Roof Method' can be explained as that the time axis is vertical and the random stress $S(t)$ represents a series of roofs on which water falls. The rules of the flow can be shown as in Figure 3.3.

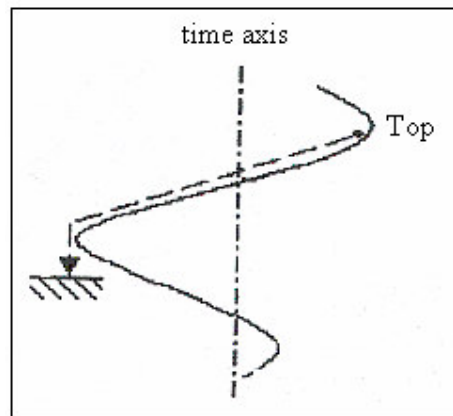


Figure 3.3. The drop released from the largest peak

The origin of the random stress is placed on the axis at the abscissa of the largest peak of the random stress. Water drops are sequentially released at each extreme. It can be agreed that the tops of the roofs are on the right of the axis, bottoms of the roofs are on the left.

If the fall starts from a peak:

- a) the drop will stop if it meets an opposing peak larger than that of departure,

- b) it will also stop if it meets the path traversed by another drop, previously determined as shown in Figure 3.4,
- c) the drop can fall on another roof and to continue to slip according to rules a and b.

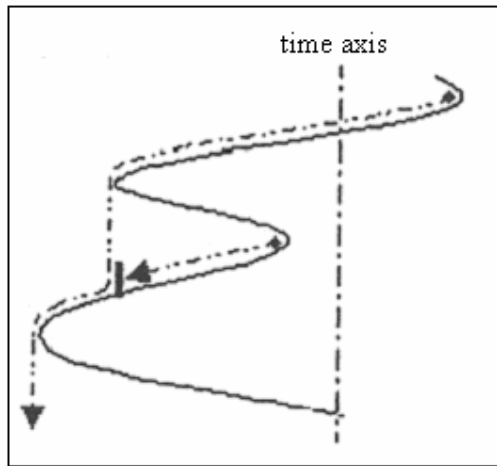


Figure 3.4. Flow rule of the drop from a peak

If the fall begins from a valley:

- d) the fall will stop if the drop meets a valley deeper than that of departure as shown in Figure 3.5,
- e) the fall will stop if it crosses the path of a drop coming from a preceding valley as given in Figure 3.6,
- f) the drop can fall on another roof and continue according to rules d and e.

The horizontal length of each rainflow defines a range which can be regarded as equivalent to a half-cycle of a constant amplitude load.

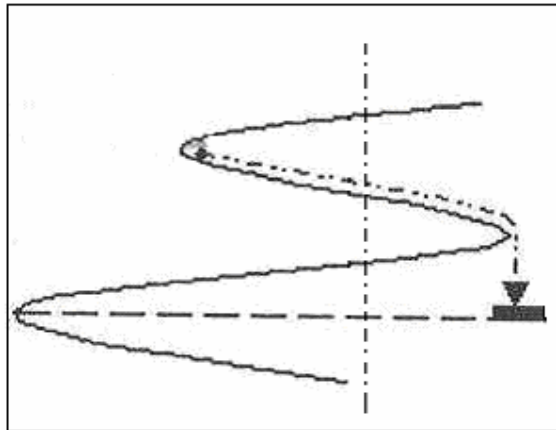


Figure 3.5. Drop departure from a valley

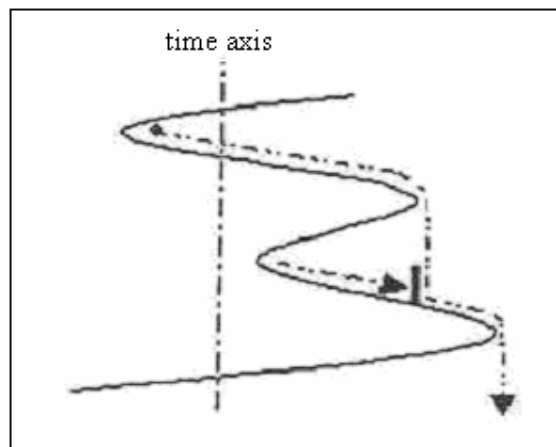


Figure 3.6. Flow rule of the drop from a valley

As the fundamentals of the original definition of the rainflow cycle counting given above, the cycles are identified in a random variable amplitude loading sequence in Figure 3.7 as an example. First, the stress $S(t)$ is transformed to a process of peaks and valleys. Then the time axis is rotated so that it points downward. At both peaks and valleys, water sources are considered. Water flows downward according to the following rules:

1. A rainflow path starting at a valley will continue down the “pagoda roofs”, until it encounters a valley that is more negative than the origin. From the figure, the path that starts at A will end at E.
2. A rainflow path is terminated when it encounters flow from a previous path. For example, the path that starts at C is terminated as shown.
3. A new path is not started until the path under consideration is stopped.
4. Valley-generated half-cycles are defined for the entire record. For each cycle, the stress range S_i is the vertical excursion of a path. The mean μ_{S_i} is the midpoint.
5. The process is repeated in reverse with peak-generated rainflow paths. For a sufficiently long record, each valley-generated half-cycle will match a peak-generated half-cycle to form a whole cycle.

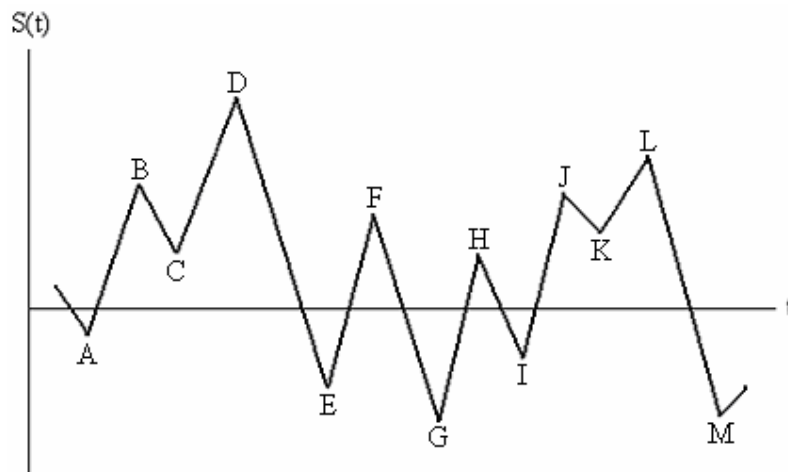


Figure 3.7. Rainflow cycle counting [13]

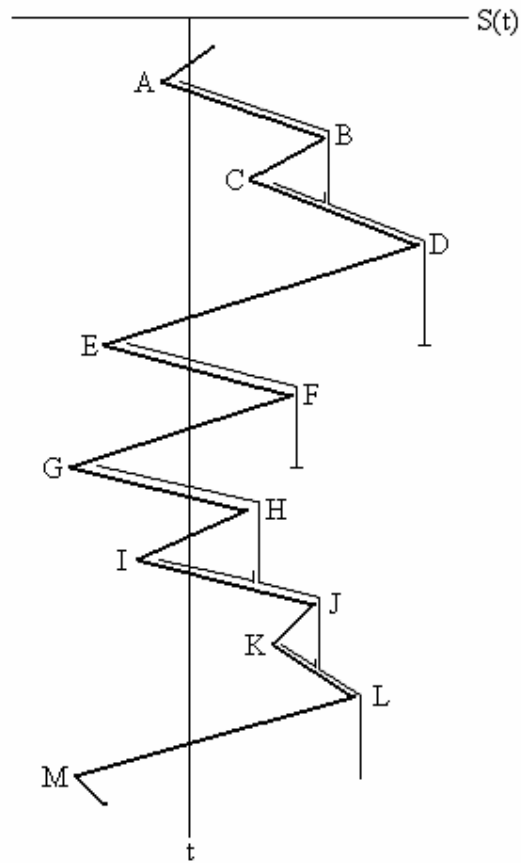


Figure 3.7. Rainflow cycle counting [13] (continued)

3.2. PRACTICAL DEFINITION

Practical definition of the rainflow cycle counting can be explained according to the ASTM E-1049 Standard Practices for Cycle Counting in Fatigue Analysis.

Rules for the rainflow counting method are given as follows:

Let X denotes range under consideration; Y, previous range adjacent to X; and S, starting point in the history.

- (1) Read next peak or valley. If out of data, go to Step 6.
- (2) If there are less than three points, go to Step 1. Form ranges X and Y using the three most recent peaks and valleys that have not been discarded.

- (3) Compare the absolute values of ranges X and Y.
 - (a) If $X < Y$, go to Step 1.
 - (b) If $X \geq Y$, go to Step 4.
- (4) If range Y contains the starting point S, go to step 5; otherwise, count range Y as one cycle; discard the peak and valley of Y; and go to Step 2.
- (5) Count range Y as one-half cycle; discard the first point (peak or valley) in range Y; move the starting point to the second point in range Y; go to Step 2.
- (6) Count each range that has not been previously counted as one-half cycle.

Figure 3.8 is used to illustrate the process. Details of the cycle counting are as follows:

- (1) $S=A$; $Y=|A-B|$; $X=|B-C|$; $X > Y$. Y contains S, that is, point A. Count $|A-B|$ as one-half cycle and discard point A; $S=B$. (Figure b)
- (2) $Y=|B-C|$; $X=|C-D|$; $X > Y$. Y contains S, that is, point B. Count $|B-C|$ as one half-cycle and discard point B; $S=C$. (Figure c)
- (3) $Y=|C-D|$; $X=|D-E|$; $X < Y$.
- (4) $Y=|D-E|$; $X=|E-F|$; $X < Y$.
- (5) $Y=|E-F|$; $X=|F-G|$; $X > Y$. Count $|E-F|$ as one cycle and discard points E and F. (Figure d. A cycle is formed by pairing range E-F and a portion of range F-G)
- (6) $Y=|C-D|$; $X=|D-G|$; $X > Y$. Y contains S, that is, point C. Count $|C-D|$ as one-half cycle and discard point C. $S=D$. (Figure e)
- (7) $Y=|D-G|$; $X=|G-H|$; $X < Y$.
- (8) $Y=|G-H|$; $X=|H-I|$; $X < Y$. End of data.
- (9) Count $|D-G|$ as one-half cycle, $|G-H|$ as one-half cycle, and $|H-I|$ as one-half cycle. (Figure f)
- (10) End of counting.

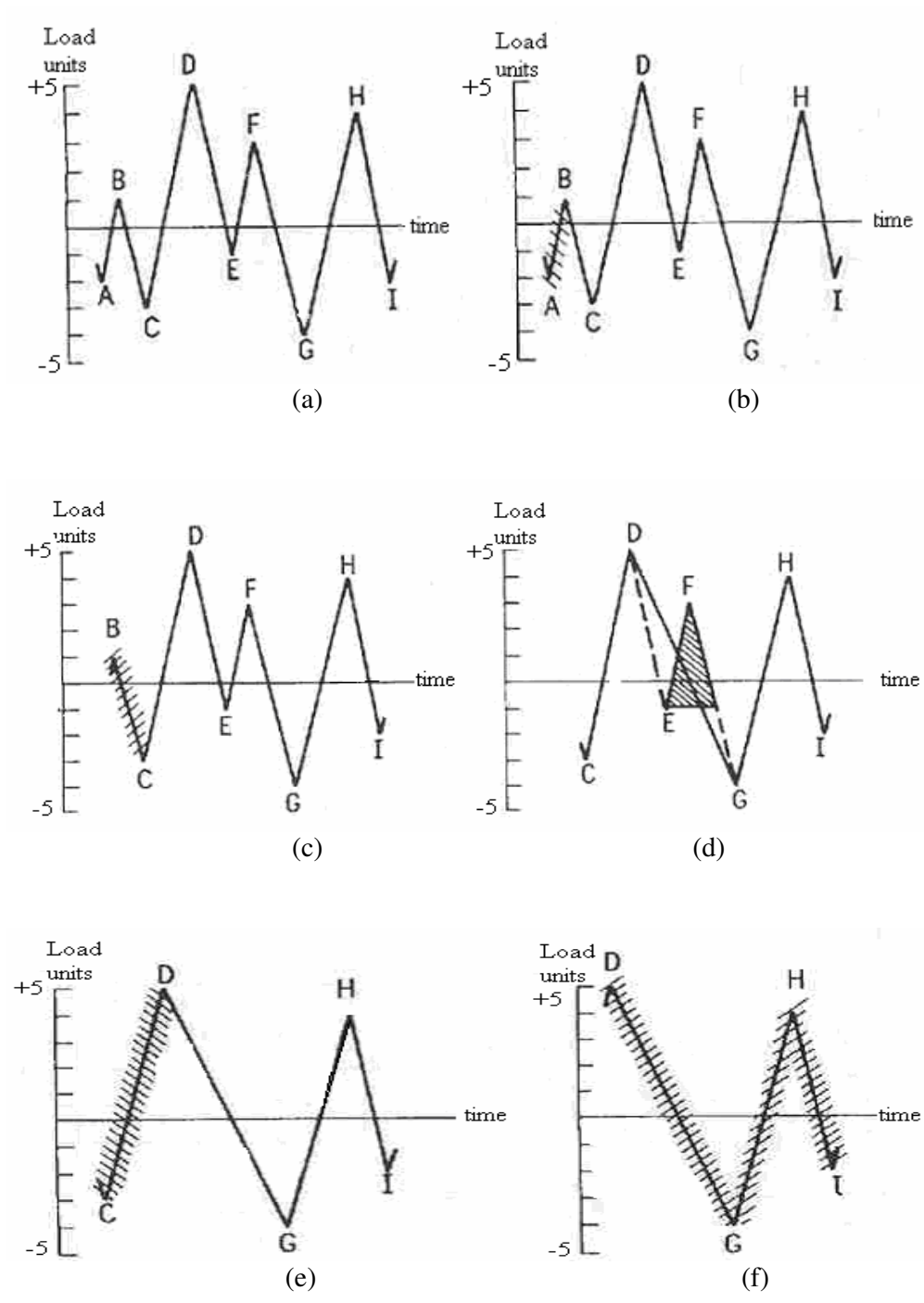


Figure 3.8. Practical definition of rainflow cycle counting

The results obtained from Figure 3.8 are tabulated in Table 3.1. It gives the number of cycle counts in the specific events.

Table 3.1. Cycle counts

Range (units)	Cycle Counts	Events
10	0	
9	0.5	D-G
8	1	C-D, G-H
7	0	
6	0.5	H-I
5	0	
4	1.5	B-C, E-F
3	0.5	A-B
2	0	
1	0	

CHAPTER 4

RAINFLOW CYCLE COUNTING IN TIME AND FREQUENCY DOMAINS

4.1. INTRODUCTION

The sample time history is actually not equivalent to the original time history. However, it is not problem: When considering the original time history was for instance 300 second segment of time signal before, or after as can be seen in Figure 4.1, the one measured is not equivalent. It does not matter, as long as the sample was long enough so that the statistics of it were the same. For instance, the mean, stress range values, and peak rate.

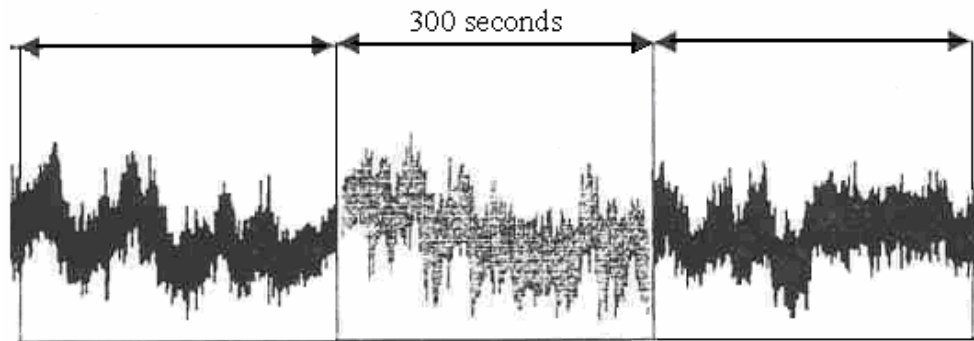


Figure 4.1. Time history [23]

If random loading input is asked to specify, then random time history should be specified as can be seen in Figure 4.1. This process can be described as random and as in the time domain. As an extension of Fourier analysis, Fourier transforms allow any process to be represented using a spectral formulation such as a power spectral density (PSD) function. This process is described as a function of

frequency and is therefore said to be in the frequency domain as can be seen in Figure 4.2. It is still a random specification of the function.

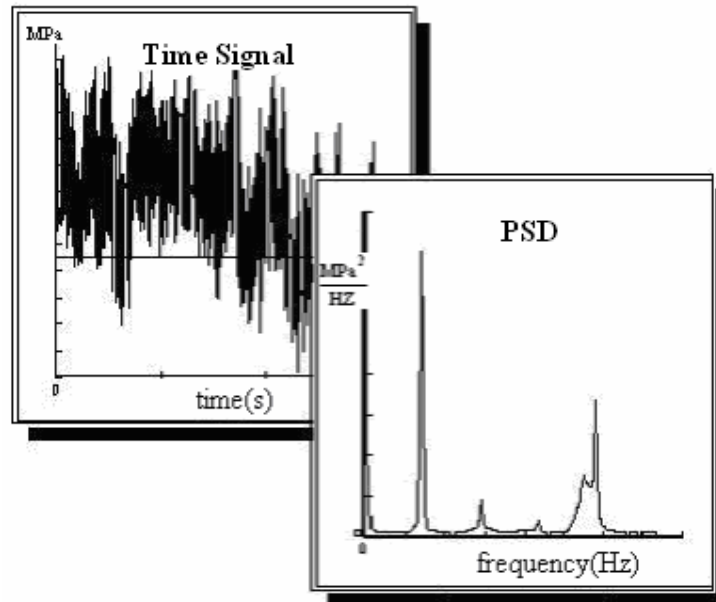


Figure 4.2. Random processes [9]

4.2. RAINFLOW CYCLE COUNTING IN TIME DOMAIN

For any fatigue analysis, the starting point is the response of the structure or component, which is usually expressed as a stress or strain time history. If the response time history is made up of constant amplitude stress or strain cycles then the fatigue design can be accomplished by referring to a typical S-N diagram. However, because real signals rarely confirm to this ideal constant amplitude situation, an empirical approach is used for calculating the damage caused by stress signals of variable amplitude. Despite its limitations, Palmgren-Miner rule is used for this purpose. This linear relationship assumes that the damage caused by parts of a stress signal with a particular range can be calculated and accumulated to the total damage separately from that caused by other ranges.

When the response time history is irregular with time as shown in Figure 4.3, rainflow cycle counting is used to decompose the irregular time history into equivalent stress of block loading. The number of cycles in each block is usually recorded in a stress range histogram. This can be used in Palmgren-Miner calculation to obtain the fatigue life.

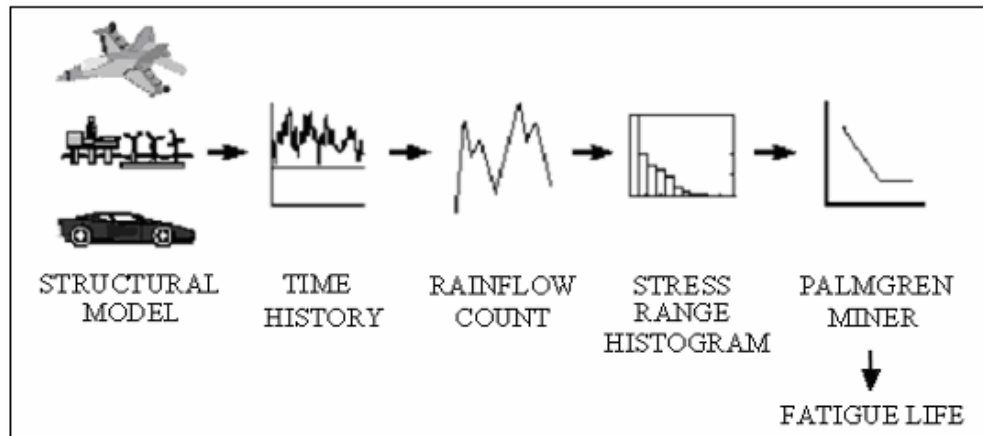


Figure 4.3. General procedure for time domain fatigue life calculation [23]

4.3. RAINFLOW CYCLE COUNTING IN FREQUENCY DOMAIN

In frequency domain, firstly, time signal data is transferred into power spectral density values. Power spectral density versus frequency data is used to find the first four moments of the power spectral density function and these four moments are used in finding the probability density function. Then, fatigue life is obtained as the steps of the process are also given in Figure 4.4.

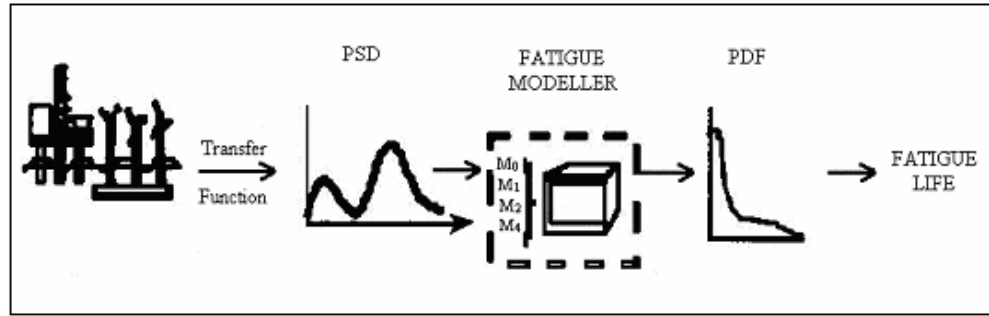


Figure 4.4. General procedure for frequency domain fatigue life calculation [23]

4.3.1. Probability Density Function (PDF)

When the stress range histogram is converted into a stress range probability density function, there is an equation to describe the expected fatigue damage caused by the loading history. [23]

$$E[D] = E[P] \cdot \frac{T}{k} \cdot \int_0^{\infty} S^b \cdot p(S) \cdot dS \quad (4.1)$$

In order to compute fatigue damage over the life time of the structure in seconds (T), the form of the material (S-N) data must also be defined using the parameters k and b as:

$$N \cdot S^b = k \quad (4.2)$$

where b and k are the material properties. There is a linear relationship exists between cycles to failure N and applied stress range S under constant amplitude cyclic loading when plotted on logarithmic paper. In addition, the total number of cycles in time T must be determined from the number of peaks per second E[P]. If the damage D caused in time T is greater than 1, then the structure is assumed to have failed. Or alternatively, the fatigue life can be obtained by setting E[D] = 1.0 and then finding the fatigue life T in seconds from the fatigue damage equation given above.

The stress range histogram information can be stored in the form of a probability density function (pdf) of stress ranges. A typical representation of this function is shown in Figure 4.5.

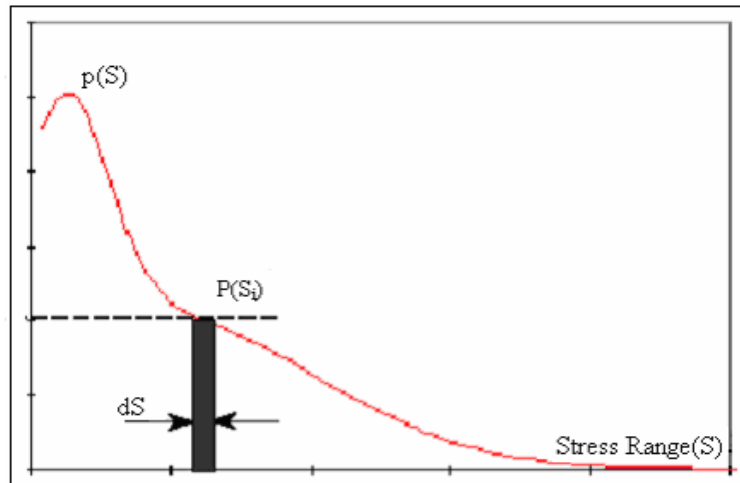


Figure 4.5. Probability density function

To get probability density function from rainflow histogram, each bin in the rainflow count has to be divided by

$$N_t \cdot dS \quad (4.3)$$

where N_t is the total number of cycles in histogram and dS is the bin width.

The probability of the stress range occurring between

$$S_i - \frac{dS}{2} \text{ and } S_i + \frac{dS}{2} \text{ is given by } p(S_i) \cdot dS.$$

4.3.2. Expected Zeros, Peaks and Irregularity Factor

The number of zero crossings and the number peaks in the signal are the most important statistical parameters. Figure 4.6 shows a one second piece cut out from the time signal.

$E[0]$ is the number of upward zero crossings, i.e. zero crossings with positive slope and $E[P]$ is the number of peaks in the same sample. The irregularity factor is defined as the number of upward zero crossings divided by the number of peaks. These points can be seen in Figure 4.5.

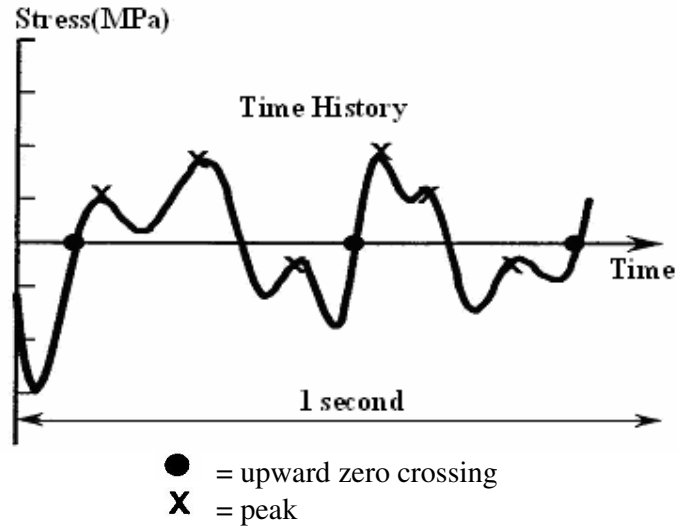


Figure 4.6. Zero and peak crossing rates

Number of upward zero crossings,

$$E[0] = 3 \quad (4.4)$$

Number of peaks,

$$E[P] = 6 \quad (4.5)$$

irregularity factor,

$$\gamma = \frac{E[0]}{E[P]} = \frac{3}{6} \quad (4.6)$$

Irregularity factor is found in the range of 0 to 1. This process is known as narrow band as shown in the Figure 4.7(a). Narrow band process is built up of sine waves covering only a narrow range of frequencies. As the divergence from narrow band increases then the value for the irregularity factor tends towards 0 and the process

is illustrated as broad band as given in Figure 4.7(b). Broad band process is made up of sine waves over a broad range of frequencies. In sine wave, shown in Figure 4.7(c), a sinusoidal time history appears as a single spike on the PSD plot. Figure 4.7(d), a white noise is shown which is a special time history. It is built up of sine waves over the whole frequency range.

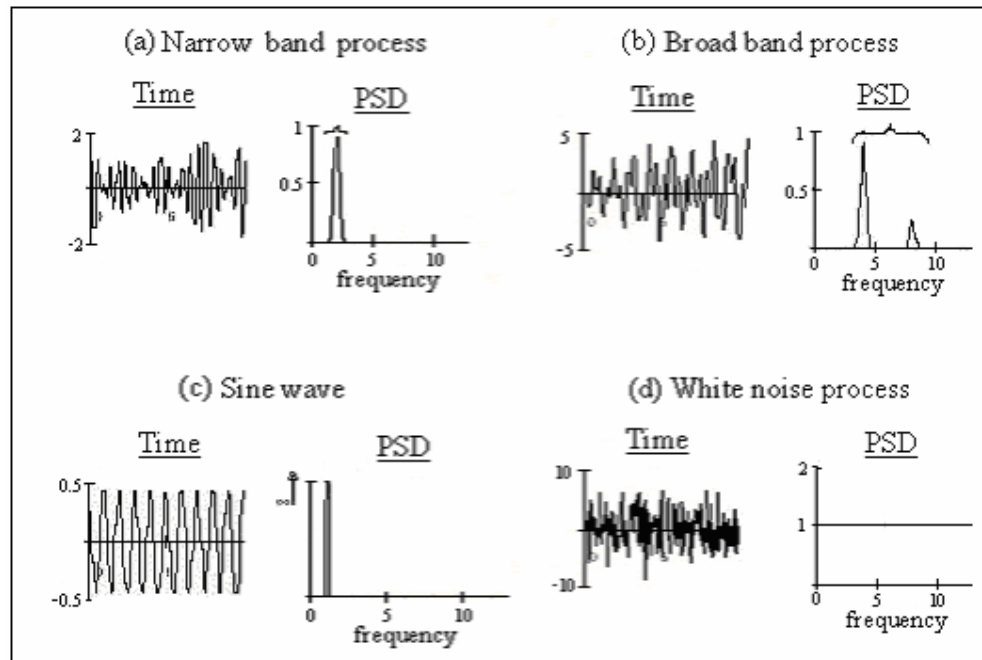


Figure 4.7. Equivalent time histories and power spectral densities

4.3.3. Moments from the Power Spectral Density

The probability density function of rainflow ranges can be extracted directly from the power spectral density (PSD) function of stress.

From the characteristics of the power spectral density, n^{th} moments of the power spectral density function are obtained. After the calculations of the moments, fatigue damage can be calculated. The relevant spectral moments are easily

computed from a one sided power spectral density, $G(f)$, using the following expression:

$$m_n = \int_0^{\infty} f^n \cdot G(f) \cdot df = \sum f_k^n \cdot G_k(f) \cdot \delta f \quad (4.7)$$

The curve is divided into small strips as shown in Figure 4.8. The n^{th} moment of area of the strip is given by the area of the strip multiplied by the frequency raised to the power n . The n^{th} moment of area of the PSD (m_n) can be calculated by summing the moments of all the strips.

In theory, all the possible moments should be calculated, however, in practice, m_0 , m_1 , m_2 , m_4 are sufficient to calculate all of the information for the fatigue analysis.

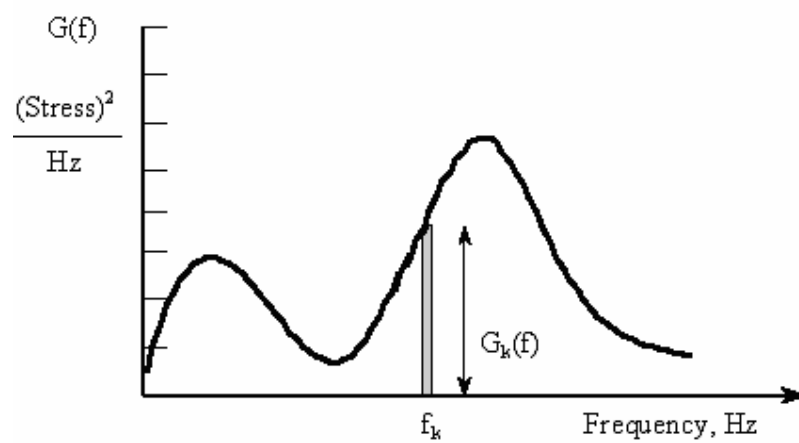


Figure 4.8. One-sided power spectral density function

4.3.4. Expected Zeros, Peaks and Irregularity Factor from a Power Spectral Density

The number of upward zero crossings per second $E[0]$ and peaks per second $E[P]$ in a random signal expressed solely in terms of their spectral moments m_n .

The number of upward zero crossings per second is [36]:

$$E[0] = \sqrt{\frac{m_2}{m_0}} \quad (4.8)$$

The number of peaks per second is:

$$E[P] = \sqrt{\frac{m_4}{m_2}} \quad (4.9)$$

Therefore, irregularity factor is found as:

$$\gamma = \frac{E[0]}{E[P]} = \sqrt{\frac{m_2^2}{m_0 \cdot m_4}} \quad (4.10)$$

Then, total number of peaks and zeros are found by multiplying E[0] and E[P] with the total record length.

$$\text{Cycles at level } i : n_i = p[S_i] \cdot dS \cdot N_i \quad (4.11)$$

$$\text{Total cycles} : N_i = E[P] \cdot T \quad (4.12)$$

where T refers to the total time.

4.3.5. Estimation of Probability Density Function from Power Spectral Density Moments (Dirlik's Solution)

Many expressions have been produced by generating sample time histories from power spectral densities (PSD) using Inverse Fourier Transform techniques. From these a conventional rainflow cycle count was then obtained.

This approach was used by Wirsching et al, Chaudhury and Dover, Tuna and Hancock [23]. It is important to note that the solutions are expressed in terms of spectral moments up to m_4 .

Dirlik [23] has produced an empirical solution for the probability density function of rainfall ranges. Dirlik's equation is given below.

$$p(S) = \frac{\frac{D_1}{Q} \cdot e^{-\frac{Z}{Q}} + \frac{D_2}{R^2} \cdot e^{-\frac{Z^2}{2}} + D_3 \cdot Z \cdot e^{-\frac{Z^2}{2}}}{2 \cdot m_0^{1/2}} \quad (4.13)$$

where,

$$Z = \frac{S}{2 \cdot m_0^{1/2}} \quad (4.14)$$

$$D_1 = \frac{2 \cdot (X_m - \gamma^2)}{1 + \gamma^2} \quad (4.15)$$

$$D_2 = \frac{1 - \gamma - D_1 + D_1^2}{1 - R} \quad (4.16)$$

$$D_3 = 1 - D_1 - D_2 \quad (4.17)$$

$$R = \frac{\gamma - X_m - D_1^2}{1 - \gamma - D_1 + D_1^2} \quad (4.18)$$

$$Q = \frac{5 \cdot (\gamma - D_1 - D_2 \cdot R)}{4 \cdot D_1} \quad (4.19)$$

where

$$\gamma = \frac{m_2}{\sqrt{m_0 \cdot m_4}} \quad (4.20)$$

$$X_m = \frac{m_1}{m_0} \cdot \sqrt{\frac{m_2}{m_4}} \quad (4.21)$$

As can be seen from the equations above X_m , D_1 , D_2 , D_3 , Q and R are all functions of m_0 , m_1 , m_2 and m_4 .

CHAPTER 5

PALMGREN-MINER RULE

Almost all available fatigue data for design purposes is based on constant amplitude tests. However, in practice, the alternating stress amplitude may be expected to vary or change in some way during the service life when the fatigue failure is considered. The variations and changes in load amplitude, often referred to as spectrum loading, make the direct use of S-N curves inapplicable because these curves are developed and presented for constant stress amplitude operation. The key issue is how to use the mountains of available constant amplitude data to predict fatigue in a component. In this case, to have an available theory or hypothesis becomes important which is verified by experimental observations. It also permits design estimates to be made for operation under conditions of variable load amplitude using the standard constant amplitude S-N curves that are more readily available.

Many different cumulative damage theories have been proposed for the purposes of assessing fatigue damage caused by operation at any given stress level and the addition of damage increments to properly predict failure under conditions of spectrum loading. Collins, in 1981, provides a comprehensive review of the models that have been proposed to predict fatigue life in components subject to variable amplitude stress using constant amplitude data to define fatigue strength. The original model, a linear damage rule, originally suggested by Palmgren (1924) and later developed by Miner (1945) [13]. This linear theory, which is still widely used, is referred to as the Palmgren-Miner rule or the linear damage rule.

Life estimates may be made by employing Palmgren-Miner rule along with a cycle counting procedure. Target is to estimate how many of the blocks can be applied before failure occurs. This theory may be described using the S-N plot.

In this rule, the assumptions can be summarized as follows:

- i) The stress process can be described by stress cycles and that a spectrum of amplitudes of stress cycles can be defined. Such a spectrum will lose any information on the applied sequence of stress cycles that may be important in some cases.
- ii) A constant amplitude S-N curve is available, and this curve is compatible with the definition of stress; that is, at this point there is no explicit consideration of the possibility of mean stress.

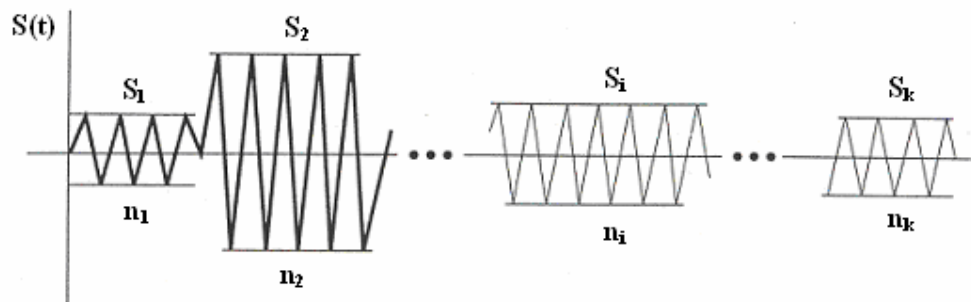


Figure 5.1. Spectrum of amplitudes of stress cycles [13]

In Figure 5.1, a spectrum of amplitudes of stress cycles is described as a sequence of constant amplitude blocks, each block having stress amplitude S_i and the total number of applied cycles n_i . The constant amplitude S-N curve is also shown in Figure 5.2.

By using the S-N data, number of cycles of S_1 is found as N_1 which would cause failure if no other stresses were present. Operation at stress amplitude S_1 for a number of cycles n_1 smaller than N_1 produces a smaller fraction of damage which can be termed as D_1 and called as the damage fraction.

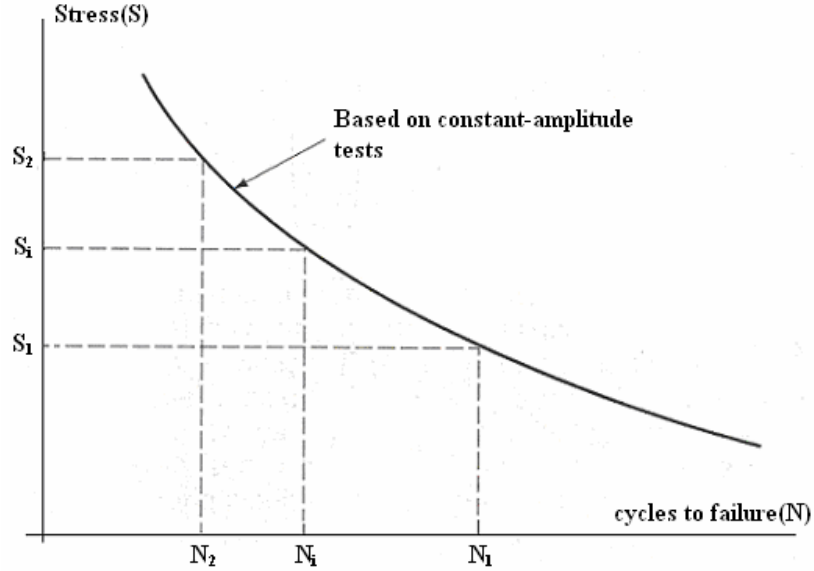


Figure 5.2. Constant amplitude S-N curve [22]

Operation over a spectrum of different stress levels results in a damage fraction D_i for each of the different stress levels S_i in the spectrum. It is clear that, failure occurs if the fraction exceeds unity:

$$D_1 + D_2 + \dots + D_{i-1} + D_i \geq 1.0 \quad (5.1)$$

According to the Palmgren-Miner rule, the damage fraction at any stress level S_i is linearly proportional to the ratio of number of cycles of operation to the total number of cycles that produces failure at that stress level, that is

$$D_i = \frac{n_i}{N_i} \quad (5.2)$$

Then, a total damage can be defined as the sum of all the fractional damages over a total of k blocks,

$$D = \sum_{i=1}^k \frac{n_i}{N_i} \quad (5.3)$$

and the event of failure can be defined as

$$D \geq 1.0 \quad (5.4)$$

The limitations of the Palmgren-Miner rule can be summarized as the following:

i) Linear: It assumes that all cycles of a given magnitude do the same amount of damage, whether they occur early or late in the life.

ii) Non-interactive (sequence effects): It assumes that the presence of S_2 etc. does not affect the damage caused by S_1 .

iii) Stress independent: It assumes that the rule governing the damage caused by S_1 is the same as that governing the damage caused by S_2 .

The assumptions are known to be faulty, however, Palmgren-Miner rule is still used widely in the applications of the fatigue life estimates.

CHAPTER 6

DESIGN OF THE EXPERIMENTS

6.1. VIBRATION TEST SYSTEM

Tests were carried on the mechanical vibration test system which is V864-640 SPA 20K, produced by Ling Dynamic Systems (LDS). The model of the system has armature in 640mm diameter and the power amplifier has 4 modules each being rated at 5kVA power. The system is shown in Figure 6.1.



Figure 6.1. Vibration test system

The essential components of a vibration test system as can be seen in Figure 6.2 are:

- Vibrator (shaker)
- Amplifier
- Controller
- Vibration transducer (typically accelerometer)

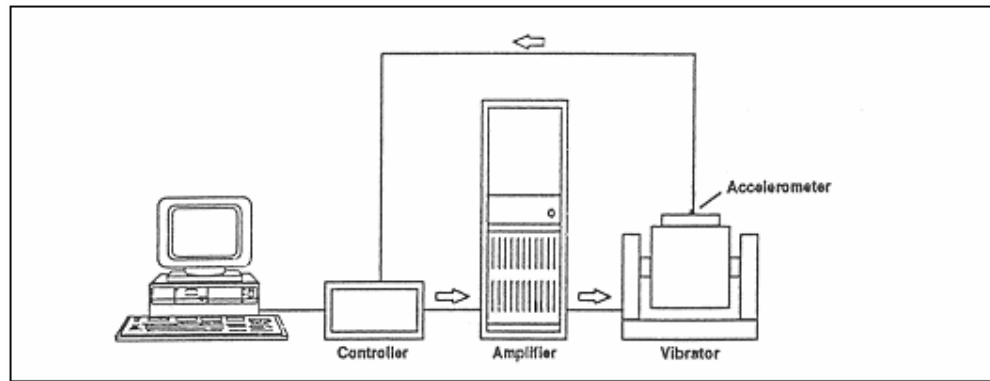


Figure 6.2. Components of the vibration test system

In principle the vibrator, which is an electrodynamic instrument, operates like a loudspeaker, where the movement of the armature is produced by an electrical current in the coil which produces a magnetic field opposing a static magnetic field. The static magnetic field is produced by an electromagnet in the vibrator. The electromagnet is a coil of wire which is commonly referred to as the field coil. The force that the armature can produce is proportional to the current flowing in the coil. To calculate the force produced, the following formula can be applied:

$$F = B \cdot I \cdot L \quad (6.1)$$

where F is the force (Newton,N), B is the magnetic flux density (Tesla,T), I is the current (Amper,A) and L is the thickness of the magnet (meter,m).

The direction of the force is well illustrated by Flemming's left hand rule.

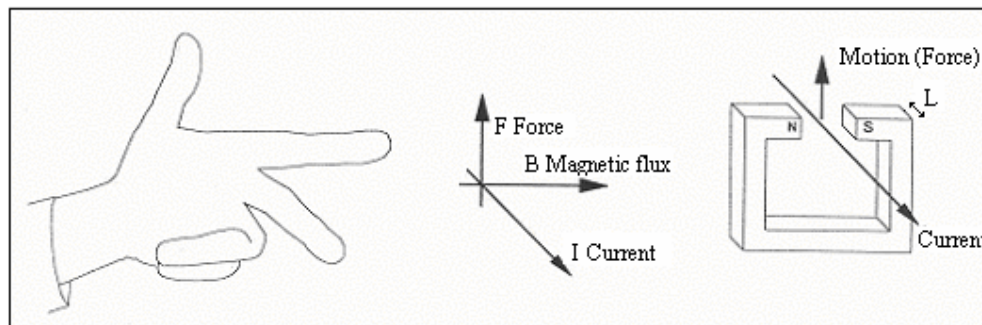


Figure 6.3. Left hand rule

The purpose of the amplifier is to provide electrical power to the vibrator's armature. The power is in the form of voltage and current. Its function is also to provide the necessary field power supply, cooling fan supply and auxiliary supplies, to monitor the system interlock signals and initiate amplifier shutdown when any system abnormality sensed. Vibration controller is used to ensure that what is seen by the control accelerometer is what has been programmed into the controller. The controller will monitor the result on the table from the output from the control accelerometer and then correct its output to match the defined test. The system behaves as a closed loop system.

In the experiment, the random vibration profile in the form of band limited noise shown in Figure 6.4 is applied to the specimen. The Minimum Integrity Test according to MIL-STD-810F is used for general purposes where the place of the specimen is not known. It is intended to provide reasonable assurance that material can withstand anywhere such as in transportation and handling including field installation, removal or repair.

The random vibration test is performed in frequencies between 5Hz and 500Hz. with $0.04\text{g}^2/\text{Hz}$ power spectral density value. The root mean square (rms) value of the acceleration (g) is obtained as 4.45 for the specified range.

6.2. TEST MATERIAL

The reality of shortened lead times, performance improvements in products and materials as well as business complexity and globalization, and regulatory compliance are factors driving the materials decisions daily. In the experimental design, the aluminum material is chosen because it is widespreadly used in the areas such as aircraft, road transport, rail transport, sea, and also in the building. Aluminum is ideal material for any transport application. Since aluminum is very strong, rugged vehicles, like the Land Rover and the Hammer military vehicle, all

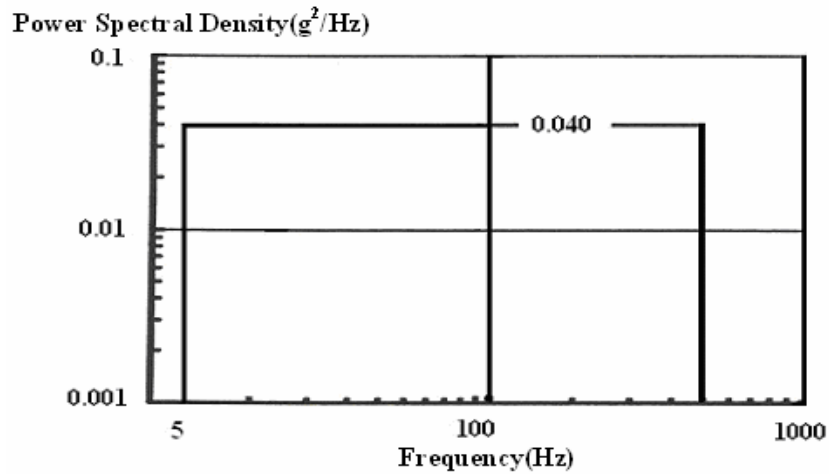


Figure 6.4. Minimum Integrity Test applied to the specimen between 5-500Hz[26]

use aluminum extensively. Aluminum is also used for railroad cars, truck and automobile engine blocks and cylinder heads, heat exchangers, transmission housings, engine parts and automobile wheels. The structures in the sea, such as craft, are weight-critical, and aluminum is the preferred material. Aluminum plate girders, which are frequently used in ships and modules in aluminum, may experience a dramatic reduction in strength due to the vulnerability of aluminum material to heating. In addition, aluminum's strength, weight and versatility make it an ideal building and cladding material since these properties encourage its use in earthquake prone zones and its resistance to corrosion means it is virtually maintenance-free. Highly resistant and rigid, they have low rates of expansion and contraction and also of condensation. They are extremely stable, durable and thermally efficient.

In conclusion, because of its properties, aluminum material is preferred in every area. Since the products are mostly seen as aluminum-made, the aluminum test specimen is chosen to analyze in the experiment. The main properties of the aluminum can be summarized as follows:

High strength-to-weight ratio: At 2700 kg/m^3 , aluminum is only one third the density of iron. Aluminum is typically used as construction material in weight-critical structures. High-strength aluminum alloys attain the tensile strength of regular construction steel.

Durability: Its natural airtight oxide skin protects aluminum against corrosion.

Electrically conductivity: An equivalent conductive cross section of aluminum is equal to 1.6 times that of copper, however brings with it a significant weight advantage or approximately 50%.

Heat conductivity: With a value of 2.03 W/cmK , aluminum exhibits excellent heat conductivity. This is why it is ideal for solar panels, cooling elements, brake discs, etc.

Ductility: Aluminum can be shaped and moulded in all the usual cutting and non-cutting ways.

Recyclability: Aluminum is almost predestined for reuse. With an energy requirement equivalent to 5% of the raw material gain, aluminum is efficiently brought back into circulation with minimal emissions.

In addition, this lightweight metal is non-toxic and completely harmless in all applicaitons.

6.3. STRAIN GAGES

In the experimental analysis, a strain gage is used to measure the strains on the surface of the aluminum plate where is the most critical point. Because the resistance change in a strain gage is very small, it can not be measured accurately with an ordinary ohmmeter. The Wheatstone Bridge is used which of its one arm is strain gage. The basic principles of the stress, strain, strain gage, measuring circuit and shunt calibration are described in this part.

The maximum benefit from strain gage measurements can only be obtained when a correctly assembled measuring system is allied with a through knowledge of the

factors governing the strength and elasticity of materials. This knowledge allows the strain gages to be in the most effective manner, so that reliable measurements can be obtained.

During the design and construction of machines and structures, the strength of the material to be used plays a very important part in the calculations. The strength of the material is used to find whether the parts can carry the loads demanded of them without excessive deformation or failure. These load carrying abilities are normally characterized in terms of stress. Stress can be calculated by dividing the force applied by the unit area for a uniform distribution of internal resisting forces:

$$\sigma = \frac{F}{A} \quad (6.2)$$

where σ is stress, F is the force and A is the unit area.

In the same way that loads are characterized in terms of stress, extension is characterized in terms of strain. Strain is defined as the amount of deformation per unit length of an object when a load is applied. Strain is measured as the ratio of dimensional change to the total value of the dimension in which the change occurs:

$$\varepsilon = \frac{\Delta L}{L} \quad (6.3)$$

where ε is the strain and L is the original length.

Poisson's ratio is the ratio of transverse to longitudinal unit strain. The modulus of elasticity is the ratio of stress to the corresponding strain (below the proportional limits). It is defined by Hooke's Law as

$$E = \frac{\sigma}{\varepsilon} \quad (6.4)$$

where E is the modulus of elasticity which is constant.

The tensile and compressive modulus of elasticity are defined separately as

$$E_T = \frac{\sigma_T}{\epsilon} \quad (6.5)$$

and

$$E_C = \frac{\sigma_C}{\epsilon} \quad (6.6)$$

Then the tensile modulus of elasticity becomes,

$$E_T = \frac{\frac{F_T}{A}}{\frac{\Delta L}{L}} \quad (6.7)$$

where F_T is the tension force, ΔL is the elongation along the direction of application force.

And, the compressive modulus of elasticity becomes,

$$E_C = \frac{\frac{F_C}{A}}{\frac{\Delta L}{L}} \quad (6.8)$$

where F_C is the compression force, ΔL is the contraction along the direction of application force.

Strain gages are one of the most universal measuring devices for the electrical measurement of mechanical quantities. As their name indicates, they are used for the measurement of strain. As a technical term 'strain' consists of tensile and compressive strain, distinguished by a positive or negative sign. Thus, strain gages can be used to pick up expansion as well as contraction. The strain of a body is always caused by an external influence or an internal effect.

6.3.1. STRAIN GAGE CHARACTERISTICS

The characteristics of the strain gage are gage dimensions, gage resistance, gage sensitivity (gage factor), the range, gage pattern, gage series, temperature and self-temperature compensation.

Gage Dimensions: The uniaxial strain gage dimensions are shown in Figure 6.5. The length of the straight portion of the grid determines the gage length of the strain gage and the width is determined by the width of the grid as can be seen in the figure. Dimensions listed for gage length, as measured inside the grid endloops and grid width refer to active or strain-sensitive grid dimensions. The endloops and solder taps are considered insensitive to strain because of their relatively large cross-sectional area and low electrical resistance. The figure also shows the overall length, overall width, matrix length, matrix width and the gridline direction.

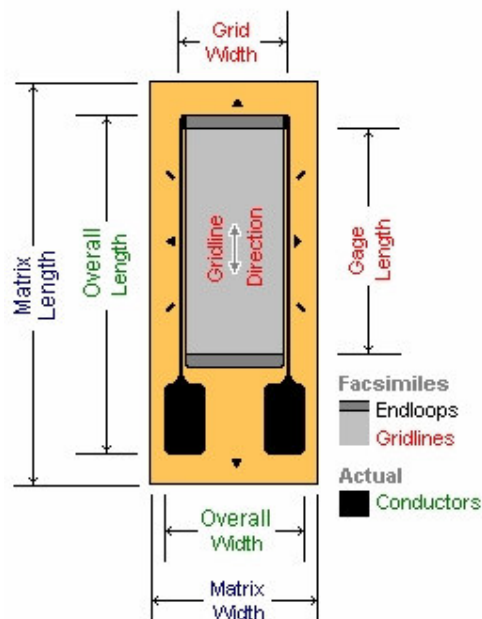


Figure 6.5. Detail description of the uniaxial strain gage [16]

A larger gage has greater grid area which is better for heat dissipation, improved strain averaging on inhomogeneous materials such as fiber reinforced composites and easier handling and installation. However, a shorter gage has advantages when measuring localized peak strains in the vicinity of a stress concentration, for example, a hole or shoulder and when very limited space available for gage mounting.

Gage Resistance: The resistance of a strain gage is defined as the electrical resistance measured between the two metal ribbons or contact areas intended for the connection of measurement cables. The range comprises strain gages with a nominal resistance of 120, 350, 600, and 700 ohms.

Strain gages with resistances of 120 and 350 ohms are commonly used in experimental stress analysis testing. For the majority of applications, 120-ohm gages are usually suitable; however, there are often advantages from selecting the 350-ohm resistance if this resistance is compatible with the instrumentation to be used. This may be because of cost considerations and particularly in the case of very small gages. In addition, 350-ohm gages are preferred to reduce heat generation, to reduce leadwire effects, or to improve signal-to noise ratios in the gage circuit. For the high resistance small gages, fatigue life reduction can also be expected.

Gage Sensitivity (Gage Factor): The strain sensitivity k of a strain gage is the proportionality factor between the relative changes of the resistance. It is a figure without dimension and is generally called gage factor which is referred as the measure of sensitivity, or output, produced by a resistance strain gage.

The strain sensitivity of a single uniform length of a conductor is given by:

$$k = \frac{\frac{dR}{R}}{\epsilon} \quad (6.9)$$

where ε is a uniform strain along the conductor and in the direction of the conductor. Whenever a conductor, for instance a wire, is wound into a strain gage grid, however, certain effects take place, which alter the resistance of the strain gage to a certain degree. This value of sensitivity is assigned to the gage.

The Range: Range represents the maximum strain which can be recorded without resetting or replacing the strain gage. The range and sensitivity are interrelated since very sensitive gages respond to small strain with appreciable response and the range is usually limited to the full-scale deflection or count of the indicator.

Gage Pattern: Gage pattern commonly refers to the number of the grid whether it is uniaxial or multiaxial. Uniaxial strain gage is selected if only one direction of strain needs to be investigated. They are available with different aspect ratios, i.e. length-to-width, and various solder tab arrangements for adaptability to different installation requirements. A biaxial strain rosette (0° - 90° tee rosette) is selected if the principal stresses need to be investigated and the principal axes are known. A tri-element strain rosette (0° - 45° - 90° rectangular rosette or 0° - 60° - 120° delta rosette) is selected if the principal stresses need to be investigated; however, the principal axes are unknown.

Gage Series: Gage series should be selected after the selection of gage size and the gage pattern. The standard gage series table is given in Appendix B, Table B.3.

Temperature: Temperature can alter not only the properties of a strain gage element, but also can alter the properties of the base material to which the strain gage is attached. Differences in expansion coefficients between the gage and base materials may cause dimensional changes in the sensor element. Expansion or contraction of the strain gage element and/or the base material introduces errors that are difficult to correct.

Self-Temperature Compensation (S-T-C): It is the approximate thermal expansion coefficient in ppm/°F of the structural material on which the gage is to be used. All gages with XX as the second code group in the gage designation are self-temperature-compensated for use on structural materials. The S-T-C numbers which are available can be given as; A alloy: 00,03,05,06,09,13,15,18; P alloy: 08; K alloy: 00,03,05,06,09,13,15. The D alloy is not available, DY is used instead of D in self-temperature-compensated form.

6.3.2. THE MEASURING CIRCUIT

The extremely small changes of the order of thousandths of an ohm, that occur in the gage resistance due to variations in the applied strain can be measured by Wheatstone Bridge. The Wheatstone Bridge was actually first described by Samuel Hunter Christie (1784-1865) in 1833. However, Sir Charles Wheatstone invented many uses for this circuit once he found the complete description in 1843 [24]. Today, the Wheatstone Bridge remains the most sensitive and accurate method for precisely measuring resistance values. Since the Wheatstone Bridge is well suited for the measurement of small changes of a resistance, it is also suitable to measure the resistance change in a strain gage. The Wheatstone Bridge is two voltage dividers, both fed by the same input. The circuit output is taken from both voltage divider outputs. It is simply shown in Figure 6.6. R_1 , R_2 , R_3 , and R_4 are the resistances in terms of ohm (Ω), E_A is voltage difference on R_3 , E_B is voltage difference on R_4 , E is voltage difference between C and D, e_o is voltage difference between A and B. Voltage differences are given in terms of volt (V).

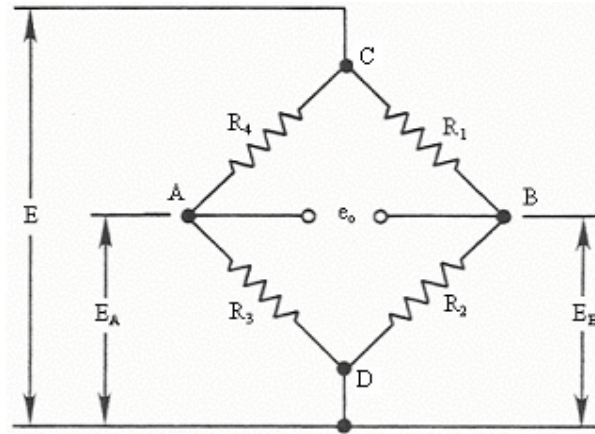


Figure 6.6. Basic Wheatstone Bridge circuit

6.3.2.1. Quarter Bridge Circuit

Quarter bridge circuit is one of the cases of Wheatstone Bridge. This arrangement is employed for many dynamic and static strain measurements where temperature compensation in the circuit is not critical.

The external circuit with active gage is illustrated with instrument in Figure 6.7. Quarter bridge circuit with active gage is shown in Figure 6.8 in which an active gage, in a three-wire circuit, is remote from the instrument and connected to gage resistance R_G by leadwires of resistance R_L . If all leadwire resistances are nominally equal, then R_1 and R_2 shown in Figure 6.6 are calculated as

$$R_1 = R_L + R_G \quad (6.10)$$

and

$$R_2 = R_L + R_G \quad (6.11)$$

This means that the same amount of leadwire resistance in series with both the active gage and the dummy. There is also leadwire resistance in the bridge output connection to the S- instrument terminal. Since the input impedance of the instrument applied across the output terminals of the bridge circuit is taken to be

infinite, the latter resistance has no effect. Thus, no current flows through the instrument leads.

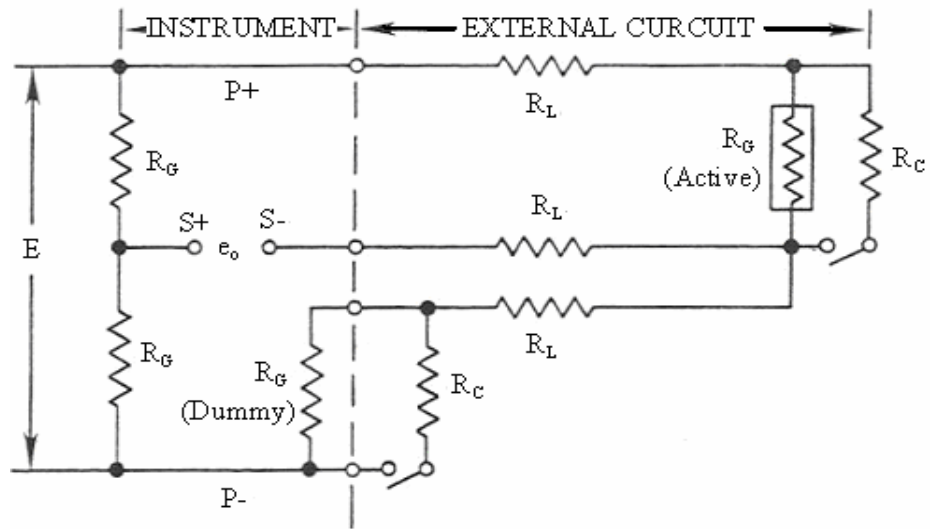


Figure 6.7. The external circuit with active gage illustrated with instrument [16]

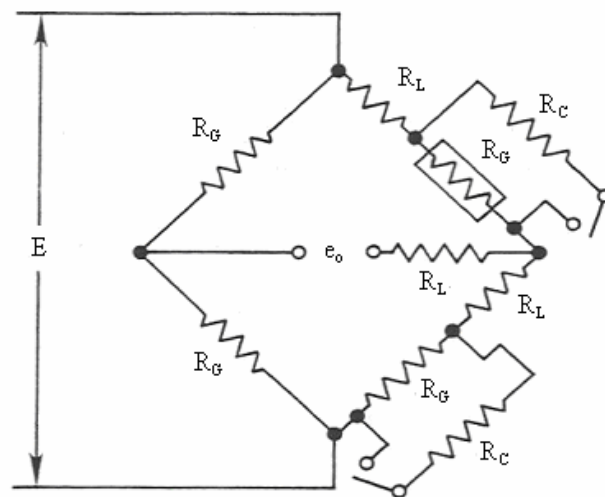


Figure 6.8. Quarter bridge circuit with active gage [16]

6.3.3. SHUNT CALIBRATION OF STRAIN GAGE

In strain measuring system, it is necessary to convert the deflection of the recording instrument into the strain quantity being measured. The process of determining the conversion factor or calibration constant is called calibration. A single calibration for the complete system is obtained so that readings from the recording instrument can be directly related to the strains which produced them.

Shunt calibration is to simulate a predetermined strain in the gage, and then adjusting the gage factor or gain of the instrument until it registers the same strain. The basic shunt calibration of single active arm is shown in Figure 6.9.

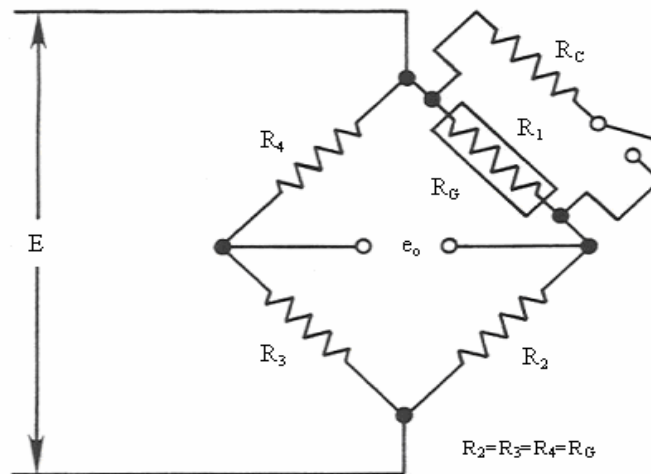


Figure 6.9. Shunt calibration of single active gage [25]

The strain measuring system is calibrated by connecting a resistor R_C of known resistance across an active arm of the bridge to produce a known change ΔR_G in resistance of this arm. For simplicity and without loss generality, it is assumed that $R_1 = R_2 = R_3 = R_4$, $R_1 = R_G$ and $\Delta R_1 = \Delta R_G$ (quarter bridge). Thus, the bridge is initially balanced. The calibration resistor R_C is shunted across R_1 by

closing the switch. The equivalent resistance of the bridge arm with the calibration resistor shunted across this arm is

$$R_e = \frac{R_1 \cdot R_C}{R_1 + R_C} \quad (6.12)$$

and the change in the arm resistance $\Delta R_1 = R_e - R_1$, by using Equation (6.12), the following is obtained:

$$\frac{\Delta R_1}{R_1} = \frac{-R_1}{R_1 + R_C} \quad (6.1)$$

where R_C is the calibration resistor.

The unit resistance change in the gage is related to strain through the definition of the gage factor, F_G :

$$\frac{\Delta R}{R_G} = F_G \cdot \varepsilon \quad (6.14)$$

Since, $R_1 = R_G$, then

$$\varepsilon_s = \frac{-R_G}{F_G \cdot (R_G + R_C)} \quad (6.15)$$

where ε_s is the calibration strain which produces the same voltage output from the bridge as the calibration resistor R_C . The minus sign indicates that the deflection of the recording system produced by the connection of R_C is along the same direction as that produced by a compressive strain in the gage resistance R_G .

6.4. TEST PROCEDURE

In the experiment, a cantilever aluminum plate with a side notch under certain loading conditions is used as a test specimen. The fatigue behavior of the test specimen subjected to random loading is investigated experimentally. The acquired experimental data are then analyzed statistically. The steps of preparing the test specimen are given as follows.

Aluminum plate, which is 79 gram mass, has 4mm thickness, 50mm width and 150mm length. An 8mm diameter hole is placed to apply an end mass on one side of the plate. The end mass which is made up of steel has mass of 486.3 gram. This configuration can be seen in Figure 6.10. Side notch is placed 50mm from the other side of the aluminum plate as shown in Figure 6.11.

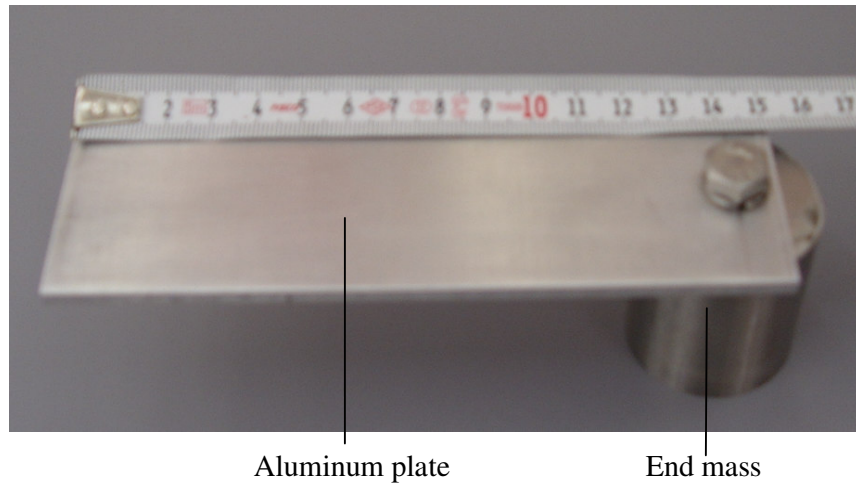


Figure 6.10. Aluminum test specimen

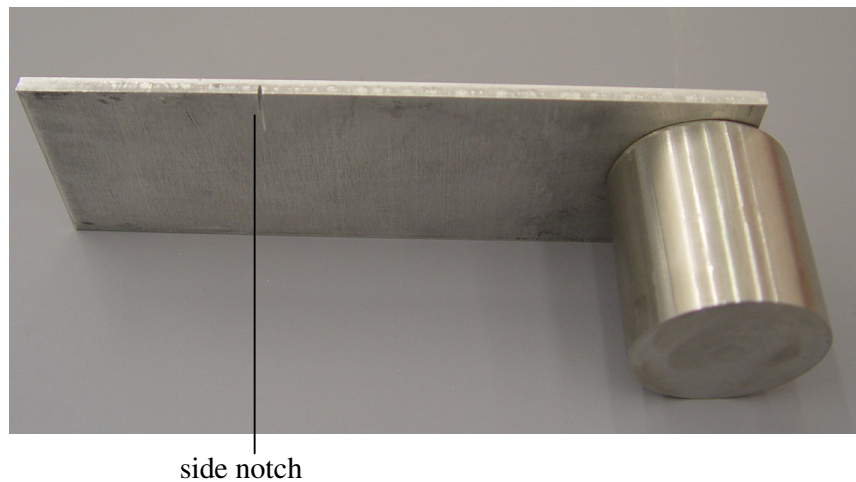


Figure 6.11. Side notch in the aluminum test specimen

The test specimen is carefully inserted between the materials from 40mm inside of the left notch side of the aluminum plate as seen in Figure 6.12. Before inserting, polyurethane foam is glued on the aluminum plate to increase the dry friction coefficient. Since notched end of the aluminum plate is fixed, a cantilever beam with base excitation is obtained.



Figure 6.12. Cantilever aluminum plate

The cantilever aluminum plate is screwed to the fixture which is used to attach the test specimen to the vibration test system, i.e. test adaptor. It is used since an intermediate element is needed to match the whole pattern of the test specimen to the pattern of the vibrator. The combined system is shown in Figure 6.13.

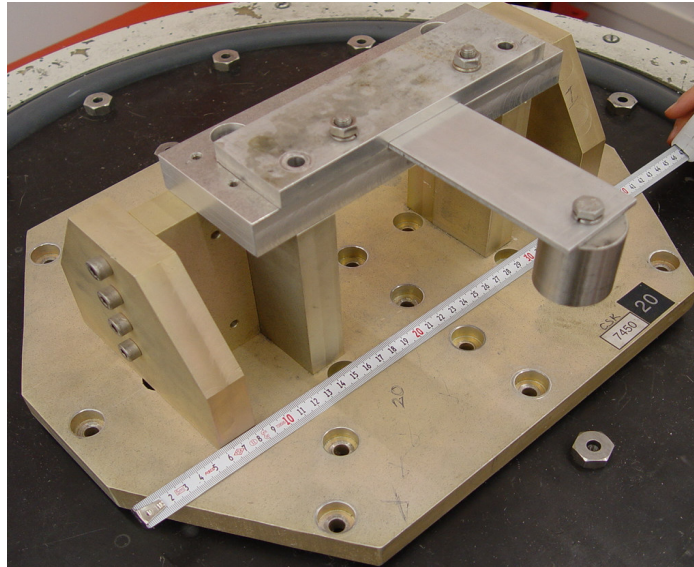


Figure 6.13. Test specimen with fixture

Strain gage is used to specify the fatigue life of the specimen. A commercial strain gage, self-compensated for aluminum, is strongly glued with the chemical consolidation behind the notch where the strain measurement is done. The process steps are the surface preparation, placing the strain gage, gluing, soldering the cable, surface protection cover and eye inspection. Figure 6.14 shows the aluminum test specimen with strain gage which is glued on. Also, in Figure 6.15, the side notch which is placed under the strain gage is seen.

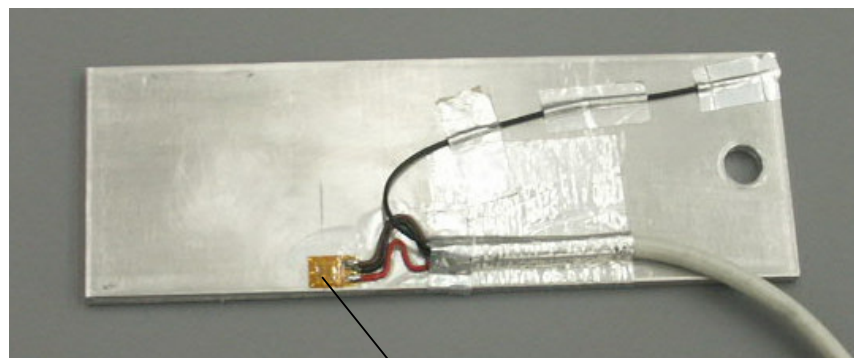


Figure 6.14. Strain gage glued on the aluminum test specimen

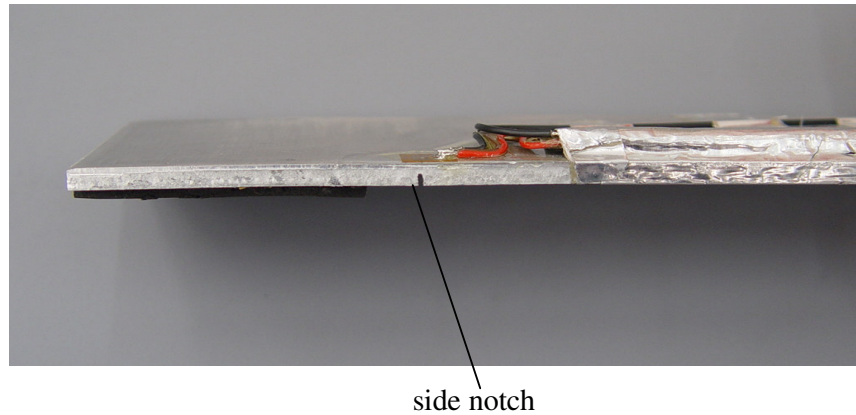


Figure 6.15. Side notch placed under the strain gage

The ideal strain gage would change resistance only due to the deformations of the surface to which the sensor is attached. It should be small in size and mass, low in cost, easily attached, and highly sensitive to strain but insensitive to ambient or process temperature variations. The uniaxial strain gage is shown separately in Figure 6.16.

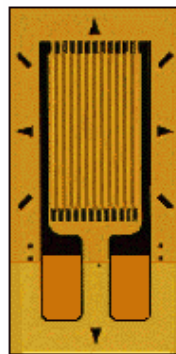
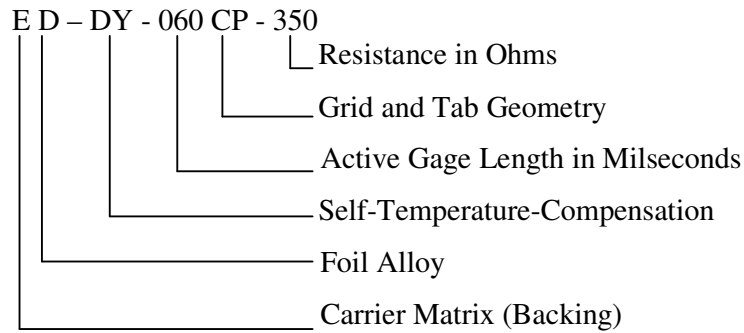


Figure 6.16. Uniaxial strain gage [16]

In the experiment, ED-DY-060CP-350 type general purpose strain gage is used. The description of the strain gage is given below:



E refers open-faced general purpose gage with tough, flexible cast polyimide backing. D refers as isoelastic alloy, high gage factor and high fatigue life excellent for dynamic measurements. The temperature range is between -195°C and $+205^{\circ}\text{C}$ and the strain range is $\pm 2\%$. Resistance is $350 \pm 0.4\% \Omega$. The dimensions of the strain gage used in the experiment are given in Table 6.2.

Table 6.2. Dimensions of the strain gage used in the experiment

Dimensions	in	mm
Gage length	0.06	1.52
Overall length	0.2	5.08
Grid width	0.18	4.57
Overall width	0.18	4.57
Matrix length	0.31	7.9
Matrix width	0.26	6.6

One side of the cable is soldered to the uniaxial strain gage and the other side is going through the connector by the quarter bridge as shown in Figure 6.17. 4-wire cable is used. One of the wires of the cable is soldered to one leg of the strain gage and two of the wires are soldered to the other leg of the strain gage. The screen is shielded to the aluminum plate to prevent the electrical noise.



Figure 6.17. Aluminum test specimen, cable and the connector

Quarter Bridge is installed as a circuit. The electrical connection of the circuit is shown in Figure 6.18. As can be seen from the figure, 6-5, 3-1, 9-15 and 8-10 are made short circuited. The other end of the cable wire, coming from one leg of the strain gage which is single soldered, is soldered to 2. The other ends of the two wires, coming from the second leg of the strain gage which is soldered at the same leg, are soldered from 10 and 11 separately to the connector. The screen is soldered to 12.

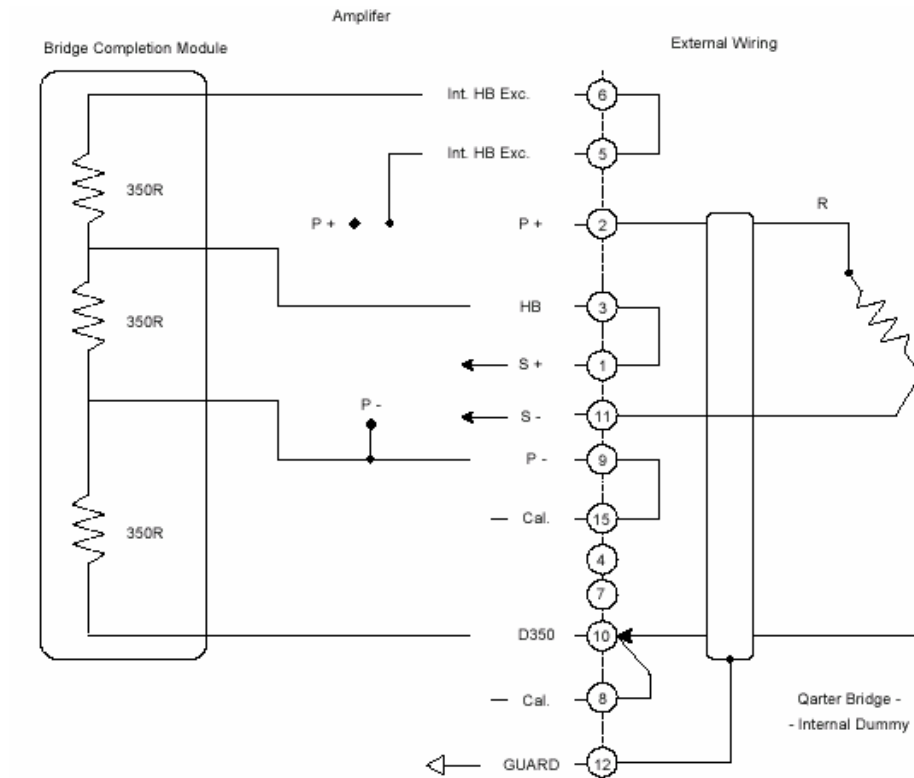
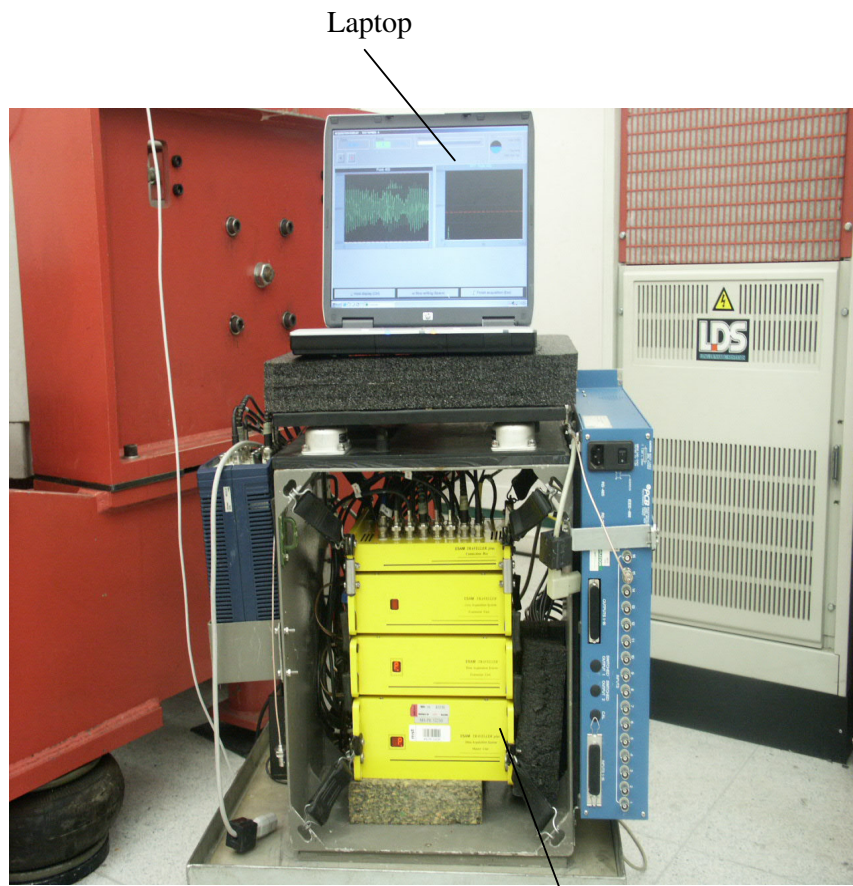


Figure 6.18. Quarter bridge circuit diagram of the strain gage connector

The connector provides the connection with the channel where the data is collected from. Traveller Plus is used as a data acquisition system. Data acquisition system, as the name implies, is a product and/or process used to collect information to document or analyze some phenomenon. The data acquisition system, Traveller Plus, can be seen in Figure 6.19, is connected to the laptop computer with USB port. ESAM (Electronic Signal Analysis Measurement) software is run from the computer to collect the data while the specimen is in the vibration test. The strain gage resistance and the gage factor; modulus of elasticity, poisson's ratio of the specimen and the environment temperature are entered to the software as input parameters. After then, ESAM software is ready to analyze the data.



Laptop

Traveller Plus Data Acquisition System

Figure 6.19. Measuring equipment

CHAPTER 7

RESULTS OF MODAL ANALYSIS AND EXPERIMENTAL STUDIES

7.1. MODAL ANALYSIS

Modal analysis has been used to determine the vibration characteristics of the specimen which are undamped natural frequencies and mode shapes. By examining the undamped natural frequencies obtained from the analysis, the sampling rate has been determined and the graphs are drawn half of the sampling frequency which is called Nyquist frequency. Nyquist frequency is the maximum frequency that can be detected from data sampled at time spacing referred as sample period. From the analysis, the behavior of the aluminum test specimen has also been examined. The material properties used in the design of a structure for dynamic loading conditions are given for the aluminum plate, steel end mass and screw are listed in Table 7.1.

Table 7.1. Material properties of the elements used in the modal analysis

Material Property	Aluminum Plate	Steel End Mass	Screw
Young's Modulus (Modulus of Elasticity)	70×10^9 Pa.	210×10^9 Pa.	210×10^9 Pa.
Density	$2,700 \text{ kg/m}^3$	$7,800 \text{ kg/m}^3$	10^{-6} kg/m^3
Poisson's Ratio	0.33	0.27	0.27

Second order element has been used in the modal analysis in ANSYS software. SOLID92 element with 10 node has been selected for the aluminum and steel elements, and BEAM4 has been selected for the screw. Screw has been modeled in 8mm diameter. In the modal analysis, Block Lanczos solver is used.

The analysis has been performed with different mesh sizes and first four undamped natural frequencies have been obtained. In the first analysis, mesh size has been taken as 0.01m. The results have been obtained as $f_1=42.96\text{Hz}$, $f_2=136.41\text{Hz}$, $f_3=254.67\text{Hz}$ and $f_4=997.85\text{Hz}$. By decreasing the mesh size to 0.005m, the second analysis results have been obtained as $f_1=46.20\text{Hz}$, $f_2=148.13\text{Hz}$, $f_3=266.38\text{Hz}$ and $f_4=1019.24\text{Hz}$. In the third analysis, mesh size has been reduced to 0.003m and the results have been found as $f_1=46.89\text{Hz}$, $f_2=148.79\text{Hz}$, $f_3=267.29\text{Hz}$, $f_4=1020.30\text{Hz}$ which have been obtained very close to the second analysis results. It has been examined that after a certain value for the mesh size, the undamped natural frequencies have been obtained very close to each other. Therefore, third analysis has been considered in the following experimental studies.

The maximum frequency of interest has been considered to define the sampling frequency. According to the third analysis results, to examine the first three natural frequencies, sampling frequency has been decided to be 1,000Hz. Mode shapes of the test specimen for the first three undamped natural frequencies are given in Figure 7.1, 7.2 and 7.3.

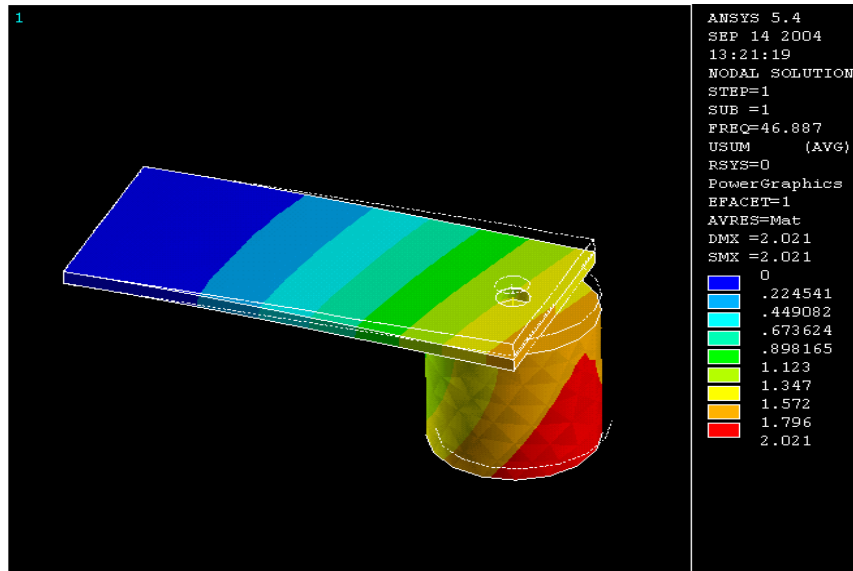


Figure 7.1. 1st mode shape of the test specimen obtained by ANSYS

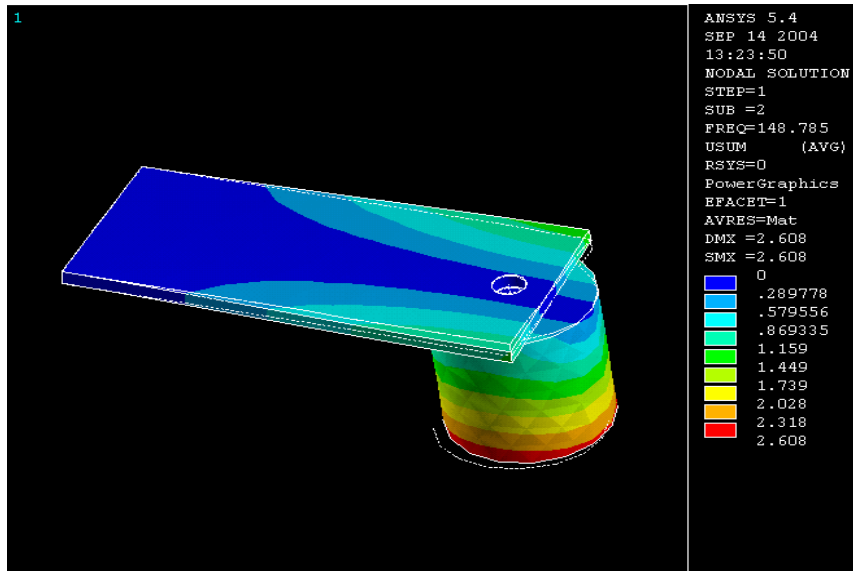


Figure 7.2. 2nd mode shape of the test specimen obtained by ANSYS

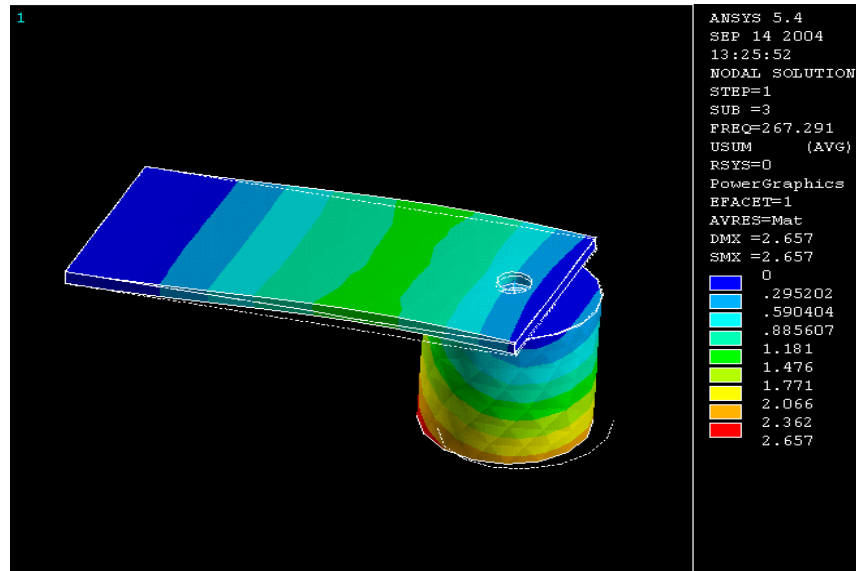


Figure 7.3. 3rd mode shape of the test specimen obtained by ANSYS

7.2. EXPERIMENTAL RESULTS

The aluminum cantilever plate has a side notch and this notch was the most critical point against the stress concentration. The strain-time data has been taken by the data acquisition system, Traveller Plus, during the vibration testing of the test specimen. The results have been obtained both in time and frequency domains. Total damage has been calculated by Palmgren-Miner rule and statistical errors associated with the spectral measurements have been performed for the analysis in frequency domain.

7.2.1. Experimental Results in Time Domain

Electronic Signal Acquisition Module (ESAM) software has been used for processing the random stresses. Each random signal has been divided into the single cycles. One of the methods of cycling implemented in the software was rainflow. The strain-time data has been collected during the experiment. The

obtained strain-time data has been used to get the stress-time data by using the equation:

$$\sigma = E \cdot \varepsilon \quad (7.1)$$

The random signal, where the abscissa shows the time values and the ordinate shows the stress ranges, has been obtained for 1,800 seconds which can be seen in Figure 7.4.

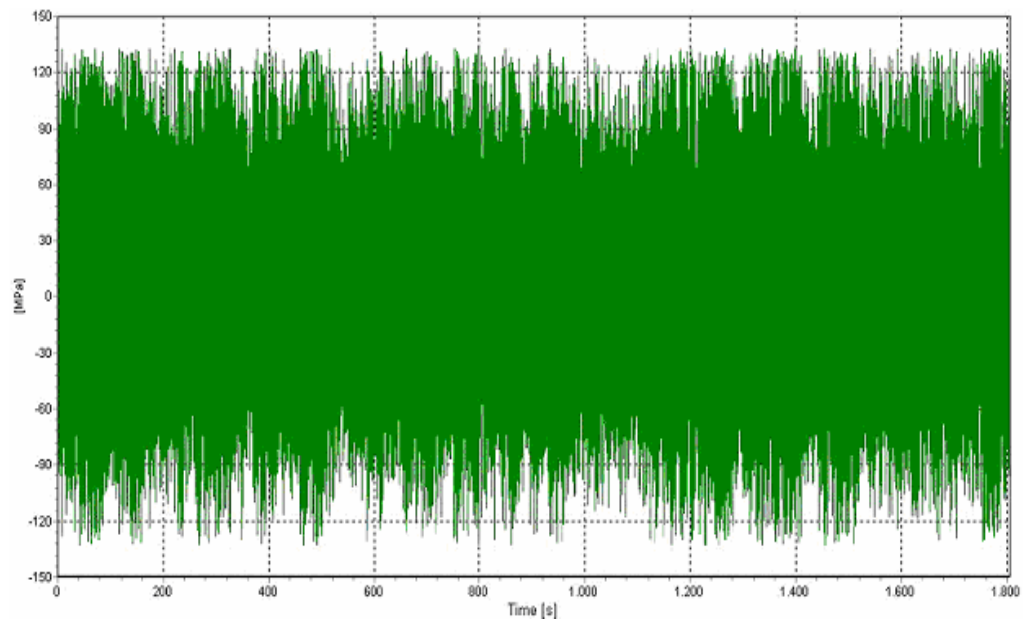


Figure 7.4. Random data acquired from the test specimen

Cycle counting by using rainflow has been executed to find the rainflow cycles in time domain for the strain gage signal. From the experiment, stress range for the test has been obtained between -132.7MPa and 132.6MPa. Each classified cycle has been described by the stress amplitude and the mean stress value by considering the stress range for the test. Full range of possible amplitudes has been divided into certain number classes to calculate classes count. Each amplitude class has been determined by class range, also amplitude tolerance has been defined as the minimal value of classified amplitude. Amplitude tolerance

has been set to the half of the amplitude class range. In the experiment, the full range for the amplitude classes has been considered such that the extreme values of the stress range for the test should be included. By taking into consideration the full range, amplitude class and the class range have been determined. When the amplitude class range has been taken as 2.5MPa and the classes count as 64, the full range has been obtained as [0..160]. Since the maximum value for the full range is 160MPa, the full range has included the maximum stress range obtained from the test. According to the amplitude class, amplitude tolerance has been taken as 1.25MPa. In Figure 7.5, cycles count versus stress amplitude is shown and cycles count as a percentage versus stress amplitude can also be seen in Figure 7.6 in the full ranges.

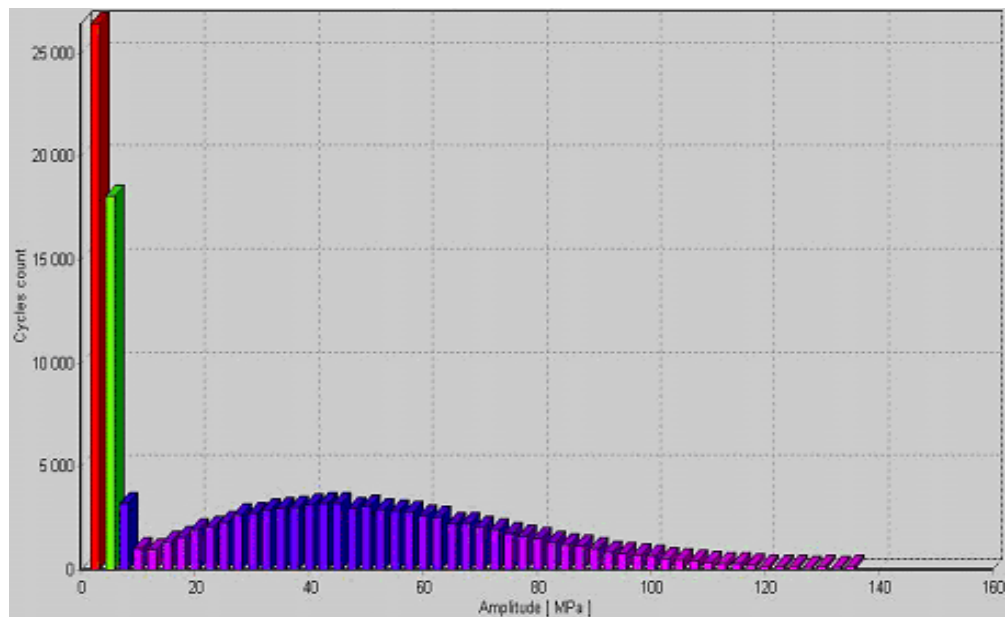


Figure 7.5. Cycle counting in full range by rainflow method on the test specimen

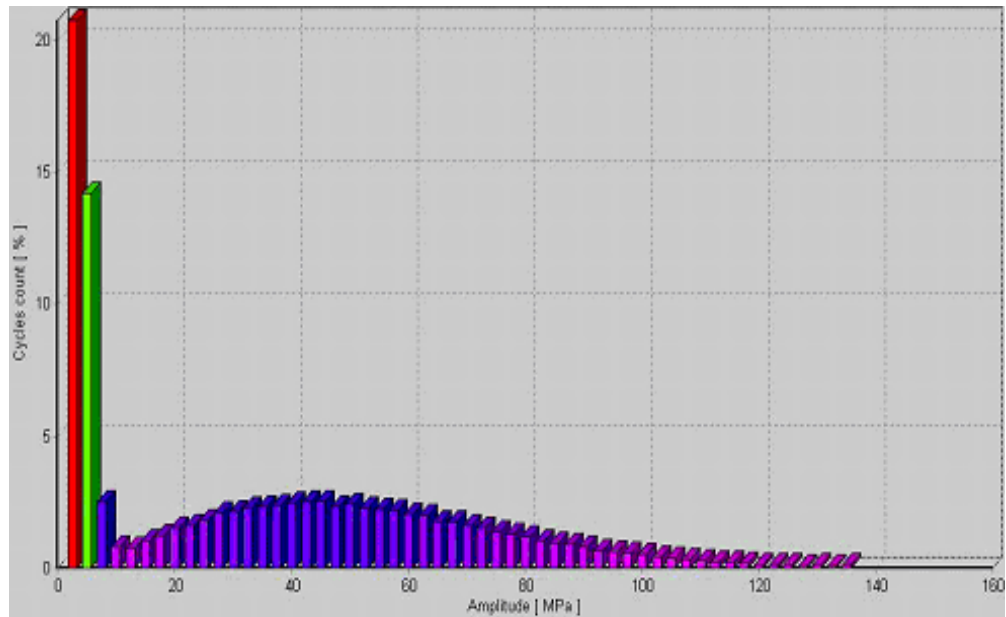


Figure 7.6. Percentage of cycle counting in full range by rainflow method on the test specimen

Mean classes have been defined similarly. The full range of the mean classes should also include the stress range obtained for the test. The full range of possible mean stress values has been divided into certain number classes which have been given as classes count. Each successive mean classes have also been determined by class range and additionally by minimal class which is the minimal value of the first mean class. By considering the stress range for test, the minimal class has been taken as -135MPa. When the class range has been taken as 5MPa and the classes count as 64, the full range has been obtained as [-135..185]. The full range for the mean classes has comprised of the stress range for test. Cycles count versus stress amplitude and mean stress value is obtained in Figure 7.7 and cycles count as a percentage versus stress amplitude and mean stress value is also shown in Figure 7.8 in the full ranges.

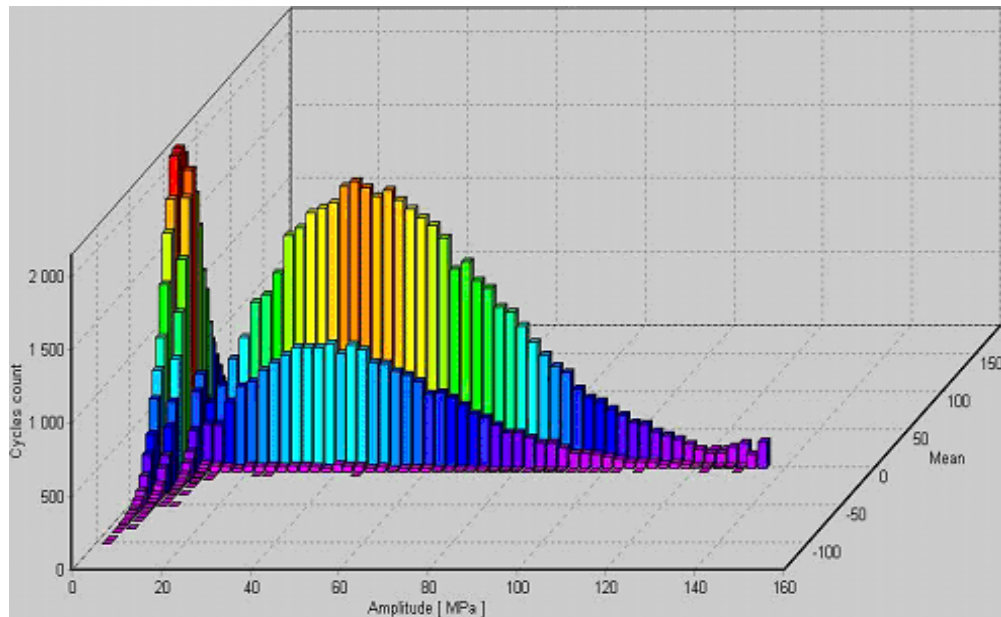


Figure 7.7. Cycle counting and mean classes in full range by rainflow method on the test specimen

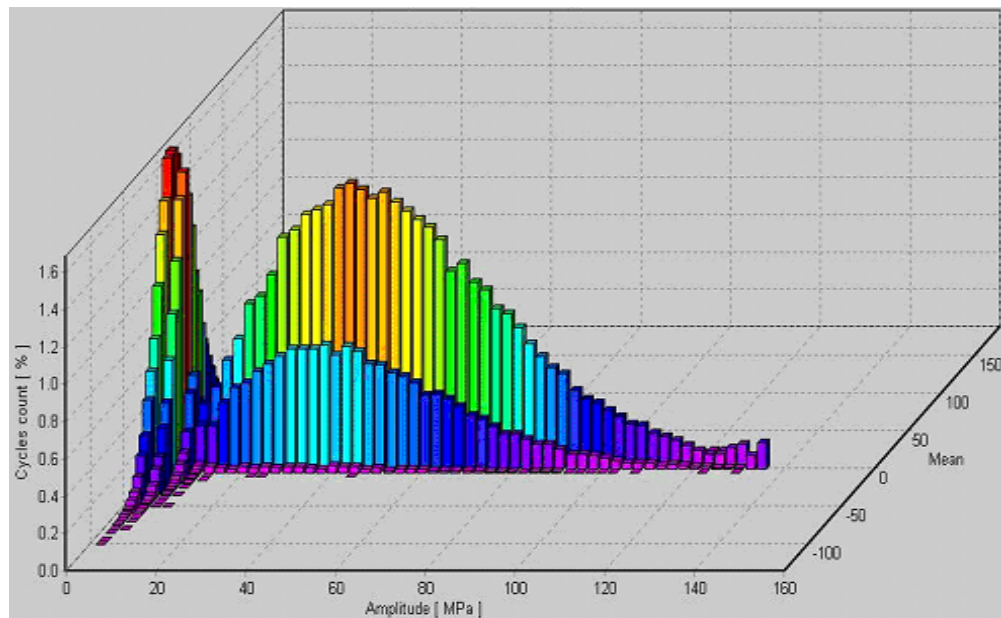


Figure 7.8. Percentage of cycle counting and mean classes in full range by rainflow method on the test specimen

The data has been analyzed for 1,800 seconds and the result for the number of cycles has been obtained as 127,413 cycles and 16 half-cycles for this time period. Since the total time has been obtained as 22,142 seconds, the total number of cycles for the whole test has been found as 1,567,420 cycles in time domain.

The number of cycles versus stress graph in Figure 7.9 can be drawn for the data collected for 1,800 seconds. The data is tabulated in Appendix A.

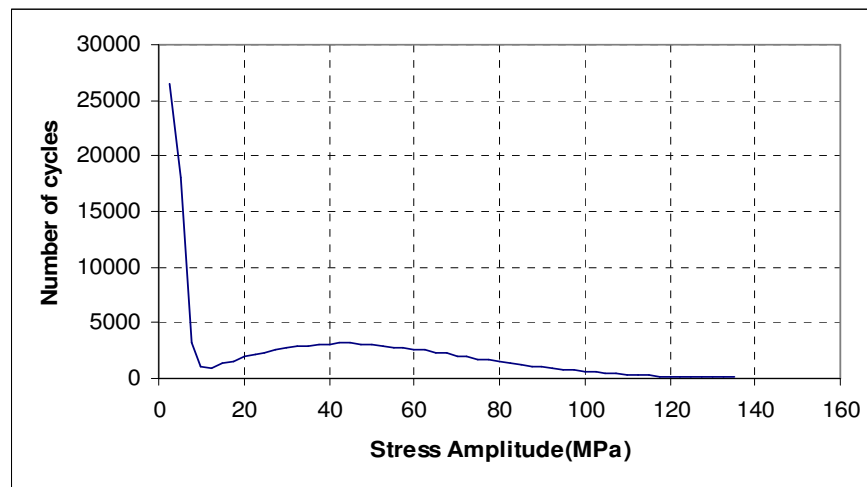


Figure 7.9. Number of cycles versus stress obtained from the test in time domain

7.2.2. Experimental Results in Frequency Domain

Frequency analysis of the test specimen has been performed to find the number of cycles for the test specimen. Since the sampling frequency has been taken as 1,000Hz, Nyquist frequency which is half of the sampling frequency has been obtained as 500Hz. Therefore, the power spectral density estimates versus frequency graph has been drawn up to 500Hz. From the graph, which has been obtained in ESAM software for the signal given in Figure 7.4, the first damped

natural frequency of the specimen is expected to find. According to Figure 7.10, a peak is obtained at frequency of 45.43Hz.

The obtained data from the graph has been exported from ESAM software to the text file. The two columns, which have been formed by power spectral density estimates and frequency, have been used to calculate the first four moments and the expected zeros, peaks and the irregularity factor in MATLAB software. The results obtained are given in Table 7.2. The total number of cycles has then been calculated. The algorithm for calculating the probability density function (pdf) estimates of stresses in Dirlik's formulation has also been written in MATLAB software. The probability density function estimates have been used to obtain the number of cycles in the stress amplitudes.

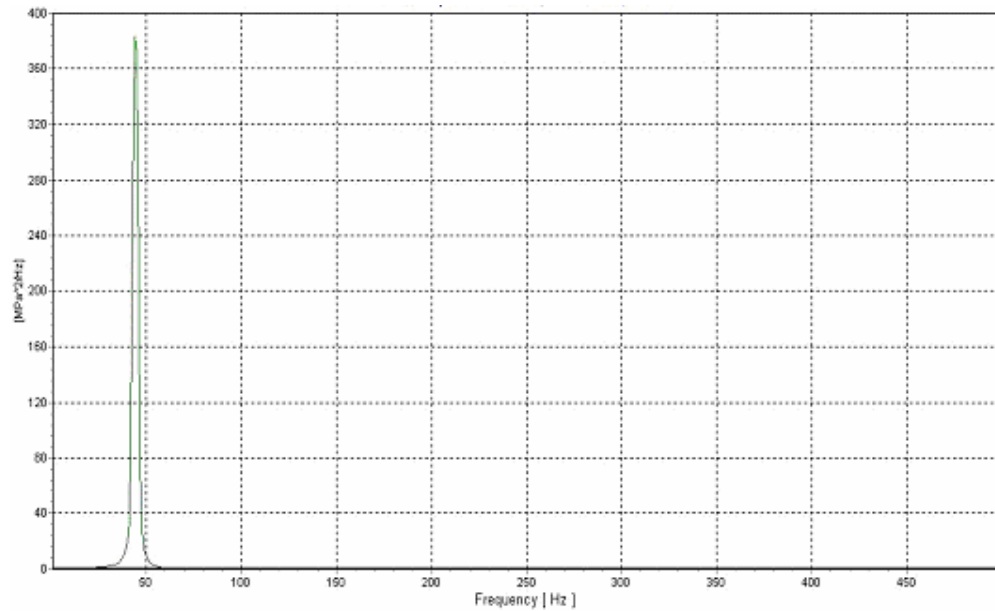


Figure 7.10. Power spectral density function estimates of the test specimen for signal in Figure 7.4

To calculate the PSD moments, expected zeros, peaks and irregularity factor, the following algorithm has been used in MATLAB software:

```
clc;
load psd_data_mat1;
psdx=psd_data;

m0=0;
for i=1:size(psd_x,1)
    m0=m0+psdx(i,2);
end;

m1=0;
for i=1:size(psd_x,1)
    m1=m1+psdx(i,1)*psdx(i,2);
end;

m2=0;
for i=1:size(psd_x,1)
    m2=m2+psdx(i,1)^2*psdx(i,2);
end;

m4=0;
for i=1:size(psd_x,1)
    m4=m4+psdx(i,1)^4*psdx(i,2);
end;

zc=sqrt(m2/m0);
nop=sqrt(m4/m2);
irf=zc/nop;

vars=[m0 m1 m2 m4 zc nop irf]';
fid = fopen('data.txt','w');
fprintf(fid,'m0= %6.4f\nm1= %6.4f\nm2= %6.4f\n m4=%6.4f\n zc=%6.4f\n
nop=%6.4f\nirf=%6.4f',vars);
fclose(fid);
```

The results taken from the algorithm are given in the tabular form:

Table 7.2. Data obtained for the test specimen by MATLAB software

Definition	Termed	Data obtained
1st psd moment value	m0	2,565
2nd psd moment value	m1	305,991
3rd psd moment value	m2	15,209,860
4th psd moment value	m4	69,677,223,407
Number of zero crossings per second	zc	77
Number of peaks per second	nop	67.7
Irregularity factor	irf	1.14

Total number of cycles can be found as by using Equation (4.12):

$$N_t = E[P] \cdot T$$

where T is the total time of the test,

$$N_t = 67.7 \cdot 22,142 = 1,499,013$$

As done above, by multiplying the number of peaks per second with the total test time, the number of cycles (N_t) has been calculated as 1,499,013 in the frequency domain.

To calculate the probability density function estimates of stress ranges using Dirlik's approach, following algorithm has been used in MATLAB software:

```
stress=2.5:2.5:135;
stress=stress';
m=0;

z=stress./(2*sqrt(m0));
xm=(m1/m0)*sqrt(m2/m4);
d1=(2*(xm-irf^2))/(1+irf^2);
r=(irf-xm-d1^2)/(1-irf-d1+d1^2);
d2=(1-irf-d1+d1^2)/(1-r);
q=(5*(irf-d1-d2*r))/(4*d1);
d3=1-d1-d2;
```

```
pdf_dirlik=((d1/q)*exp(-z./q)+(d2/r^2)*exp((-z.^2)./r^2)+d3*z.*exp(-z.^2/2))./(2*sqrt(m0));
```

```
fid = fopen('data1.txt','w');
fprintf(fid,'%18.9f\n ',pdf_dirlik);
fclose(fid);
```

According to the algorithm written to find the probability density function estimates, the first stress value was 2.5MPa and by the increment of 2.5MPa, the values have been calculated up to 135MPa. The probability density function estimates has been found by Dirlik's formulation from the power spectral density (PSD) estimates graph in Figure 7.10. The tabulated form of the stress-pdf_dirlik has been listed in Appendix A. The graph is given in Figure 7.11.

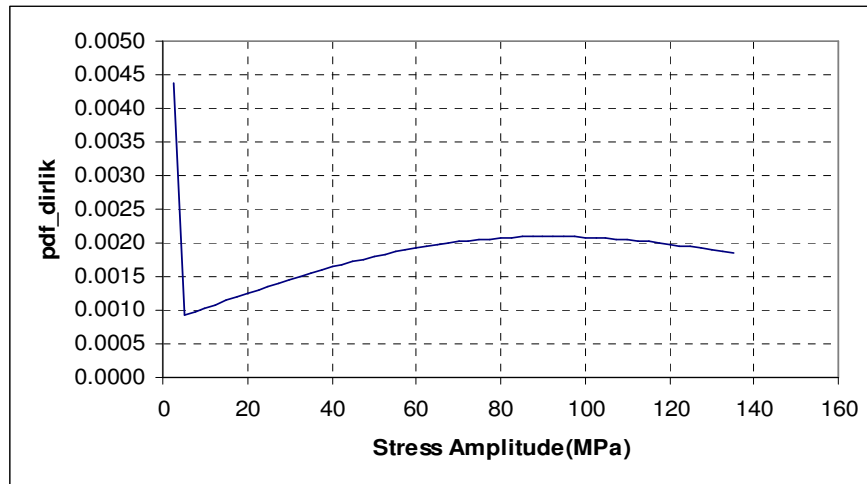


Figure 7.11. Probability density function estimates versus stress amplitude obtained from PSD graph of the test specimen in Figure 7.10 by Dirlik's formulation

From Equation 4.10, cycles at level i has been given as:

$$n_i = p[S_i] \cdot dS \cdot N_t$$

where N_t value is 1,800 seconds for the total analyzed period of time and dS is 2.5 MPa.

$$n_i = p[S_i] \cdot 2.5 \cdot 67.7 \cdot 1,800$$

The number of cycles obtained for the stress amplitudes have also been listed in Appendix A. The number of cycles versus stress amplitude graph which has been obtained from Dirlik's solution is given in Figure 7.12.

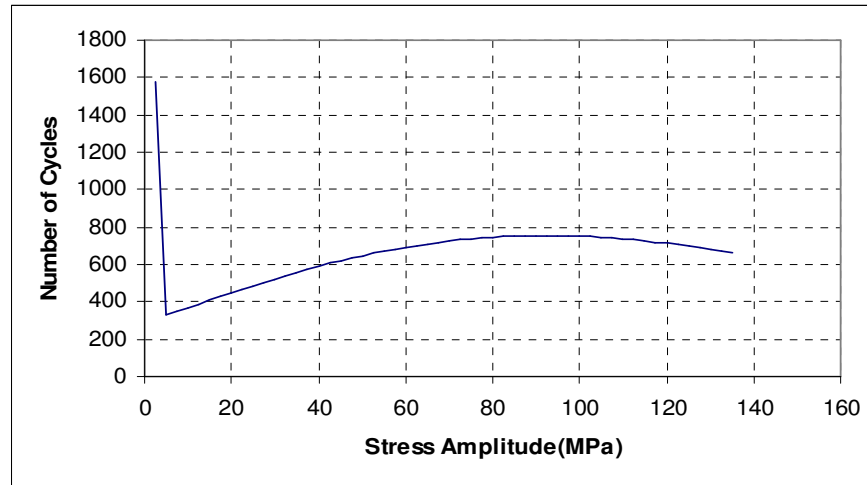


Figure 7.12. Number of cycles versus stress obtained from the test in frequency domain

7.3. PALMGREN-MINER RULE APPLICATION

Palmgren-Miner rule, linear damage rule, has been applied to find the fatigue damage of the test specimen which is accepted for the Stress-Life method. This has been confirmed by Mr. Neil Bishop referring to the mail given in Appendix D. Fatigue life calculation has been done by using Palmgren-Miner rule along with a cycle counting procedure. In the test specimen, Al 2024 T351 has been used as an aluminum plate. According to the S-N graph, the equation of the aluminum material has been obtained [34]:

$$\log(S) = 4.23 - 0.48 \cdot \log(N) \quad (7.2)$$

Then, number of cycles, N , can be found from the Equation (7.2):

$$N = 10^{\frac{4.23 - \log(S)}{0.48}} \quad (7.3)$$

By putting the stress data into Equation 7.3, the number of cycles can be obtained. The data has been tabulated in Appendix A, named ‘N theoretical’.

The total damage has been defined as the sum of all the fractional damages over a total number of blocks as given in Equation (5.3):

$$D = \sum_{i=1}^k \frac{n_i}{N_i}$$

where, since the stress values were between 2.5MPa and 135MPa by an increment of 2.5MPa, the number of blocks, k, has been calculated as 54.

Then, the total damage can be written as:

$$D = \sum_{i=1}^{54} \frac{n_i}{N_i} \tag{7.4}$$

According to Equation (7.4), total damage in time and frequency domains can be found.

7.3.1. Total Damage Calculation in Time Domain by Palmgren-Miner Rule

Total damage has been calculated by dividing the number of cycles found in the time domain for each stresses to the number of cycles found from the Equation 7.13 for Al 2024 T351:

$$\sum_{i=1}^{54} \frac{n_i}{N_i} = 0.61$$

That is, total damage obtained from the time domain analysis:

$$D = 0.61$$

7.3.2. Total Damage Calculation in Frequency Domain by Palmgren-Miner Rule

Total damage has been calculated by dividing the number of cycles found in the frequency domain for each stresses to the number of cycles found from the Equation 7.13 for Al 2024 T351:

$$\sum_{i=1}^{54} \frac{n_i}{N_i} = 0.54$$

That is, total damage obtained from the frequency domain analysis:

$$D = 0.54$$

7.4. STATISTICAL ERRORS ASSOCIATED WITH THE SPECTRAL MEASUREMENTS

The accuracy of the measurement of the power spectral density estimates may have been affected, since a limited length has been analyzed. Therefore, errors should be introduced into the measured spectrum. Even assuming that random process is ergodic, in which any one sample function completely represents the infinity of functions which make up the ensemble, errors should still be defined when only dealing with a limited length of a sample function.

Spectral linear analysis parameters have been taken as the sampling frequency, Nyquist frequency (cut-off frequency), bandwidth and the number of blocks of frequency versus power spectral density estimates.

By considering the modal analysis results, sampling frequency has been taken as 1,000Hz. Since Nyquist frequency is half of the sampling frequency, the analysis has been performed up to 500Hz. Sample time history has been taken as 1.024 seconds and statistically independent subrecords have been taken as 64. Average

power spectral density estimates have been found for the total record length of 1.024×64 seconds which can be given as

$$G_{ave}(f_k) = \frac{1}{64} \cdot \sum_{i=1}^{64} G_i(f_k) \quad (7.5)$$

where the frequency is in the range of $0 \leq f \leq 500$ Hz. and $k = 1..64$. The result is obtained as in Figure 7.13.

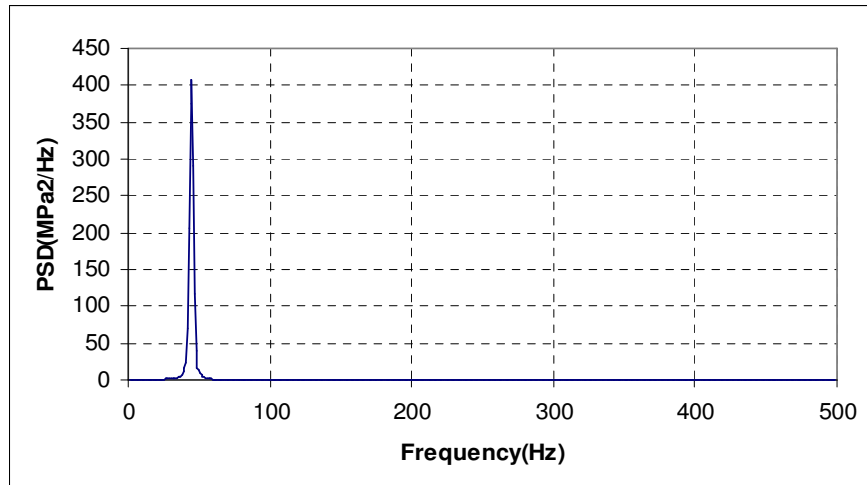


Figure 7.13. Average result of power spectral density estimates versus frequency for 1.024 seconds of each 64 sample time history

Power spectral density estimates in dB form have been examined to see the second and third damped natural frequencies of the specimen along with the first natural frequency. By taking the reference value as $1 \text{ MPa}^2/\text{Hz}$, average power spectral density estimates can be written as:

$$L_{G_{ave}}(f) = 10 \cdot \log(G_{ave}(f)) \quad (7.6)$$

From Equation 7.6, the graph of average power spectral density estimates versus frequency is obtained as in Figure 7.14. The first three damped natural frequencies can be seen clearly in the graph.

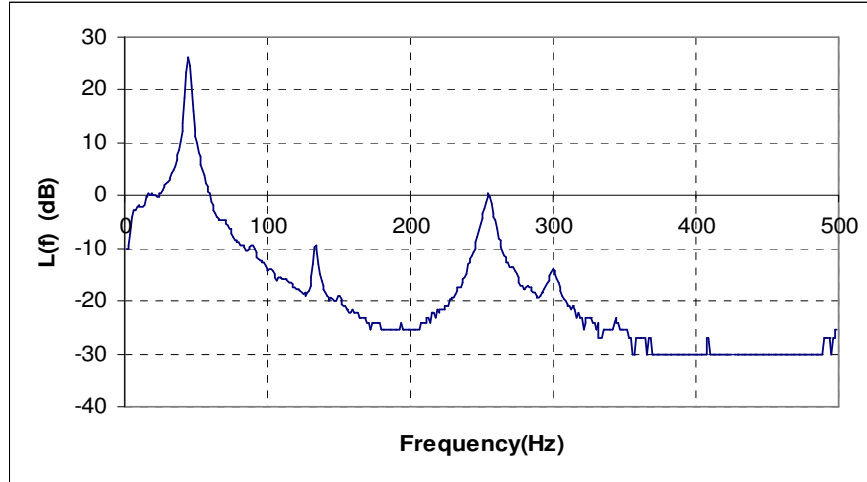


Figure 7.14. Average power spectral density estimates versus frequency

The statistical errors which are random and bias errors have been examined in the computation of desired quantities from random process. Frequency domain quantities occurring in the analysis have been discussed.

7.4.1. Random Error

The estimate $G_{ave}(f)$ has a variance error [33]

$$Var(G_{ave}(f)) \approx \frac{G^2(f)}{B_e \cdot T_{total}} \quad (7.7)$$

where T_{total} is the total record length and knowing that statistically independent subrecords n_d , the record length T , the equation can be given as:

$$T_{total} = n_d \cdot T \quad (7.8)$$

and B_e is the effective bandwidth and given as:

$$B_e = \Delta f = \frac{1}{T} \quad (7.9)$$

Then, equation becomes

$$\text{Var}(G_{ave}(f)) = \frac{G_{ave}^2(f)}{n_d} \quad (7.10)$$

Equation 7.10 yields the normalized random error formula

$$\varepsilon_r(G_{ave}(f)) = \frac{1}{\sqrt{n_d}} \quad (7.11)$$

The random error formula for the measurements of the average power spectral density estimates is only determined by n_d . In the frequency analysis of the experiment, $n_d = 64$, then random error is found as:

$$\varepsilon_r(G_{ave}(f)) = \frac{1}{\sqrt{64}} = 0.125$$

The random error is obtained as 12.5%.

7.4.2. Bias Error

The estimate of $G_{ave}(f)$ is a biased estimate where

$$b(G_{ave}(f)) \approx \frac{B_e^2}{24} \cdot \frac{d^2}{df^2} G_{ave}(f) \quad (7.12)$$

The normalized bias error is given by

$$\varepsilon_b(G_{ave}(f)) \approx \frac{B_e^2}{24} \cdot \left(\frac{\frac{d^2}{df^2} G_{ave}(f)}{G_{ave}(f)} \right) \quad (7.13)$$

The frequency response function for the single degree of freedom system can be represented by

$$H(f) = \frac{\frac{1}{k}}{1 - \left(\frac{f}{f_n}\right)^2 + j \cdot 2 \cdot \zeta \cdot \left(\frac{f}{f_n}\right)} \quad (7.14)$$

where ζ is the damping ratio and f_n is the undamped natural frequency.

If a theoretical white noise input with power spectral density function $G_w(f) = K$, a constant, then the output average power spectral density function takes the form

$$G_{ave}(f) = |H(f)|^2 \cdot G_w(f) \quad (7.15)$$

Then,

$$G_{ave}(f) = \frac{\frac{K}{k^2}}{\left[1 - \left(\frac{f}{f_n}\right)^2\right]^2 + \left[2 \cdot \zeta \cdot \left(\frac{f}{f_n}\right)\right]^2} \quad (7.16)$$

This result describes realistic bandwidth-limited white noise data. The peak value of $G_{ave}(f)$ occurs at the resonance frequency f_r and is given by

$$G_{ave}(f_r) = \frac{K}{4 \cdot k^2 \cdot \zeta^2 \cdot (1 - \zeta^2)} \quad (7.17)$$

where

$$f_r = f_n \cdot \sqrt{1 - 2 \cdot \zeta^2} \quad \text{for } \zeta^2 \leq 0.50$$

It is seen that if $\zeta^2 \ll 1$, then,

$$f_r \approx f_n$$

and

$$G_{ave}(f_n) = \frac{K}{4 \cdot k^2 \cdot \zeta^2} \quad (7.18)$$

Second derivative of $G_{ave}(f)$ with respect to f is:

$$\frac{d^2}{df^2} G_{ave}(f) \approx \frac{-K}{2 \cdot k^2 \cdot \zeta^4 \cdot f_r^4} \quad (7.19)$$

$$\frac{\frac{d^2}{df^2} G_{ave}(f_r)}{G_{ave}(f_r)} \approx \frac{-2}{\zeta^2 \cdot f_r^2} \quad (7.20)$$

When the damping ratio is relatively small, i.e. $\zeta^2 \ll 1$, the half-power point bandwidth B_r around f_r is given approximately by

$$B_r \approx 2 \cdot \zeta \cdot f_r \quad (7.21)$$

Hence,

$$\frac{\frac{d^2}{df^2} G_{ave}(f_r)}{G_{ave}(f_r)} \approx \frac{-8}{B_r^2} \quad (7.22)$$

Then, substituting (7.12) into (7.10) yields

$$\varepsilon_b(G_{ave}(f)) \approx -\frac{1}{3} \cdot \left(\frac{B_e}{B_r} \right)^2 \quad (7.23)$$

$$B_e = \frac{1}{T} = \frac{1}{1.024} = 0.977$$

The half-power bandwidth, $B_r = 3.481$ is obtained from the power spectral density estimates versus frequency graph for the test specimen.

In the frequency analysis of the experiment, the bias error is found as:

$$\varepsilon_b(G_{ave}(f)) \approx 0.026$$

The bias error is approximately obtained as 2.6%.

CHAPTER 8

SUMMARY AND CONCLUSION

8.1. SUMMARY

In this study, the fatigue behavior of cantilever aluminum plate with a side notch under certain loading conditions, i.e. base excitation, has been investigated. An experimental approach has been presented for the stress state of the cantilever aluminum plate by using strain gage. The strain gage has been glued on the critical stress location at the specimen where the strain measurement has been done. The test specimen has been exposed to random vibration test. The Traveller Plus, which is the data acquisition system, has been used in the experiment. During the random vibration test, the strain data has been collected by Traveller Plus and the results have been followed by laptop computer. The experimental data has then been analyzed statistically. The structural fatigue analysis has been carried out in time and frequency domains. The experimental results have also been used to check the accuracy of fatigue damage estimation based on Palmgren-Miner rule.

The aim of the fatigue analysis was to predict the crack initiation after a certain number of cycles by the strain gage approaches. To achieve this target, firstly the stress-time graph has been derived from the strain-time data by converting the strain data into stress data. The strain data for the graph has been taken from the uniaxial strain gage measurement while the test specimen was excited by random vibration simultaneously.

Modal analysis of the test specimen has been carried on ANSYS software to determine the undamped natural frequencies and mode shapes of a structure. The finite element model was developed employing second order BEAM4 and

SOLID92 elements. The first modal analysis has been performed by taking the mesh size as 0.01m. The undamped natural frequencies have been obtained as $f_1=42.96\text{Hz}$, $f_2=136.41\text{Hz}$, $f_3=254.67\text{Hz}$ and $f_4 = 997.85\text{Hz}$. In the second modal analysis, the mesh size has been taken as 0.005m, and the results have been found as $f_1=46.20\text{Hz}$, $f_2=148.13\text{Hz}$, $f_3=266.38\text{Hz}$ and $f_4=1019.24\text{Hz}$. Taking the mesh size equal to 0.003m in the third modal analysis, the results have been found as $f_1=46.89\text{Hz}$, $f_2=148.79\text{Hz}$, $f_3=267.29\text{Hz}$ and $f_4=1020.30\text{Hz}$. Since the undamped natural frequencies obtained were very close in the second and the third analysis, the third analysis results have been considered in the experimental analysis. According to the range of undamped natural frequencies, the sampling frequency is determined and the analysis has been performed up to the Nyquist frequency (cut-off frequency) which is the half of the sampling frequency of 1000Hz.

In time domain approach, the fatigue state has been determined by the cycle counting used. The experimental random stress data converted from strain measurements has been obtained as shown in Figure 7.4. The analysis has been done by processing the random signal in rainflow cycle counting to obtain the stress intervals and the number of cycles at these stress intervals by using the stress-time graph. Consequently, the number of cycles has been calculated in the stress amplitude which has been started from 2.5MPa and by the increment of 2.5MPa, ended at 135MPa. The graph for the cycles count has been found with respect to the stress amplitudes as given in Figure 7.5. This graph has also been given in terms of percentage of the cycles count in Figure 7.6. For the specific stress amplitudes, their mean values have also been obtained. This result has been shown in Figure 7.7 in terms of cycles count and in Figure 7.8 in terms of percentages of cycles count. By rainflow cycle counting, 127,413 cycles and 16 half-cycles have been found for a sample length of 1,800 seconds. The total number of cycles for the whole test has been found as 1,567,420 in time domain according to the total time of 22,142 seconds. The number of cycles obtained for

each stress ranges has been used in the cumulative damage theory to achieve an estimate of the structural fatigue life.

In frequency domain approach, by using the frequency analysis in ESAM software, power spectral density estimates versus frequency data has been obtained from the stress-time data. The graph of the power spectral density estimates versus frequency, which has been obtained from the time history, has been presented in Figure 7.10. In the graph, a peak has been observed at frequency of 45.43Hz. When the modal analysis result has been compared with the experimental result, 3.2% higher first undamped natural frequency has been obtained from the modal analysis which has been found as 46.89Hz. The second damped natural frequency has been obtained at frequency of 142.79Hz in the experiment. Therefore, the second undamped natural frequency of 148.79Hz, found from the modal analysis, has been investigated 4.2% higher than the experimental result. The third damped natural frequency has also been obtained at frequency of 263.70Hz in the experiment. The modal analysis result has been found 1.36% higher, since it has been obtained as 267.29Hz.

From the characteristics of the power spectral density estimates, the first four spectral moments have been obtained as 2,565.3, 305,991, 15,209,860 and 69,677,223,407 , respectively. These moments have been used to find the number of zero crossings per second, number of peaks per second and the irregularity factor which have been calculated as 77, 67.7 and 1.14 respectively. And finally, Dirlik's empirical solution has been employed to find the probability density function estimates of rainflow ranges and the graph of the probability density function estimates versus stress amplitude has been given as in Figure 7.11. The algorithm for the Dirlik's solution has been implemented in MATLAB software. The number of cycles has been determined for each stress value and the graph of the number of cycles versus stress amplitude has been illustrated in Figure 7.12. The total number cycles in frequency domain approach has been obtained by

multiplying the total time by the number of peaks per second. As a result, 1,499,013 cycles have been found as total number of cycles to failure in frequency domain.

Palmgren-Miner rule application has been performed both in frequency and time domains to estimate the structural fatigue life. Fraction of damage has been obtained for each of the stress levels and then total damage has been calculated as the sum of all the fraction of damages over the total number of blocks. In the time domain approach, total damage has been calculated as 0.61 whereas in the frequency domain approach, total damage has been calculated as 0.54.

The statistical errors associated with the spectral measurements have also been investigated. The reliability has been achieved by calculating the average of the power spectral density estimates when sample time history has been taken as 1.024 seconds and independent subrecords have been taken as 64. The graph for the average result of power spectral density estimates versus frequency has been given in Figure 7.13. It is also clearly seen from Figure 7.14 that taking the power spectral density estimates, the first three natural frequencies have been obtained sufficiently close to those found from the modal analysis. Random and bias errors have also been calculated for the desired quantities. By referencing the statistical errors for the measurement; random error, which is only a function of the statistical independent subrecords, has been found as 12.5%. In the same way, bias error, which has been determined by the effective and half-power point bandwidths, has been obtained as 2.6%.

8.2. CONCLUSION

If the cracks through the material are not detected in time to perform the necessary repairs, then fatigue failures can be catastrophic. Fatigue cracks contribute to serious structural failures. Unfortunately, most loadings that occur in nature do so in a random manner. Therefore, a phenomenon of random vibrations has been used to study responses of structural components.

Since the calculation of fatigue damage under certain loading histories requires an appropriate cycle counting method, the rainflow cycle counting method, which emerges as one of more popular techniques, has been used in the thesis. The rainflow cycle counting is a procedure for determining damaging events in variable amplitude loadings. Generally damage of the cycles has been quantified by considering Wöhler curves (S-N curves) from constant amplitude tests.

Modal analysis of the test specimen has been carried to examine the vibration characteristics of the test specimen. Numerical experiments have been conducted to improve the accuracy in the calculation of undamped natural frequencies by varying the mesh size. Through continuously decreasing the mesh size, after a certain value, almost the same results have been calculated. As a result, the first four undamped natural frequencies have been examined by taking the mesh size as 0.003m which is small enough for the test specimen. Results of modal analysis have been utilized to determine the sampling frequency to be employed in data acquisition. Therefore, the experimental analysis in frequency domain has been examined up to the Nyquist frequency of 500Hz corresponding to a sample frequency of 1,000Hz.

In the experimental stress analysis, minimum possible values have been taken for the amplitude class range and classes count to obtain the accurate results in time domain. It has been understood from the graph of cycles count versus stress

amplitude given in Figure 7.5 that higher number of cycles has been obtained in small stress amplitudes. Sharp decrease in the number of cycles has been observed when the stress amplitude has been increased. Small increases have occurred up to 50MPa stress amplitude and then, stress amplitude has again decreased. That is, after a certain stress amplitude, when the stress range increases, the number of cycles counted decreases. In maximum stress amplitudes, less number of cycle counting have been observed. The same conclusion can be made for the graph of percentages of the cycles count versus stress amplitude presented in Figure 7.6. For the specific stress amplitudes, their mean values have also been given in Figure 7.7 in terms of cycles count and in Figure 7.8 in terms of percentages of cycles count. From the graphs, it has been concluded that for certain stress amplitude, when the mean value is zero, higher number of cycles have been obtained. As the mean value has increased in magnitude, the number of cycles has decreased. In addition, larger mean values have been observed for small stress ranges and few cycles counted at these points.

In the frequency analysis, the graph of the power spectral density estimates versus frequency has been obtained as given in Figure 7.10. Since the excitation is of band limited white noise type, it is expected peaky response around natural frequencies due to low damping characteristics of the cantilever plate. Experimentally observed frequencies at which such peak behavior is observed are lower than the corresponding calculated theoretical undamped natural frequencies due to presence of damping. Since the small percentage errors have been obtained when comparing the modal analysis and frequency analysis results for the first three of the natural frequencies, the differences are found reasonable.

It has been seen that the results of rainflow cycle counting method obtained from time and frequency domain approaches were close to each other. This can also be shown by Figures 8.1 and 8.2 given below. Frequency domain approach is found

to provide a marginally safer prediction tool when compared with time domain approach.

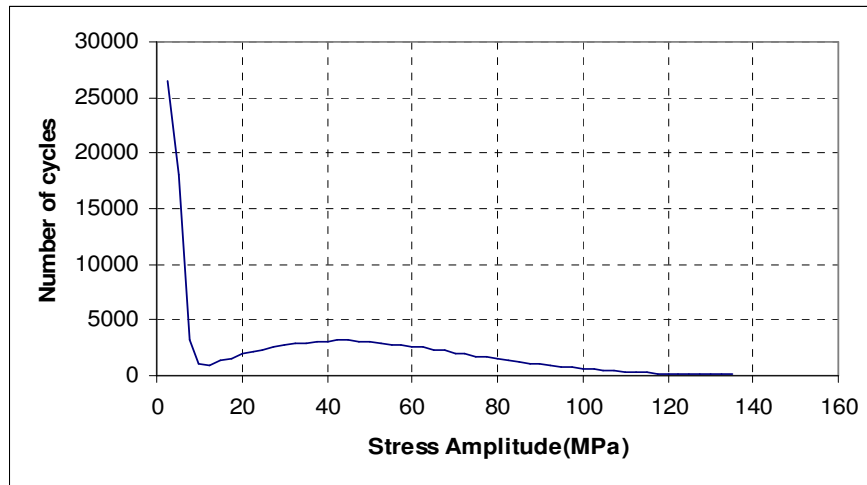


Figure 8.1. Number of cycles vs stress diagram (time domain approach)

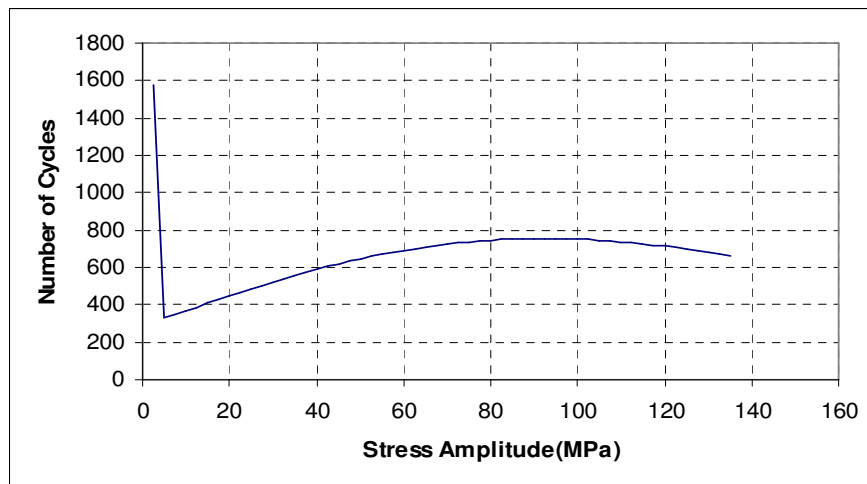


Figure 8.2. Number of cycles vs stress diagram (frequency domain approach)

The Palmgren-Miner rule predicts, in theory, that the specimen should fail when the total damage is equal to 1. Practically, additional complexity has been

introduced for different areas of application. For instance, for aerospace electronic structures, a more conservative limit is used, which is accepted as 0.7 [11]. This conservative limit has also been suggested for the mechanical structures and the electronic equipment by Steinberg [14]. In addition, a conservative limit of 0.6 has been proposed by W. Schutz [14]. Since Palmgren-Miner rule is an approach and this approach has some assumptions, it has become very difficult to obtain the same result as given by the approach. It is assumed that the same amount of damage has been incurred by all cycles of a given magnitude whether they occur early or late in the life. It is also assumed that the damage accumulates without being influence of one level on the other and rate of damage is a function of n / N independent of the amplitude of the cyclic stress. Therefore, by considering the assumptions, Palmgren-Miner rule is a linear law independent of stress level and without interaction. On the other hand, the S-N equation for the aluminum plate which has been given in Equation 7.2 should be regarded as an approximation and S-N curves are empirical. Because of these reasons, the estimated fatigue damage based on Palmgren-Miner rule is known as non-conservative, but, it is still widely used since, no rule more applicable than Palmgren-Miner's rule, is developed. However, in the result of the Palmgren-Miner rule application for the experiment, reasonable values have been found since close damage fraction have been obtained for both time and frequency domains. The error is inherent within the rule itself and but also depends on the precision of the S-N curve used.

The same power spectral density estimates versus frequency graph has been obtained with the graph found in frequency analysis by calculating the average power spectral density estimates when sample time history has been taken as 1.024 seconds and independent subrecords have been taken as 64 with the graph found for 1,800 seconds. In addition, the expected three natural frequencies have been obtained from the power spectral density estimates. Therefore, it is concluded that reliable test results have been found from the analysis. From the calculations of the statistical errors which have been found for the measurement, it

has been resulted that acceptable random error and negligible bias error have been observed from the analysis. A bias error value has been accepted to be ignored when effective bandwidth has been obtained 0.28 times of the half-power point bandwidth.

In this study, some important and critical points have been considered to obtain sensitive results for the experimental test. For instance, care has been exercised in the selection of the strain gage. Ideally the conductor should have a high gage factor, so that small strains give as large changes as possible to the resistance. Therefore, the possible smaller strain gage has been preferred. Before the vibration test has been started, the voltage value for the quarter bridge has also been selected as high as possible to get better signal; the screen of the cable, the cable which has provided the connection between the strain gage and the connector have all been shielded to reduce the electrical noise in the measured data. Shunt calibration has been done in ESAM software for the sensitivity.

Fatigue may cause significant property damage as well as loss of life. Therefore, the goal in the design process is to perform fatigue calculations at earlier stages. This would reduce and/or eliminate the need for expensive redesign. The calculated fatigue life has represented the predicted number of cycles that can be applied to the component before failure.

REFERENCES

- [1] Richard C.Rise, Brian N.Leis, Drew V.Nelson, Henry D.Berns, Dan Lingenfelter, M.R. Mitchell, 1988. Fatigue Design Handbook, Society of Automotive Engineers, Inc.
- [2] Par Johannesson, 1999. Rainflow Analysis of Switching Markov Loads, Lund Institute of Technology, Centre for Mathematical Sciences, Mathematical Statistics, Lund Institute of Technology, Sweden, pp.1-27.
- [3] Paul W.Winter and Don A.MacInnes, 1993. Fatigue Under Variable Amplitude Loading: A New Approach, Volume II, Safety and Reliability, AEA Technology, pp. 99-106.
- [4] Georg Lindgren and Jesper Ryden, 2002. Transfer Function Approximations of the Rainflow Filter, Mechanical Systems and Signal Processing 16(6), pp. 979-989.
- [5] R.J. Anthes, 1997. Modified Rainflow Counting Keeping the Load Sequence , ABB Daimler-Benz Transportation GmbH, Am Rathenaupark, 16761 Hennigsdorf, Germany, pp.529-535.
- [6] Par Johannesson, 2000. On Rainflow Cycles and The Distribution of the Number of Interval Crossings by a Markov Chain , Mathematical Statistics, Chalmers University of Technology, 412 96, Sweden, pp.123-130.
- [7] X.Pitoiset, A.Preumont, A.Kernilis, 1998. Tools for a Multiaxial Analysis of Structures Submitted to Random Vibrations, Active Structures Laboratory and Foret de Vernon, Brussels, Vernon, pp.1-6.

- [8] X.Pitoiset, A.Preumont, 1999. Spectral Methods for Multiaxial Random Fatigue Analysis of Metallic Structures, International Journal of Fatigue, pp. 541-550.
- [9] T.P.Byrne and G.D.Morandin, 1998. A Multiaxial Fatigue Cycle Counting Technique Based on the Rainflow Method, PVP-Vol.370, Finite Element Applications: Linear, Non-Linear, Optimization and Fatigue and Fracture, pp.19-25.
- [10] Richard C.Rice, Brian N.Leis, Drew V.Nelson, Henry D.Berns, Dan Lingenfelter, M.R.Mitchell, 1988. Fatigue Design Handbook, Society of Automotive Engineers Inc., 400 Commonwealth Drive, Warrendale.
- [11] Tom Irvine, 2003. Random Vibration Fatigue, Revision B.
- [12] Steven R.Lampman, Grace M.Davidson, Faith Reidenbach, Randall L.Boring, Amy Hammel, Scott D.Henry, William W.Scott, 1996. Fatigue and Fracture Volume 19, ASM International.
- [13] Paul H.Wirsching, Thomas L.Paez, Keith Ortiz, 1995. Random Vibrations, Theory and Practice, A Wiley-Interscience Publication, John Wiley & Sons, Inc.
- [14] Christian Lalanne, 1999. Mechanical Vibration & Shock, Fatigue Damage, Volume IV, Taylor and Francis Books, Inc.
- [15] Maurice L.Sharp, Glenn E.Nordmark, Craig C.Menzemer, 1996. Fatigue Design of Aluminum Components and Structures, McGraw Hill Companies, Inc.
- [16] Traveller Plus and ESAM Software Manual, 2000. Measurements Group Inc.

- [17] John Vaughan, October 1975. Application of B&K Equipment to Strain Measurements, Brüel & Kjaer.
- [18] Akhtar S.Khan, Xinwei Wang, 2001. Strain Measurements and Stress Analysis, Prentice Hall, Inc.
- [19] Shunt Calibration, Tech. Note TN-514, Measurements Group, Inc., Raleigh (North Carolina), 1988.
- [20] Harry N.Norton, 1989. Handbook of Transducers, Prentice Hall, Inc. A Division of Simon&Schuster.
- [21] Hermann K.P.Neubert, 1975. Instrument Transducers, An Introduction to Their Performance and Design, Oxford Clarendon Press, Second Edition.
- [22] Jack A.Collins, 1993. Failure of Materials in Mechanical Design, Analysis, Prediction, Prevention, Second Edition, A Wiley-Interscience Publication.
- [23] NWM Bishop and F.Sherratt, 2000. Finite Element Based Fatigue Calculations, Nafems Publication.
- [24] Wheatstone Bridge,
http://www.play-hookey.com/dc_theory/wheatstone_bridge.html , April 2004
- [25] James W.Dally and William F.Riley, Experimental Stress Analysis.
- [26] MIL-STD-810F, 2000. Department of Defense Test Method Standard for Environmental Engineering Considerations and Laboratory Tests.
- [27] ASTM E-1049, Standard Practices for Cycle Counting in Fatigue Analysis.

- [28] Jorgen Amdahl, Nina Kristin Langhelle, Steinar Lundberg, 2001. Aluminum Plated Structures at Elevated Temperatures, Proceedings of OMAE 2001: 20th Offshore Mechanics and Arctic Engineering Conference.
- [29] Dr.Alex Morris, 1998. Material World, Aluminum Alloys for Aerospace, Azom.com Pty. Ltd.
- [30] T. Warner, Pechiney CRV, Voreppe, France; R. Macé, 2004. The Future for Aluminum Alloys in Aerospace: Solutions Tailored for Specific Applications.
- [31] L.S.Srinath, M.R.Raghavan, K.Lingaiah, G.Gargesha, 1984. Experimental Stress Analysis, Tata McGraw-Hill Publishing Company Limited.
- [32] James W. Dally, I.Riley, William Franklin, 1991. Experimental Stress Analysis International Edition, McGraw-Hill Book Co.
- [33] Julius S.Bendat and Allan G.Piersol, 1980. Engineering Applications of Correlation and Spectral Analysis, John Wiley & Sons, Inc.
- [34] A.K.Lynn, D.L.DuQuesnay, 2002. International Journal of Fatigue 24, pp. 977-986.
- [35] W.F.Wu, H.Y.Liou&H.C.Tse, 1997. Estimation of Fatigue Damage and Fatigue Life of Components under Random Loading, Int. J. Pres. Ves. & Piping 72, pp. 243-249.
- [36] F.Socie Darrell,
www.mie.uiuc.edu/content/files/FCP/Socie%20presentation.pdf , May 2004

APPENDIX A

EXPERIMENTAL WORK FOR THE TEST SPECIMEN DETERMINATION

In the experimental design part of the thesis, many tests have been performed to decide the test specimen. The specimens made of aluminum alloy have been studied and the analysis has been done in the thesis according to the selected specimen. The form of the aluminum specimens used in the test is given in Figure A.1.



Figure A.1. Aluminum test specimens

In the first experiments, perpendicular S-shaped specimen which is standby with the welded part and under certain loading condition has been tested in the vibration test system. The specimen which is on the vibrator has been shown in Figure A.2. The crack initiation has been observed from the welded points in the vibration test as in Figure A.3 and it has been observed that the specimen has been started to bend from end of the support part. Since the crack initiation under

control has been aimed, it would not be a suitable solution for the test specimen. In Figure A.4, bending of the specimen can be seen clearly.

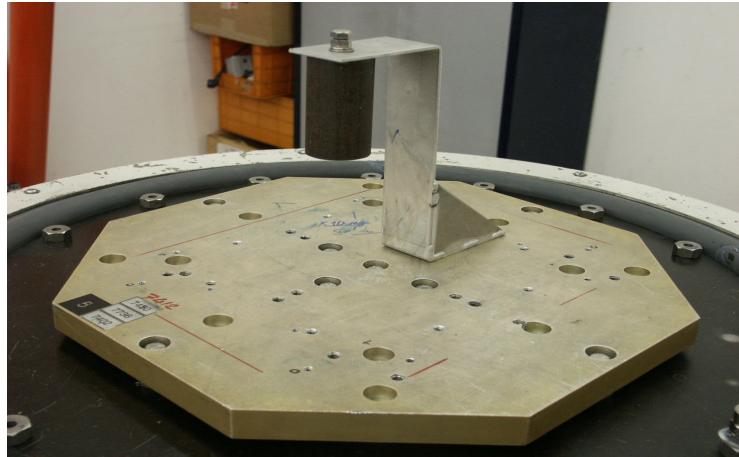


Figure A.2. Perpendicular S-shaped test specimen under vibration test

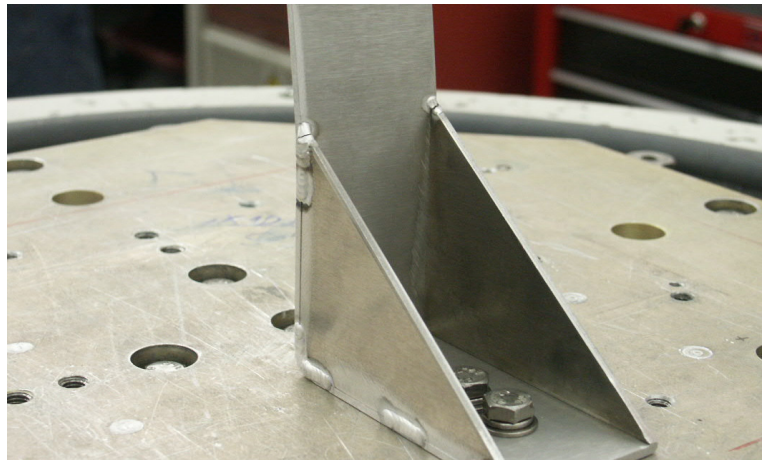


Figure A.3. Crack initiation occurred in the welded points in the vibration test

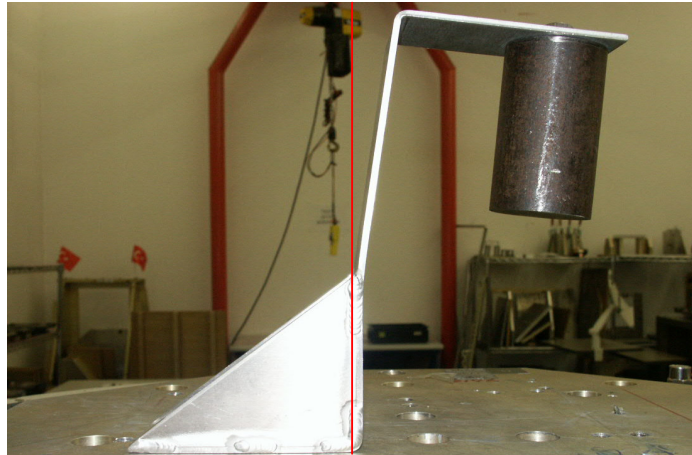


Figure A.4. Bending started from the end of the support part in the test specimen

A cantilever beam form has then been used for the test specimen. A cantilever aluminum plate has been decided to use which is under a certain loading condition. For the first experiment, the end mass has been selected less in weight according to the first end mass. The test specimen has been shown in Figure A.5. The vibration test is done to the specimen. It has been seen that, the crack has been started to occur around the screw, however for this specimen it would be difficult to examine the crack initiation position.



Figure A.5. Aluminum cantilever plate under a certain loading condition

In the next experiment, the aluminum plate has been compressed from the top side as well as the under side as can be seen in Figure A.6. The heavier end mass has been used in the test. An accelerometer has been put on the aluminum plate to watch over the vibration level on it. During the vibration test, the crack has been started from the fixed side as shown in Figure A.7.

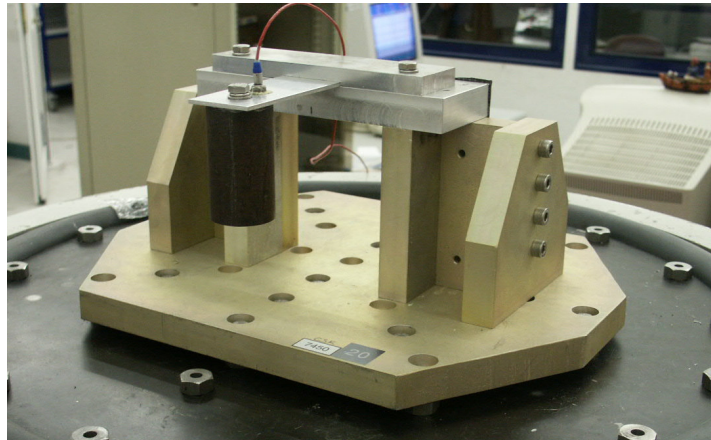


Figure A.6. Cantilever aluminum test specimen

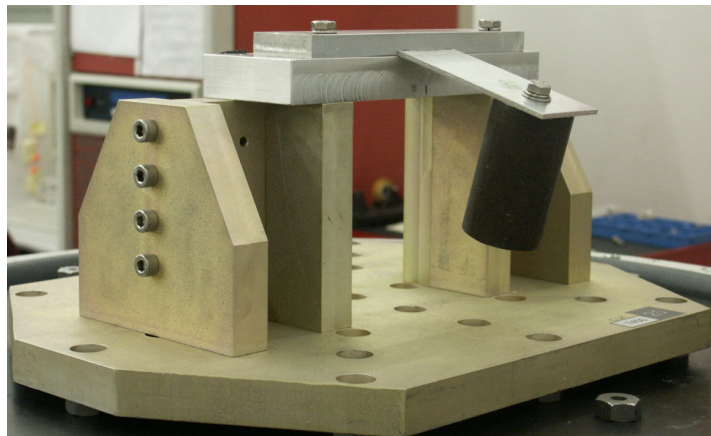


Figure A.7. Crack occurred in the fixed side of the aluminum plate in the vibration test

To make the crack under control, the notch has been placed 1cm away from the fixed side of the aluminum plate as shown in Figure A.8. The weight of the end mass has also been decreased to increase the vibration test time period. The test has been done to a specimen given in Figure A.9. The notch has been made by the fret saw. The polyurethane foam is glued on the compressed part of aluminum plate surface, as given in Figure A.10, to increase the friction. In this way, notch is obtained as the critical position.



Figure A.8. The notch placed on the aluminum plate

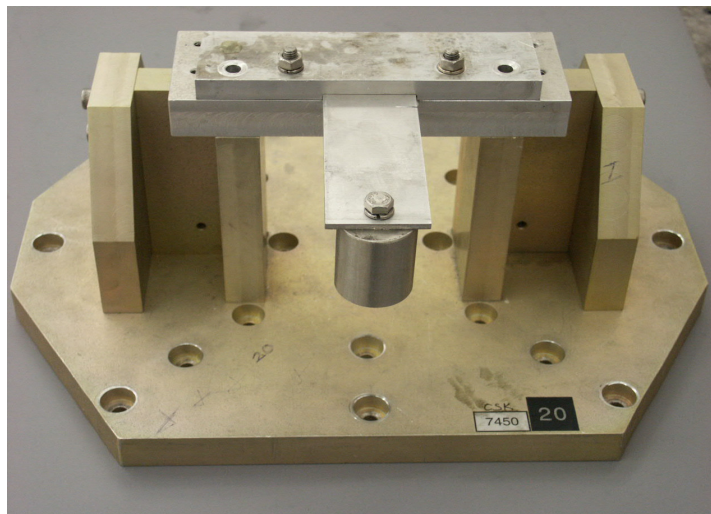


Figure A.9. The notch placed on top surface of the cantilever aluminum plate

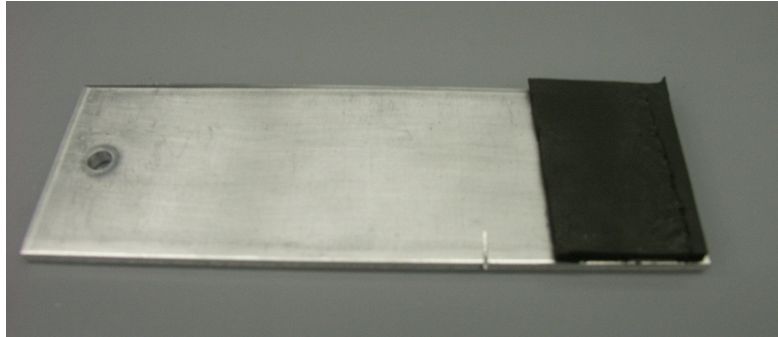


Figure A.10. Polyurethane foam glued on the aluminum plate

In the same configuration, only by changing the position of the crack, vibration test has been performed. The crack has been made on the aluminum plate such that it has been positioned under the plate which can be seen clearly in Figure A.11 and strain gage has been decided to stick on aluminum plate that has been placed above the notch. Test specimen with side notch which is placed under the aluminum plate has been given in Figure A.12.

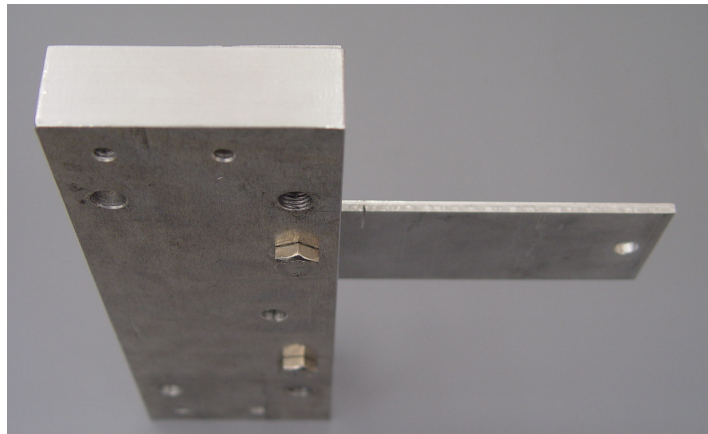


Figure A.11. Notch position on the aluminum plate



Figure A.12. The notch placed on the bottom surface of the aluminum plate

During the vibration test, the test specimen has been watched for the crack initiation and it has been examined under the microscope. In one of the experiment, the vibration test has been continued to watch over the crack propagation also. In Figure A.13, the crack has been zoomed to see the propagation of the crack clearly.

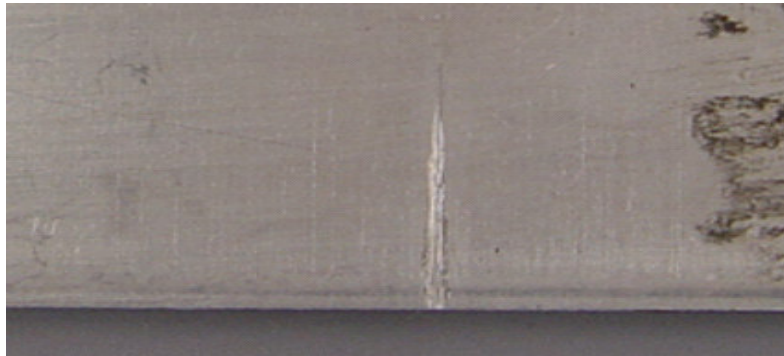


Figure A.13. Crack propagation occurred in the vibration test

APPENDIX B

TABLES

Stress amplitudes (MPa) versus number of cycles (n) and half-cycles found from the rainflow cycle counting in time domain are tabulated as follows:

Table B.1. Stress versus number of cycles in time domain

Stress (MPa)	Number of Cycles	Number of Half-cycles	N theoretical
2.5	26,437	0	96,262,761.3
5.0	18,079	1	22,714,986.9
7.5	3,192	0	9,760,132.2
10.0	1,034	1	5,360,023.2
12.5	973	0	3,367,214.7
15.0	1,354	0	2,303,084.5
17.5	1,603	0	1,670,465.1
20.0	1,927	0	1,264,797.0
22.5	2,082	0	989,585.0
25.0	2,299	0	794,556.9
27.5	2,642	0	651,463.7
30.0	2,748	0	543,455.6
32.5	2,903	0	459,984.3
35.0	2,955	0	394,177.3
37.5	3,020	0	341,403.7
40.0	3,129	0	298,452.4
42.5	3,213	0	263,040.8
45.0	3,177	0	233,511.0
47.5	2,989	0	208,635.6
50.0	3,094	0	187,490.5
52.5	2,929	0	169,369.3
55.0	2,831	1	153,725.0
57.5	2,759	0	140,128.1
60.0	2,626	0	128,238.4
62.5	2,548	0	117,783.2
65.0	2,246	0	108,541.8
67.5	2,258	1	100,334.5
70.0	2,029	0	93,013.4
72.5	1,925	0	86,456.1
75.0	1,749	1	80,560.5

Table B.1. Stress versus number of cycles in time domain (continued)

Stress (MPa)	Number of Cycles	Number of Half-cycles	N theoretical
77.5	1,630	0	75,241.0
80.0	1,523	1	70,425.4
82.5	1,348	0	66,052.2
85.0	1,205	1	62,069.4
87.5	1,137	0	58,431.9
90.0	1,026	0	55,101.2
92.5	853	1	52,044.1
95.0	797	0	49,231.4
97.5	719	0	46,638.1
100.0	660	0	44,241.9
102.5	564	0	42,023.5
105.0	480	1	39,965.8
107.5	440	0	38,053.9
110.0	379	0	36,274.3
112.5	308	0	34,615.1
115.0	289	1	33,065.8
117.5	224	1	31,617.0
120.0	175	0	30,260.2
122.5	173	2	28,987.9
125.0	162	0	27,793.1
127.5	133	0	26,669.8
130.0	152	1	25,612.5
132.5	104	0	24,616.0
135.0	182	2	23,675.8

Stress versus probability density function (pdf) estimates obtained from Dirlik's algorithm in frequency domain and number of cycles is found as follows:

Table B.2. Stress versus probability density function estimates and number of cycles in frequency domain

Stress(MPa)	pdf_dirlik	Number of Cycles	N theoretical
2.5	0.004383	1,577.7	96,262,761.3

Table B.2. Stress versus probability density function estimates and number of cycles in frequency domain (continued)

Stress(MPa)	pdf_dirlik	Number of Cycles	N theoretical
5.0	0.000922	331.9	22,714,986.9
7.5	0.000967	347.9	9,760,132.2
10.0	0.001024	368.7	5,360,023.2
12.5	0.001081	389.2	3,367,214.7
15.0	0.001138	409.5	2,303,084.5
17.5	0.001193	429.5	1,670,465.1
20.0	0.001248	449.1	1,264,797.0
22.5	0.001301	468.4	989,585.0
25.0	0.001354	487.3	794,556.9
27.5	0.001405	505.7	651,463.7
30.0	0.001455	523.6	543,455.6
32.5	0.001503	541	459,984.3
35.0	0.00155	557.9	394,177.3
37.5	0.001595	574.2	341,403.7
40.0	0.001639	589.9	298,452.4
42.5	0.001681	605	263,040.8
45.0	0.001721	619.4	233,511.0
47.5	0.001759	633.2	208,635.6
50.0	0.001796	646.4	187,490.5
52.5	0.00183	658.8	169,369.3
55.0	0.001863	670.5	153,725.0
57.5	0.001893	681.4	140,128.1
60.0	0.001922	691.6	128,238.4
62.5	0.001948	701.1	117,783.2
65.0	0.001972	709.8	108,541.8
67.5	0.001994	717.8	100,334.5
70.0	0.002014	724.9	93,013.4
72.5	0.002032	731.3	86,456.1
75.0	0.002047	736.9	80,560.5
77.5	0.002061	741.7	75,241.0
80.0	0.002072	745.8	70,425.4
82.5	0.002081	749.1	66,052.2
85.0	0.002088	751.6	62,069.4
87.5	0.002093	753.3	58,431.9
90.0	0.002096	754.3	55,101.2
92.5	0.002097	754.6	52,044.1
95.0	0.002095	754.2	49,231.4

Table B.2. Stress versus probability density function estimates and number of cycles in frequency domain (continued)

Stress(MPa)	pdf_dirlik	Number of Cycles	N theoretical
97.5	0.002092	753	46,638.1
100.0	0.002087	751.1	44,241.9
102.5	0.00208	748.6	42,023.5
105.0	0.002071	745.4	39,965.8
107.5	0.00206	741.5	38,053.9
110.0	0.002048	737	36,274.3
112.5	0.002034	731.9	34,615.1
115.0	0.002018	726.3	33,065.8
117.5	0.002	720	31,617.0
120.0	0.001982	713.3	30,260.2
122.5	0.001961	706	28,987.9
125.0	0.00194	698.2	27,793.1
127.5	0.001917	690	26,669.8
130.0	0.001893	681.3	25,612.5
132.5	0.001868	672.2	24,616.0
135.0	0.001841	662.7	23,675.8

Table B.3. Standard gage series

Code	Definition
EA	Constantan grid, polyimide backing
CEA	Encapsulated constantan grid, copper solder tabs
N2A	Constantan grid, thin polyimide backing
WA	Encapsulated constantan grid, high endurance lead wires
SA	Encapsulated constantan grid, high endurance lead wires
EP	High elongation constantan grid
ED	Isoelastic foil, polyimide backing
WD	Encapsulated isoelastic grid, high endurance lead wires
SD	Encapsulated isoelastic grid, solder dots
EK	K-alloy grid, polyimide backing

Table B.3. Standard gage series (continued)

CEA	Encapsulated constantan grid, copper solder tabs
WK	Encapsulated K-alloy grid, high endurance lead wires
SK	Encapsulated K-alloy grid, solder dots

APPENDIX C

FIRST NATURAL FREQUENCY CALCULATION OF THE ALUMINUM CANTILEVER PLATE

The first natural frequency of the aluminum cantilever plate has been calculated. It is known as the most damaging frequency. The cantilever aluminum plate is assumed in such a structure that a simple mass m supported by a pure spring stiffness k , which when deflected, resonates at a frequency:

$$f_n = \frac{w_n}{2 \cdot \pi} = \frac{1}{2 \cdot \pi} \cdot \sqrt{\frac{k}{m}} \quad \text{Hz} \quad (\text{C.1})$$

For the single degree of freedom model of a cantilever plate, first natural frequency is given as:

$$w_n = \sqrt{\frac{k_{eq}}{m_{eq}}} \quad (\text{C.2})$$

The equivalent stiffness can be calculated from the equation:

$$k_{eq} = \frac{3 \cdot E \cdot I}{L^3} \quad (\text{C.3})$$

where E is the Young's modulus(N/m^2), I is the cross-sectional moment of inertia(m^4) and the mass can be calculated from the equation:

$$m_{eq} = m + 0.24 \cdot m_{Al} \quad (\text{C.4})$$

where m is the end mass(kg) and m_{Al} is the mass of aluminum plate.

For a rectangular section, cross-sectional moment of inertia is

$$I = \frac{1}{12} \cdot b \cdot h^3 \quad (\text{C.5})$$

where b is width(m), h is thickness of the plate(m).

By giving the inputs for the cantilever aluminum plate, the equations can be solved as in the following:

$$m_{Al} = 79 \cdot 10^{-3} \text{ kg} \quad m = 486.3 \cdot 10^{-3} \text{ kg}$$

$$m_{eq} = m + 0.24 \cdot m_{Al}$$

$$m_{eq} = 0.505 \text{ kg}$$

$$b = 5 \cdot 10^{-2} \text{ m} \quad h = 4 \cdot 10^{-3} \text{ m}$$

$$I = \frac{1}{12} \cdot b \cdot h^3$$

$$I = 2.667 \cdot 10^{-10} \text{ m}^4$$

$$E = 70 \cdot 10^9 \text{ N/m}^2 \quad L = 11 \cdot 10^{-2} \text{ m}$$

$$k_{eq} = \frac{3 \cdot E \cdot I}{L^3}$$

$$k_{eq} = 4.207 \cdot 10^4 \text{ N/m}$$

$$w_{eq} = \sqrt{\frac{k_{eq}}{m_{eq}}}$$

$$w_{eq} = 288.568 \text{ rad/s}$$

$$w_n = \frac{1}{2 \cdot \pi} \cdot w_{eq}$$

$$w_n = 45.927 \text{ Hz}$$

The first natural frequency of the cantilever aluminum plate is calculated as 45.927Hz. It is obtained almost the same with the experimental result of first natural frequency which has been obtained as 45.43Hz.

APPENDIX D

COMMUNICATION

Experimental stress analysis has been defined to Mr. Neil Bishop and asked whether Palmgren-Miner rule can be used for the crack initiation method. The answer has been mailed by Mr. Neil Bishop as following:

‘ Actually the term crack initiation is a very misleading term since most conventional metals have cracks in from the beginning and so all you are actually doing when applying loads is to grow these cracks to detectable lengths. So the crack initiation method (Strain-Life) is conceptually the same as the S-N or Stress-Life method. For both methods the Palmgren-Miner rule is generally accepted as the only method to accumulate damage. ’

It is also approved by Mr. Neil Bishop that Palmgren-Miner rule can be used for the Stress-Life method to find the cumulative damage.

APPENDIX E

SUBROUTINE FOR RAINFLOW COUNTING

The routine below makes it possible to determine the ranges of a signal to use for the calculation of the fatigue damage according to this method. The signal must be first modified in order to start and to finish by the largest peak. The total number of peaks and valleys must be even and an array of the peaks and valleys (Extrema()) must be made up from the signal thus prepared.

The boundaries of the ranges from the peaks are provided in arrays *Peak_Max()* and *Peak_Min()* and those of the ranges resulting from the valleys in *Valley_Max()* and *Valley_Min()*. These values make it possible to calculate the two types of ranges *Range_Peak()* and *Range_Valley()*, as well as their mean

value $\frac{Peak_Min(i) + Peak_Max(i)}{2}$ and $\frac{Valley_Min(i) + Valley_Max(i)}{2}$.

Procedure Rainflow of Peaks Counting

According to D.V. NELSON

The procedure uses as input/output data:

Extremum(Nbr_Extrema+2) = array giving the list of Nbr_Extrema extrema successive and starting from the largest peak

At output, obtained:

Peak_Max(Nbr_Peaks) and Peak_Min(Nbr_Peaks) = limits of the ranges of the peaks

Valley_Max(Nbr_Peaks) and Valley_Min(Nbr_Peaks) = limits of the valley ranges

These values make it possible to calculate the ranges and their mean value.

Range_Peak(Nbr_Peaks) = array giving the listed ranges relating to the peaks

Range_Valley(Nbr_Peaks) = array of the ranges relating to the valleys

Procedure rainflow (Nbr_Extrema,VAR Extremum())

LOCAL i,n,Q,Output,m,j,k

Separation of peaks and valleys

Nbr_Peaks=(Nbr_Extrema+1)/2

FOR i=1 TO Nbr_Peaks

 Peak(i)=extremum(i*2-1)

NEXT i

FOR i=2 TO Nbr_Peaks

 Valley(i)=Extremum(i*2-2)

NEXT i

Research of the deepest valley

Valley_Min=Valley(2)

FOR i=2 TO Nbr_Peaks

 IF Valley(i)<Valley_Min

 Valley_Min=Valley(i)

 ENDIF

NEXT i

Valley(Nbr_Peaks+1)=1.01*Valley_Min

Treatment of valleys

FOR i=2 TO Nbr_Peaks

(Initialization of the tables with Peak(1))

 L(i)=Peak(1)

 LL(i)=Peak(1)

NEXT i

FOR i=2 TO Nbr_Peaks

 n=0

 Q=i

 Output=0

 DO

(Calculation of the Ranges relating to the Valleys)

 IF LL(i+n)<Peak(i+n)

 Range_Valley(i)=ABS(LL(i+n)-Valley(i)) *(Array of the Valleys Ranges)*

 Valley_Max(i)=LL(i+n) *(Array of the Maximum of the Ranges of the Valleys)*

 Valley_Min(i)=Valley(i) *(Array of the Minimum of the Ranges of the Valleys)*

 Output=1

 ELSE

 IF Valley(i+n+1)<Valley(i)

 Range_Valley(i)=ABS(Peak(Q)-Valley(i))

 Valley_Max(i)=Peak(Q)

 Valley_Min(i)=Valley(i)

 Output=1

 ELSE

 IF Peak(i+n+1)<Peak(Q)

```

    L(i+n+1)=Peak(Q)
    n=n+1
ELSE
    L(i+n+1)=Peak(Q)
    Q=i+n+1
    n=n+1
ENDIF
ENDIF
ENDIF
LOOP UNTIL Output =1
m=i+1
IF m<=Q
    FOR j=m TO Q
        LL(j)=L(j)
    NEXT j
ENDIF
NEXT i

Treatment of peaks
FOR i=2 TO NBR_Peaks+1      (Initialization of the arrays with Valley_Min)
    L(i)=Valley_Min
    LL(i)=Valley_Min
NEXT i
For i=1 TO Nbr_Peaks
n=0
k=i+1
Q=k
Output=0
DO
    IF LL(k+n)>Valley(k+n)
        Range_Peak(i)=ABS(Peak(i)-LL(k+n))      (Array of the Ranges of the Peaks)
        Peak_Max(i)=Peak(i)      (Array of the Maximum of the Ranges of the Peaks)
        Peak_Min(i)=LL(k+n)      (Array of the Minimum of the Ranges of the Peaks)
        Output=1
    ELSE
        IF Peak(k+n)>Peak(i)
            Range_Peak(i)=ABS(Peak(i)-Valley(Q))
            Peak_Max(i)=Peak(i)
            Peak_Min(i)=Valley(Q)
            Output=1
        ELSE
            IF Valley(k+n+1)>Valley(Q)
                L(k+n+1)=Valley(Q)
                n=n+1
            ELSE
                L(k+n+1)=Valley(Q)
            ENDIF
        ENDIF
    ENDIF
NEXT i

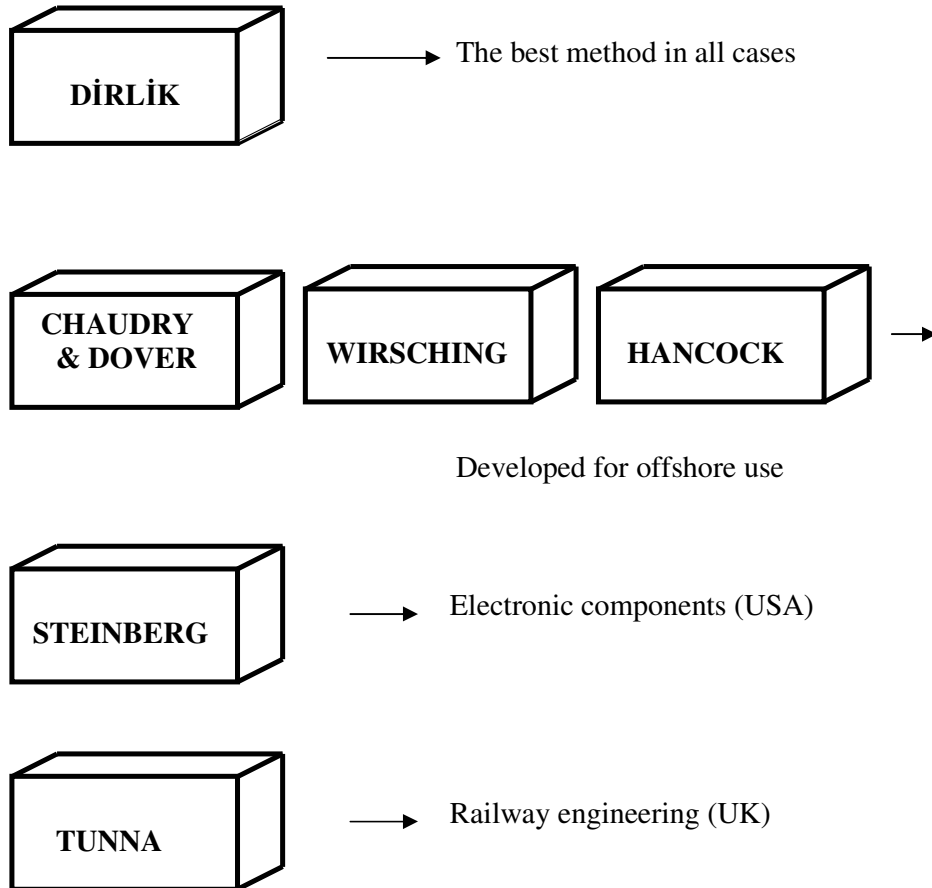
```

```
    Q=k+n+1  
    N=n+1  
    ENDIF  
    ENDIF  
    ENDIF  
    LOOP UNTIL Output=1  
    m=k+1  
    IF m<=Q  
        FOR j=m TO Q  
            LL(j)=L(j)  
        NEXT j  
    ENDIF  
    NEXT i  
    RETURN
```

APPENDIX F

SOLUTION METHODS

There are various approaches for estimating the probability density functions from power spectral density moments. There were expressions developed with reference to offshore platform design where interest in the techniques has existed for many years. In general, they were produced by generating sample time histories from power spectral density using Inverse Fourier Transform techniques. From these a conventional Rainflow cycle count was then obtained. The solutions of Wirsching, Chaudry and Dover, Tuna and Hancock were all derived using this approach [23]. They are all expressed in terms of the spectral moments up to m_4 .



HAUDRY AND DOVER SOLUTION

$$S_{eqCandD} = (2 \cdot \sqrt{2 \cdot m_0}) \cdot \left[\left(\frac{\varepsilon^{m+2}}{2 \cdot \sqrt{\pi}} \right) \cdot \Gamma\left(\frac{m+1}{2}\right) + \frac{\gamma}{2} \cdot \Gamma\left(\frac{m+2}{2}\right) + erf(\gamma) \cdot \frac{\gamma}{2} \cdot \Gamma\left(\frac{m+2}{2}\right) \right]^{1/m}$$

WIRSCHING SOLUTION

$$E(D)_{Wirsch} = E(D)_{NB} \cdot [a(m) + (1 - a(m)) \cdot (1 - \varepsilon)^{c(m)}]$$

where m is the slope of the S-N curve and

$$a(m) = 0.926 - 0.033m, \quad c(m) = 1.587m - 2.323, \quad \varepsilon = \sqrt{1 - \gamma^2}$$

HANCOCK SOLUTION

$$S_{eqHanc} = (2 \cdot \sqrt{2 \cdot m_0}) \cdot \left(\gamma \cdot \Gamma\left(\frac{m}{2} + 1\right) \right)^{1/m}$$

STEINBERG SOLUTION

'THREE BANDED TECHNIQUE'

Three banded technique is used for testing electronic equipment in the USA.

$$S_{eqStein} = f(m_0)$$

$$S_{eqStein} = \left[0.683 \cdot (2 \cdot \sqrt{m_0})^m + 0.271 \cdot (4 \cdot \sqrt{m_0})^m + 0.043 \cdot (6 \cdot \sqrt{m_0})^m \right]^{1/m}$$

This solution is based on the assumption that stress levels occur for 68.3% time at 1rms, 27.1% time at 2rms, 4.3% time at 3rms.

TUNNA SOLUTION

$$p(S)_T = \left(\frac{S}{4 \cdot \gamma^2 \cdot m_0} \cdot e^{\frac{-S^2}{8 \cdot \gamma^2 \cdot m_0}} \right)$$

APPENDIX G

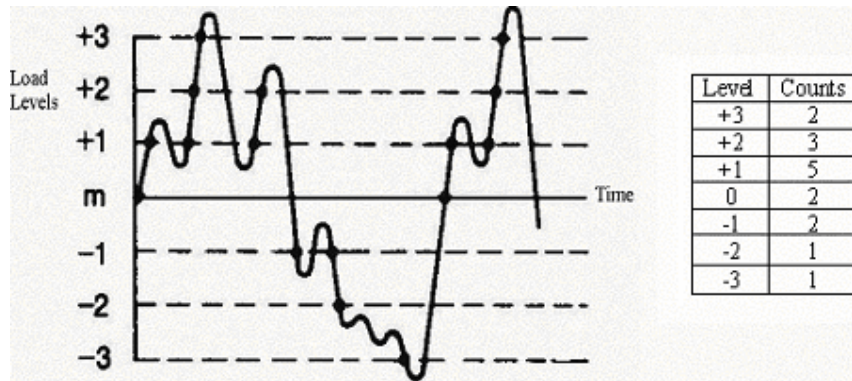
COUNTING METHODS FOR THE ANALYSIS OF THE RANDOM TIME HISTORY

Various methods of counting were proposed, leading to different results and, thus, for some, to errors in the calculation of the fatigue lives. Although various methods may still be in use, Rainflow Counting is the preferred method. This method includes a family of various computer algorithms. Older methods which often utilized analog logic circuits are Level Crossing, Peak Counting, Simple Range.

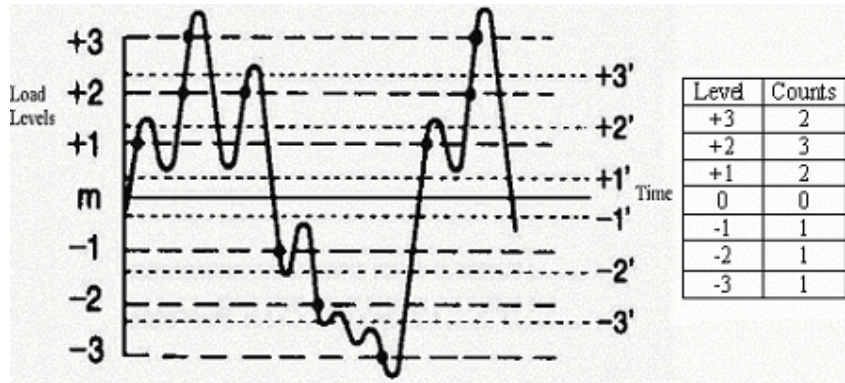
LEVEL CROSSING COUNTING

The results of the level crossing count are shown in Figure G.1. There are practical restrictions on the level crossing counts which are often specified to eliminate small amplitude variations. By this way, small amplitude variations can give rise to a large number of counts. This can be accomplished by making no counts at the reference load and to specify that only one count be made between successive crossings of a secondary level associated with each level above the reference load, or a secondary higher level associated with each level below the reference load. Figure G.1(b) illustrates this method.

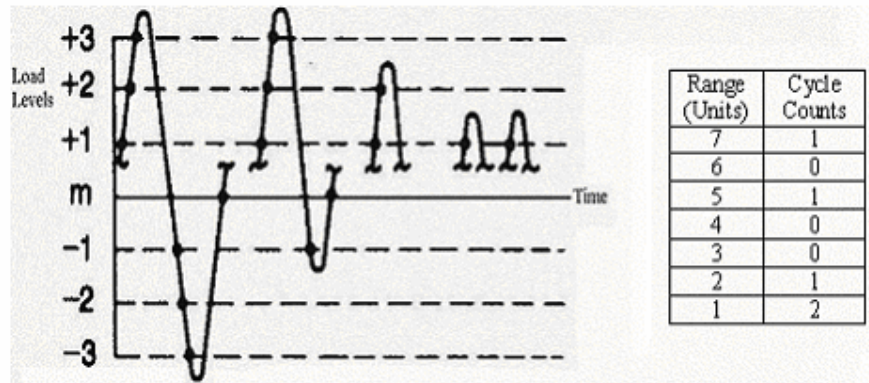
The most damaging cycle count for fatigue analysis is derived from the level crossing count by first constructing the largest possible cycle, followed by the second largest, etc., until all level crossings are used. Reversal points are assumed to occur halfway between levels. This process is shown in Figure G.1(c). Once this most damaging cycle count is obtained, the cycles could be applied in any desired order, and this order could have a secondary effect on the amount of damage.



(a) Level crossing counting



(b) Restricted level crossing counting



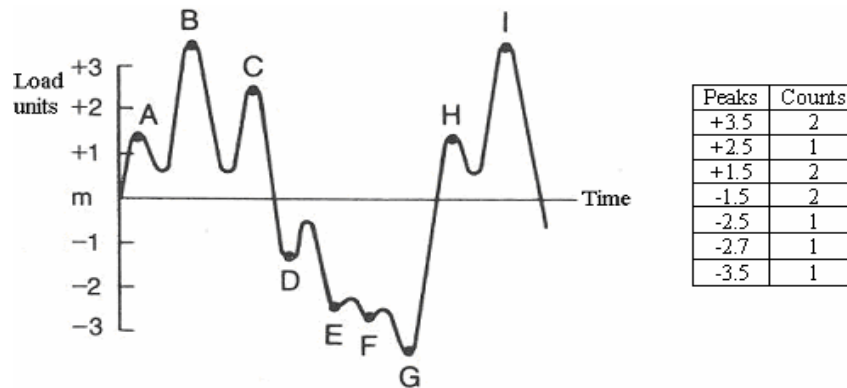
(c) Cycles derived from level crossing counting of (a)

Figure G.1. Level crossing counting example

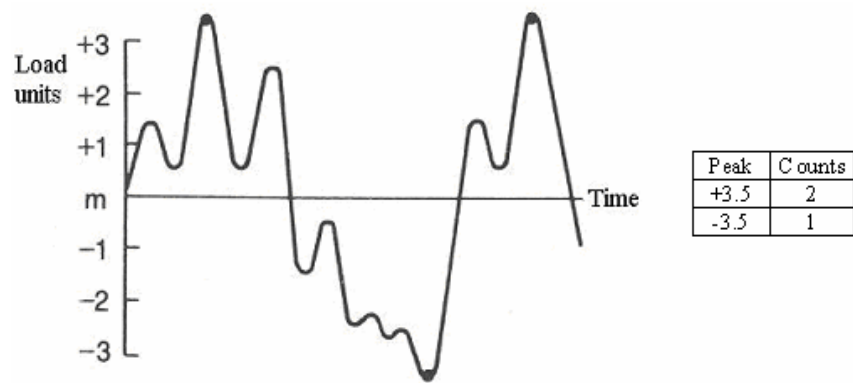
PEAK COUNTING

Peak counting identifies the occurrence of a relative maximum or minimum load value. Peaks above the reference load level are counted, and valleys below the reference load level are counted. This illustrates in Figure G.2(a). Results for peaks and valleys are reported separately. A variation of this method is to count all peaks and valleys without regard to the reference load. To eliminate small amplitude loadings, mean crossing peak counting is often used. Instead of counting all peaks and valleys, only the largest peak or valley between two successive mean crossings is counted as can be seen in Figure G.2(b).

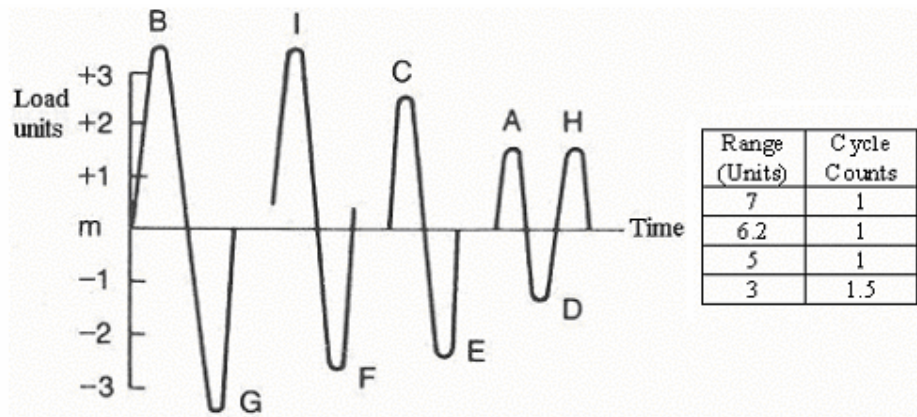
The most damaging cycle count for fatigue analysis is derived from the peak count by first constructing the largest possible cycle, using the highest peak and lowest valley, followed by the second largest cycle, etc., until all peak counts are used. This process can be seen in Figure G.2(c). Once this most damaging cycle count is obtained, the cycles could be applied in any desired order, and this order could have a secondary effect on the amount of damage.



(a) Peak crossing



(b) Mean crossing peak counting



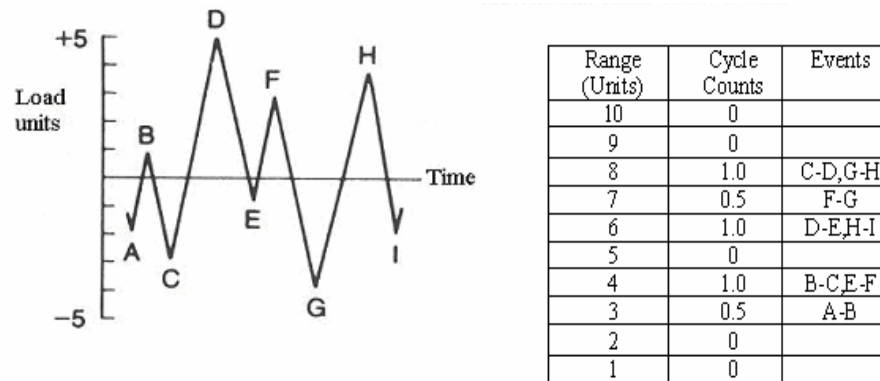
(d) Cycles derived from peak count of (a)

Figure G.2. Peak counting example

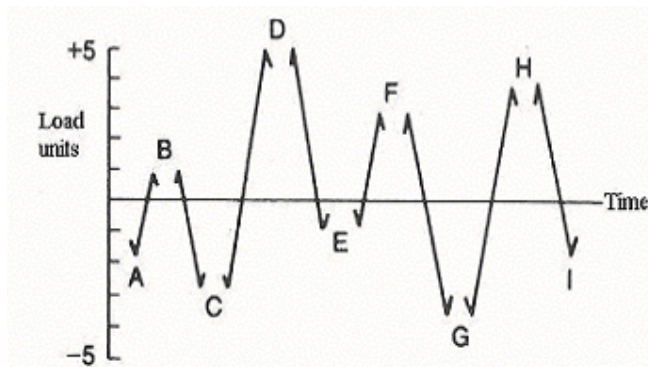
SIMPLE RANGE COUNTING

For this method, a range is defined as the difference between two successive reversals, the range being positive when a valley is followed by a peak and negative when a peak is followed by a valley. Positive ranges, negative ranges, or both may be counted with this method. If only positive or only negative ranges are counted, then each is counted as one cycle. If both positive and negative ranges

are counted, then each is counted as one-half cycle. Ranges smaller than a chosen value is usually eliminated before counting. An example is given in Figure G.3 which shows that both positive and negative ranges are counted.



(a) Simple range counting



(b) Counting from simple range counting (a)

Figure G.3. Simple range counting example